THE LONG RANGE DISPERSION OF RADIOACTIVE PARTICULATES

by

Joshua Michael Aaron Ryder Wurman

S.B. Massachusetts Institute of Technology, 1982

Submitted to the Department of
Meteorology and Physical Oceanography
in Partial Fulfillment of the
Requirements of the Degree of

MASTER OF SCIENCE IN METEOROLOGY

at the

MASSACHUSETTS INSTITUTE OF TECHNOLOGY

June 1982

Signature of Author_____
Department of Meteorology and Physical Oceanography
18 June 1982

Certified by_____
Dr. Raymond Pierrehumbert
Thesis Supervisor

Accepted by_____
Dr. Peter Stone
Chairman, Department of Meteorology and Physical Oceanography

THE LONG RANGE DISPERSION OF RADIOACTIVE PARTICULATES

by

Joshua Michael Aaron Ryder Wurman

S.B. Massachusetts Institute of Technology, 1982

Submitted to the Department of
Meteorology and Physical Oceanography
in Partial Fulfillment of the
Requirements of the Degree of
Master of Science in Meteorology

ABSTRACT

Particle advection in the upper troposphere and lower stratosphere was modeled using the Arakawa scheme to approximate the Jacobian of the height of constant pressure field and the concentration field in the concentration advection equation. The scheme was tested with three different initializations of particle distributions. The numerical properties of the scheme were studied. Wakes of alternating sign produced by the scheme to the lee side of the particle cloud were found to be unacceptable and a modification to the scheme was proposed. The modified scheme was tested with the same three initializations. The modification was found to eliminate the wakes with only a small resultant numerical diffusion. A crude model for the deposition of particles to the ground was added to the advection scheme. The resultant scheme was tested and produced a realistic fallout pattern. Horizontal diffusion was neglected in all the tests. The tests used an idealized height field representing purely zonal flow. The model is adaptable to real synoptic height fields, real diffusion coefficients, and more realistic deposition schemes.

Thesis Supervisor: Dr. Raymond Pierrehumbert

Title: Assistant Professor of Meteorology

ACKNOWLEDGMENTS

This research was begun in January, 1981 under the Undergraduate Research Opportunities Program. I wish to thank the people who run this program, without which this project may never have started. I wish to thank my thesis advisor, Raymond Pierrehumbert, whose guidance was invaluable during the past eighteen months. I wish to thank Ken Morey whose assistance and patience with me and efforts at keeping the computer facility running permitted the computational phase of this research to occur.

Finally, I wish to thank my parents, who instilled in me the greatest of all gifts, the desire to learn.

TABLE OF CONTENTS

LIST OF FIGURES

LIST OF TABLES

DEFINITION OF SYMBOLS

symbol	description	page first used
a	concentration in primary grid box	126
b	concentration in secondary grid box	126
cc	used to calculate smoothed height field	198
C	concentration	30
cos	cosine	33
d	differential operator	30
∂	partial differential operator	30
D	total differential operator	30
D_V	vertical distance scale	30
D_E	diffusion constant	27
dd	used to calculate smoothed height field	198
ee	used to calculate smoothed height field	198
f	coriolis parameter	32
ff	used to calculate smoothed height field	199
g	gravitational acceleration of the Earth	35
gg	used to calculate smoothed height field	199
gp	gridpoint	53
H	vertical depth of the cloud of particles	163
hh	used to calculate smoothed height field	199
J	Jacobian	35
$\hat{k}$	unit vector perpendicular to the Earth's surface	41
kg	kilograms	49

symbol	description	page first used
L	horizontal distance scale	30
ln	longitudinal grid coordinate	198
lt	latitudinal grid coordinate	198
m	meters	27
mb	millibars	49
om	angular rotation rate of the Earth	34
O	of order	39
p	density of air	32
P	pressure	32
Pa	pascals	49
ph	zonal distance coordinate in natural system	33
r	gas constant for air	35
R_e	radial distance from the center of the Earth	33
R_s	Rossby number	30
R_o	radius of Earth	37
R_L	radius of curvature of wind flow	32
s	seconds	27
sin	sine	34
t	time	28
T	temperature	35
th	meridional distance coordinate in natural system	33
tstp	timestep	53
u	zonal velocity	30
u_g	zonal geostrophic wind velocity	32
U	zonal velocity	30

symbol	description	page first used
v	meridional velocity, velocity	28
v_g	meridional geostrophic wind velocity	32
V	meridional velocity, velocity	32
V_g	geostrophic wind velocity	32
V_c	cyclostrophic wind velocity	32
w	vertical velocity	30
x	zonal distance coordinate in cartesian system	30
y	meridional distance coordinate in cartesian system	30
z	vertical distance coordinate in cartesian system	30
ζ	vorticity	41
Δ	incremental change	47
*	multiplication operator	34
X	cross product operator	41
.	dot product operator	41
∇	del operator	41
∇^2	Laplacian operator	36
v	mean terminal velocity	161

The units used in this paper are MKS unless otherwise specified. Units are expressed in exponent form (e.g. velocity is expressed as a certain number of m s-1)

I. Introduction

It is likely that a large scale military conflict between the United States and the Soviet Union would involve the exchange of nuclear weapons. The explosive force of these devices is orders of magnitude greater than that of conventional, non-nuclear, weapons. The blast damage caused by the detonation of these devices is, of course, much greater than that from a conventional explosion. But the effects of nuclear detonations extend far beyond the initial damage caused by the force of the explosion. The focus of this paper is the study of a phenomenon unique to nuclear weapons: radioactive fallout.

Radioactive fallout is comprised of radioactive particles from the bomb itself and from debris that is exposed to the nuclear blast. The amount and nature of radioactive fallout is dependent on the nature of the bomb and the altitude of the detonation above the ground. In an explosion far above the Earth's surface there is little solid material present from which fallout can be created. When the explosion occurs near the ground, however, a large amount of the surface is exposed to the blast and thrown into the atmosphere, to become fallout. In the event of a war, weapons that are targeted at strengthened missile silos and other military targets would, likely, be detonated near ground level in order to maximize

their destructive force. During such an event, much of the debris that is thrown into the atmosphere will become radioactive. The effects of the resultant radioactivity when these particles eventually fall to the ground are commonly known and can be disastrous.

The fallout, just described, is divided into two basic types, distinguished by the time that is necessary for the radioactivity to reach the ground. Near range fallout consists of large radioactive particles that fall to the ground rapidly and near the site of the explosion. Also included in this category are small particles that are not thrown far into the atmosphere and, thus, settle rapidly to the ground. This near range fallout is due to particles that have only a short residence time in the atmosphere and only a short exposure to the transport effects of the wind. This paper deals with the long range fallout that is caused by nuclear explosions. This fallout consists of particles thrown into the upper troposphere and lower stratosphere by large blasts at the surface. These particles, often very small, require from hours to years to fall to the surface. During this time, high winds at that altitude cause the particles to advect away from the site of the explosion. The particulate cloud may circuit the globe many times before nearly all of the particles fall and the cloud diffuses and loses identity. Most of the destructive fallout, however, falls during the cloud's first day or two of advection on its first circuit

around the Earth.

Studies of the movement of these clouds and the resultant fallout from them have been made by other investigators. Wit and Zagurek (1981) calculated the fallout amounts that would be expected from an attack on the, once, proposed MX missile silos in Utah, Nevada, Texas, and New Mexico. They used a prediction model utilized by the Federal Emergency Management Agency called the WSEG 10 Fallout Model. The scheme was tested on a wind field that was described as a "'typical day' in March". Their study, while only indicating the effects predicted for a non-existent, "typical" day, indicated the scale of mortality and morbidity that would occur in such an attack on the MX missile silos. Harmful levels of fallout were predicted to fall from the blast area in the West all the way to the Atlantic coast. A study of particle trajectories in variable wind fields was conducted by Kao and Henderson (1970). This study modeled individual particle trajectories in a Lagrangian manner. The subject of their paper was the magnitude of the eddy diffusivity and statistics about the particle displacements after very long time periods. Tanaevsky and Blanchet (1966) studied the fallout from nuclear detonations in the atmosphere over Semipalatinsk and Novaya Zemlya in the Soviet Union. They found it difficult to plot cloud trajectories, especially in regions of difluent flow. Instead, they plotted a "line of probability" which represented the front along which the first fallout was likely

to occur. Due to the indeterminate prediction of the location of the cloud, no attempt was made to predict fallout amounts at specific locations.

In this paper, the movement of the particulate cloud during its first day of advection is modeled in an Eulerian scheme involving the fields of concentration and of constant pressure heights. The height field of constant pressure is directly related to the wind field by the geostrophic approximation to the momentum equation. The advection term in the rate of concentration change equation is written in terms Of a Jacobian of the concentration and height fields. The Jacobian is approximated by a scheme developed by Arakawa (1966).

The Arakawa scheme has advantages and drawbacks that are discussed, at length, in the text. Its basic advantages are designed to be the conservation of mass and the suppression of spurious numerical diffusion. In the trials presented in this paper, the scheme conserves mass very closely. The quantity designed to measure resistance to numeric diffusion, the sum of the squares of the masses in all grid boxes, is also conserved fairly well. The drawback to this scheme was that, in order to conserve the quantity just described, the sum of the squares of the masses in all portions of the cloud, the model produced unrealistic results. The scheme caused a series of wakes, alternating in sign, to develop behind and

around the cloud. These wakes eventually dominated the cloud and obscured any useful results. The cloud, if the wakes were included, actually expanded very rapidly to continental dimensions. The sum of the squares quantity is conserved at the expense of creating the series of negative and positive wakes. While the wakes cause the pure Arakawa scheme to not be usable in this context, a scheme is presented here which eliminates the wakes and produces good results. The small resultant degree of numerical diffusion, that is noticeable by inspection of the cloud and by the drop in the sum of the squares quantity, is acceptable and the cloud appears very realistic.

Real turbulent diffusion is ignored in the tests of the modified scheme that are presented in this paper. This is done so that the properties of the advection scheme can be studied without the complications introduced by the physical diffusion of the cloud. The advection pattern is not changed significantly by this omission. Davidson, et. al. (1966) determined that the range of horizontal diffusion coefficients in the troposphere and stratosphere was between D_E = 10000 m+2 s-1 and D_E = 100000 m+2 s-1. In their model of the very long term diffusion of Tungsten-185, a value of D_E = 40000 m+2 s-1 produced the best agreement with the observed distribution of the element months after its injection into the atmosphere by nuclear detonations. Dyer (1966) studied the distribution of volcanic dust in the Southern Hemisphere

during the two years following the eruption of Mount Bali in 1963. He determined that the concentration of dust found at Aspendale, Victoria, Australia could best be explained if the value of the diffusion constant was D_E = 40000 m+2 s-1. The amounts found at the South Pole were best explained by a value of D_E= 140000 m+2 s-1. Even with the largest of these values, the diffusive length scale is much smaller than the advective length scale after one day. The diffusive length scale, $L \sim \sqrt{D\ t}$, assuming D_E = 100000 m+2 s-1 and t= 100000 s, is of order 100000M. The deposition pattern has a length scale in the direction of the wind velocity that is of order L ~ v * t. If a wind speed of 10 m s-1 and the same time scale is assumed, then this distance is of order 1,000,000 m. Thus the long axis of the deposition pattern will not be significantly affected by the neglect of diffusion. The width of the deposition pattern is much less than its length. But, if, as will be shown in the trials, the minimum stable cloud size is of order five gridpoints or 100,000 m, then the diffusion will only double this scale. Thus, the bulk properties of the deposition remain the same even with the neglect of diffusion. This is especially true in the trials where the numerical diffusion that is present helps produce more realistic results.

An idealized height field is used in order to test the properties of advection scheme. The purpose of this study was not to make actual predictions of real fallout patterns. The

scheme described in the text is, however, fully adaptable to real synoptic situations.

The deposition scheme used in this paper is very crude. This scheme is included to indicate the general intensity of fallout that could be expected to fall from a particulate cloud. The assumptions of no vertical diffusion and a mono-disperse particle size distribution are made and they are clearly not realistic.

This paper is intended to provide some basic groundwork towards the prediction of actual distributions under realistic and varying atmospheric conditions. The assumptions of an idealized wind field, zero horizontal or vertical diffusion, a crude deposition scheme, and the neglect of other effects such as the radioactive decay of the particles and the scavenging effects of precipitation in the lower portions of the atmosphere, cause the trials presented here to be of little, actual predictive, significance.

The techniques described here should be expanded to include these, and possibly other, effects and the model should be applied to real wind fields. Once this is done, a better understanding of the long range effects of nuclear explosions will be achieved.

II. Derivation of exact equations

In order to predict the concentration of particulates at a particular location at a particular time, it is necessary to know both the concentration at an initial time and then be able to integrate the time rate of change of concentration at that location. The total time rate of change of particle concentration can be expressed as

$$\frac{DC}{Dt} = \frac{dC}{dt} + u\frac{\partial C}{\partial x} + v\frac{\partial C}{\partial y} + w\frac{\partial C}{\partial z} \qquad (1)$$

where C is the particle concentration, and u, v, and w are the flow velocities in the x, y, and z directions respectively, and the particles are assumed to be moving at the same velocity as the wind.

Scaling arguments can be used to simplify (1). The vertical motions associated with synoptic scale flow are quite small in the atmosphere. The following scaling of the vertical wind (Pedlosky, 1979) shows this explicitly.

$$w \sim U \left[\frac{D_v}{L} \right] R_s \qquad (2)$$

where U is a typical horizontal velocity, D_v is a typical scale of vertical distance , L is a typical scale of horizontal

distance, and R_s is the Rossby number.

The ratio of the vertical advection term to the horizontal advection terms is then:

$$\frac{w\,\frac{\partial C}{\partial z}}{u\,\frac{\partial C}{\partial x}} \sim \frac{U\left[\frac{D_v R_s}{L}\right]\left[\frac{C}{D_v}\right]}{U\left[\frac{C}{L}\right]} = R_s \qquad (3)$$

Thus, if the Rossby number is small, then the last term in (1) can be neglected with respect to the other two.

The advective terms in (1) explicitly contain wind velocities. For calculation purposes, it is inconvenient to utilize observed upper tropospheric and lower stratospheric winds directly. It is more useful to use the height field of certain standard pressure values to calculate particle advection. In order to calculate the particle advection from this height data it is first necessary to transform (1) into pressure coordinates. The horizontal momentum equations are used in order to do this. The simplified momentum equations are (Holton, 1979):

$$\frac{du}{dt} - f v = -\frac{1}{p}\frac{\partial P}{\partial x} \tag{4}$$

$$\frac{dv}{dt} + f u = -\frac{1}{p}\frac{\partial P}{\partial y} \tag{5}$$

where f is the coriolis parameter, p is the density of the air, and P is the local pressure. If the acceleration terms are small, then the first terms can both be dropped and the results, after rearranging terms are (6a) and (6b), the geostrophic approximation.

$$v_g = \frac{1}{p f}\frac{\partial P}{\partial x} \tag{6a}$$

$$u_g = \frac{-1}{p f}\frac{\partial P}{\partial y} \tag{6b}$$

This approximation is accurate to order R_s, the Rossby number. The greatest deviations from geostrophy will occur in the highest curvature regions of mid-latitude jets. The deviation from the more accurate, but more computationally involved gradient, or cyclostrophic, wind is:

$$\frac{V_c}{V_g} = 1 + \frac{V}{f R_L} \tag{7}$$

where R_L is the radius of curvature of the flow pattern. R_L is positive in cyclonic flow and negative in anticyclonic flow. The departure from geostrophy is rarely more than ten or twenty percent in middle and high latitudes, but can be great in the tropics. Thus, with the geostrophic approximation, this study confines itself to the examination of advection in the middle and high latitudes.

The substitution of (6a) and (6b) into (1) gives,

$$\frac{DC}{Dt} = \frac{dC}{dt} - \frac{1}{pf}\frac{\partial C}{\partial x}\frac{\partial P}{\partial y} + \frac{1}{pf}\frac{\partial C}{\partial y}\frac{\partial P}{\partial x} \qquad (8)$$

It is now necessary to expand (8) into natural coordinates. The coordinate system chosen is the latitude, longitude convention in the western portion of the northern hemisphere. In this system, ph, the longitude, increases to the west and th, the latitude, is zero at the equator and increases northward. With this choice of coordinates, the differential transformations are:

$$\partial x = - R_e \cos(th)\, \partial(ph) \qquad (9a)$$

$$\partial y = R_e\, \partial(th) \qquad (9b)$$

Where R_e is the radial distance from the center of the Earth. It is also convenient to express the coriolis parameter explicitly as,

$$f = 2\ om\ \sin(th) \tag{10}$$

where om is the angular rotation rate of the earth. When (9a), (9b), and (10) are substituted into (8) the result is,

$$\frac{DC}{Dt} = \frac{dC}{dt} + \frac{1}{2\ om \sin(th)\ R_e\ p \cos(th)} \frac{\partial P}{\partial(th)} \frac{\partial C}{\partial(ph)}$$

$$- \frac{1}{2\ om \sin(th)\ R_e\ p \cos(th)} \frac{\partial P}{\partial(th)} \frac{\partial C}{\partial(ph)} \tag{11}$$

This can be modified to give,

$$\frac{DC}{Dt} = \frac{dC}{dt} - \left[\frac{1}{2\ om \sin(th)\ R_e\ p \cos(th)}\right] *$$

$$\left[\frac{\partial P}{\partial(ph)} \frac{\partial C}{\partial(th)} - \frac{\partial P}{\partial(th)} \frac{\partial C}{\partial(ph)}\right] \tag{12}$$

The data that is usually used to represent the weather patterns in the middle and upper atmosphere is not expressed in terms of pressure fields. The data commonly gives the height of a standard pressure surface at the location of the observation. Thus, it is useful to convert (12) into an equation using a height coordinate. The hydrostatic approximation, valid for ideal gases and small vertical accelerations, gives a relationship between a vertical height coordinate and the pressure coordinate,

$$dP = \frac{-g\ p}{r\ t}\ dz \tag{13}$$

where g is the acceleration of gravity, r is the gas constant for air, and T is the temperature of the air. When (13) is substituted into (12) the result is,

$$\frac{DC}{Dt} = \frac{dC}{dt} - \left[\frac{g\ P}{2\ om\ \sin(th)\ R_e\ p\ \cos(th)\ r\ T}\right] * \left[\frac{\partial C}{\partial(ph)}\frac{\partial z}{\partial(th)} - \frac{\partial C}{\partial(th)}\frac{\partial z}{\partial(ph)}\right] \tag{14}$$

The last two terms in (14) can be expressed as a Jacobian where,

$$J(C,z) = \begin{vmatrix} \frac{\partial C}{\partial(ph)} & \frac{\partial C}{\partial(th)} \\ \frac{\partial z}{\partial(ph)} & \frac{\partial z}{\partial(th)} \end{vmatrix} \tag{15}$$

Thus,

$$\frac{DC}{Dt} = \frac{dC}{dt} - \frac{g\ P}{2\ om\ \sin(th)\ R_e\ p\ \cos(th)\ r\ T}\ J(C,z) \tag{16}$$

If the assumption is made that the atmosphere is an ideal gas, then P/(p r T) is unity and can be eliminated in this equation.

DC/Dt is the time rate of change of concentration moving with the flow of particles. To obtain a final set of equations, DC/Dt is set equal to the rate at which particles are redistributed or removed from the atmosphere by physical processes, such as horizontal and vertical diffusion, radioactive decay, and deposition on the ground. In the model studied here, the assumption is made that the diffusion can be modeled in terms of a single diffusion constant. The simplified form of the diffusion is assumed to be,

$$\frac{DC}{Dt} = D_E \nabla^2 (C) \qquad (17)$$

where D_E is the diffusion constant. In natural coordinates, this expands to,

$$\frac{DC}{Dt} = D_E \left[\frac{1}{R_e} \frac{\partial}{\partial R_e} \left\{ R_e^2 \frac{\partial C}{\partial R_e} \right\} + \frac{1}{R_e \cos(th)} \frac{\partial}{\partial (th)} \left\{ \cos(th) \frac{\partial C}{\partial (th)} \right\} + \frac{1}{R_e \sin(th)} \frac{\partial^2 C}{\partial (ph)} \right] \qquad (18)$$

Deposition is dealt with in a later section and the radioactive decay of the particles is neglected in the model studied here.

The model used in this study contains only a single

layer. The essential assumptions in this single layer approximation are that the concentration of particulates in the debris cloud and the wind velocities do not vary significantly with height, or that the particles only exist in a certain thin layer that is characterized by uniform or nearly uniform winds and other physical properties. This assumption greatly simplifies the computational problem, but neglects important vertical variations in the atmosphere. In particular, real winds do show considerable shear in both direction and speed through the depth of the atmosphere. The one layer model used here assumes that the particles are always being advected by winds that are present at one particular level.

The first term in (18) contains the radial variation of concentration. This term can be eliminated because:

$$R_e = R_o + z \tag{19a}$$

Where R_o is the radius of the Earth.
The differentiatial form of (19a) is:

$$dR_e = dz \tag{19b}$$

Thus,

$$\frac{dC}{dR_e} = \frac{dC}{dz} = 0 \qquad \text{In the single layer approximation} \tag{19c}$$

Thus, by substituting (18) into (16) and rearranging terms, the local rate of change of particle concentration becomes,

$$\frac{dC}{dt} = D_E \left[\frac{1}{R_e \cos(th)} \frac{\partial}{\partial(th)} \left\{ \cos(th) \frac{\partial C}{\partial(th)} \right\} + \frac{1}{R_e \sin(th)} \left\{ \frac{\partial^2 C}{\partial(ph)} \right\} \right] + \frac{g P}{2\ om \sin(th) R_e p \cos(th) r T} J(C,z) \qquad (20)$$

As will be seen in the trials calculated in section IV, the finite difference approximations used to calculate the advection introduce numerical diffusion. Since some diffusion is already present, and it is desirable to study the model's properties without physical diffusion, the constant D_E in (20) was set to zero in the trials presented here. The derivation here includes the diffusion term for completeness and an appropriate diffusion constant should be chosen for more detailed trials and in order to make accurate predictions of the deposition onto the ground of radioactive particles. A crude calculation of deposition rates is discussed in section IV.3.

III. Derivation of finite difference forms

In order to solve this equation numerically, it is necessary to convert it to finite difference form. The finite difference analogues to the diffusion terms can be found in a straightforward manner. The standard two point center differenced expansion of a derivative gives,

$$\left.\frac{\partial C}{\partial(th)}\right|_{th+\frac{\Delta th}{2}} = \frac{1}{\Delta th}\left(C(th+\Delta th)-C(th)\right) + O\left[\frac{\Delta th}{2}\right]^2 \qquad (21)$$

and,

$$\left.\frac{\partial C}{\partial(th)}\right|_{th-\frac{\Delta th}{2}} = \frac{1}{\Delta th}\left(C(th)-C(th-\Delta th)\right) + O\left[\frac{\Delta th}{2}\right]^2 \qquad (22)$$

Thus,

$$\left.\frac{\partial}{\partial(th)}\left(\cos(th)\frac{\partial C}{\partial(th)}\right)\right|_{th} = \frac{1}{(\Delta th)^2}\left(\cos\left(th+\frac{\Delta th}{2}\right)\left(C(th+\Delta th)-C(th)\right)-\cos\left(th-\frac{\Delta th}{2}\right)\left(C(th)-C(th-\frac{\Delta th}{2})\right)\right) \qquad (23)$$

The second order derivative in (20) can be found by using two Taylor expansions near the point in question.

$$C(ph+\Delta ph) = C(ph) + \Delta ph\frac{\partial C(ph)}{\partial(ph)} + \frac{1}{2}(\Delta ph)^2\frac{\partial^2 C(ph)}{\partial(ph)^2} + \frac{1}{6}(\Delta ph)^3\frac{\partial^3 C(ph)}{\partial(ph)^3} + \frac{1}{24}(\Delta ph)^4\frac{\partial^4 C(ph)}{\partial(ph)^4} + O\left[\Delta(ph)^5\right] \qquad (24)$$

$$C(ph-\Delta ph) = C(ph) - \Delta ph\frac{\partial C(ph)}{\partial(ph)} + \frac{1}{2}(\Delta ph)^2\frac{\partial^2 C(ph)}{\partial(ph)^2} - \frac{1}{6}(\Delta ph)^3\frac{\partial^3 C(ph)}{\partial(ph)^3} + \frac{1}{24}(\Delta ph)^4\frac{\partial^4 C(ph)}{\partial(ph)^4} - O\left[\Delta(ph)^5\right] \qquad (25)$$

The addition of (24) and (25) gives,

$$C(\rho_h+\Delta\rho_h)-C(\rho_h-\Delta\rho_h)=2C(\rho_h)+(\Delta\rho_h)^2\frac{\partial^2 C}{\partial(\rho_h)^2}+O\left[\frac{\Delta(\rho_h)^4}{12}\right] \qquad (26)$$

thus,

$$\frac{\partial^2 C(\rho_h)}{\partial(\rho_h)^2}=\frac{C(\rho_h+\Delta\rho_h)-2C(\rho_h)+C(\rho_h-\Delta\rho_h)}{(\Delta\rho_h)^2}-O\left[\frac{(\Delta\rho_h)^2}{12}\right] \qquad (27)$$

To approximate the Jacobian advection term, the method described by Arakawa (1966) was used. This approximation for the Jacobian is accurate to high order in spatial derivatives and is resistant to computational instabilities that can arise in long term numerical integration. The Arakawa scheme should also conserve the square of the area-weighted particle concentrations in the cloud. The approximation for the Jacobian is,

$$\begin{aligned}J(C(\rho_h,t_h),z(\rho_h,t_h))=\frac{-1}{12\Delta\rho_h\Delta t_h}\Big[&\big(z(\rho_h,t_h-\Delta t_h)+z(\rho_h+\Delta\rho_h,t_h-\Delta t_h)\\&-z(\rho_h,t_h+\Delta t_h)-z(\rho_h+\Delta\rho_h,t_h+\Delta t_h)\big)*\\&\big(C(\rho_h+\Delta\rho_h,t_h)-C(\rho_h,t_h)\big)\\&+\big(z(\rho_h-\Delta\rho_h,t_h-\Delta t_h)+z(\rho_h,t_h-\Delta t_h)-z(\rho_h-\Delta\rho_h,t_h+\Delta t_h)-z(\rho_h,t_h+\Delta t_h)\big)\big(C(\rho_h,t_h)-C(\rho_h-\Delta\rho_h,t_h)\big)\\&+\big(z(\rho_h+\Delta\rho_h,t_h)+z(\rho_h+\Delta\rho_h,t_h+\Delta t_h)-z(\rho_h-\Delta\rho_h,t_h)-z(\rho_h-\Delta\rho_h,t_h+\Delta t_h)\big)\big(C(\rho_h,t_h+\Delta t_h)-C(\rho_h,t_h)\big)\\&+\big(z(\rho_h+\Delta\rho_h,t_h-\Delta t_h)+z(\rho_h+\Delta\rho_h,t_h)-z(\rho_h-\Delta\rho_h,t_h-\Delta t_h)-z(\rho_h-\Delta\rho_h,t_h)\big)\big(C(\rho_h,t_h)-C(\rho_h,t_h-\Delta t_h)\big)\\&+\big(z(\rho_h+\Delta\rho_h,t_h)-z(\rho_h,t_h+\Delta t_h)\big)\big(C(\rho_h+\Delta\rho_h,t_h+\Delta t_h)-C(\rho_h,t_h)\big)\\&+\big(z(\rho_h,t_h-\Delta t_h)-z(\rho_h-\Delta\rho_h,t_h)\big)\big(C(\rho_h,t_h)-C(\rho_h-\Delta\rho_h,t_h-\Delta t_h)\big)\\&+\big(z(\rho_h,t_h+\Delta t_h)-z(\rho_h-\Delta\rho_h,t_h)\big)\big(C(\rho_h-\Delta\rho_h,t_h+\Delta t_h)-C(\rho_h,t_h)\big)\\&+\big(z(\rho_h+\Delta\rho_h,t_h)-z(\rho_h,t_h-\Delta t_h)\big)\big(C(\rho_h,t_h)-C(\rho_h+\Delta\rho_h,t_h-\Delta t_h)\big)\Big]\end{aligned} \qquad (28)$$

The Arakawa scheme was developed in order to have the advection Jacobian conserve certain properties and be stable to long term numerical integration. Arakawa's derivation was directed towards the solution of the vorticity advection equation for two-dimensional, incompressible, flow. That equation is:

$$\frac{d\zeta}{dt} + v \cdot \nabla \zeta = 0 \qquad (28.5)$$

where v is the velocity and ζ is the vorticity, $\hat{k} \times \nabla \cdot v$. The quantities that were to be conserved were mean vorticity, mean kinetic energy of the flow, and mean square vorticity. The first constraint just forces the conservation of the scalar quantity that is undergoing advection. The latter two constraints were derived for incompressible, two dimensional, flow by Fjortoft (1953). These constraints, when applied to the concentration advection equation, (1), require that the total mass, the total sum of the squares of the masses, and the kinetic energy of the flow remain constant. Since the velocity field is not altered by the advection of concentrations, the kinetic energy constraint is not of interest here.

The stability of the second order Arakawa scheme was investigated by Lilly (1965). He studied certain stability

measures under several time differencing schemes. With the time differencing used here, the Eulerian method, (30), Lilly found that the Jacobian could become unstable when applied to (28.5). It should be noted that the coupling between the vector and scalar fields that is present in (28.5), is absent in the concentration advection equation that is used here.

The conservation properties of the scheme were studied by Arakawa (1970). The mean square vorticity was found to be almost exactly conserved. Small errors were found to be introduced in this quantity due to time differencing errors, Arakawa and Lamb (1977). While the mean vorticity is exactly conserved by the scheme, the mean square vorticity is only semi-conserved to within time differencing errors.

Numerous investigators have used the Arakawa scheme for numerical integration. Bretherton and Karweit (1975) used the fourth order scheme with the same conservation properties to solve the vorticity equation for ocean flows. Lilly (1969) used the second order scheme to study simulations of two dimensional turbulence. Two detailed studies of the Arakawa scheme and other alternate methods have been done. The first, Molenkamp (1967), compared the schemes to other finite difference schemes in their ability to accurately advect a region of an arbitrary scalar quantity in a field characterized by purely cyclonic flow. The second and fourth order schemes were found to produces solutions which preserved

the mean vorticity and the mean square vorticity. The Arakawa schemes compared favorably with other simple schemes in terms of preserving the peak value of the scalar quantity and in terms of the velocity of the peak value. Negative values were produced at some gridpoints, but their detailed nature was not discussed. Molenkamp's paper only considered the first forty timesteps of an advection. Orzag (1971) studied the Arakawa schemes with similar velocity and scalar fields. His results show that the schemes do preserve the basic features of the scalar field, but that there are significant problems in the patterns. Specifically, there were a number of what Orzag called "wakes of bad numbers" upwind of the main distribution. These wakes were attributed to phase lag errors in the Arakawa scheme. The wakes were said to be components of the distribution that were lagging the main area. Thus, some of the information necessary to construct the distribution was not centered in the proper location. A diagram of these wakes is shown below in figure 1, reproduced from Orzag (1971), p. 84.

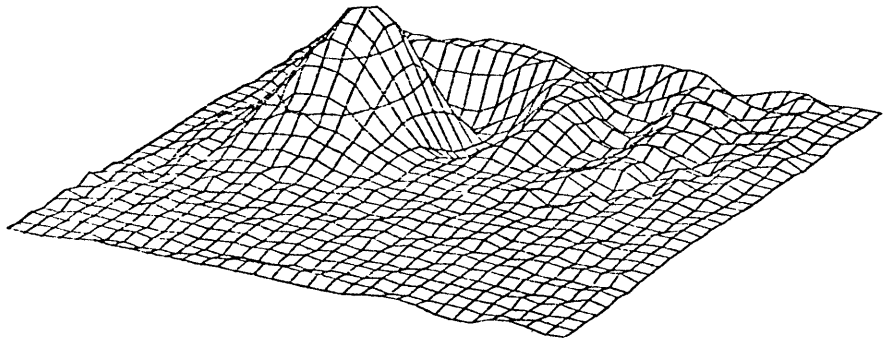

Figure 1: Wakes in Orzag's advection trials

The substitution of (23), (27), and (28) into (20) gives,

$$\frac{\partial C(\rho_h,\theta_h)}{\partial t} = D_E\left[\frac{1}{R_e^2\cos(\theta_h)(\Delta\theta_h)^2}\left(\cos\left(\theta_h+\frac{\Delta\theta_h}{2}\right)\left(C(\rho_h,\theta_h+\Delta\theta_h)-C(\rho_h,\theta_h)\right)\right.\right.$$

$$\left.-\cos\left(\theta_h-\frac{\Delta\theta_h}{2}\right)\left(C(\rho_h,\theta_h)-C(\rho_h,\theta_h-\Delta\theta_h)\right)\right)$$

$$\left.+\frac{1}{R_e^2\sin^2(\theta_h)(\Delta\rho_h)^2}\left(C(\rho_h+\Delta\rho_h,\theta_h)-2C(\rho_h,\theta_h)+C(\rho_h-\Delta\rho_h,\theta_h)\right)\right]$$

$$-\frac{9}{24\,\text{om}\,R_e^2\sin(\theta_h)\cos(\theta_h)\,\Delta\rho_h\,\Delta\theta_h}\Bigg[$$

$$\left(z(\rho_h,\theta_h-\Delta\theta_h)+z(\rho_h+\Delta\rho_h,\theta_h-\Delta\theta_h)-z(\rho_h,\theta_h+\Delta\theta_h)-z(\rho_h+\Delta\rho_h,\theta_h+\Delta\theta_h)\right)\left(C(\rho_h+\Delta\rho_h,\theta_h)-C(\rho_h,\theta_h)\right)$$

$$+\left(z(\rho_h-\Delta\rho_h,\theta_h-\Delta\theta_h)+z(\rho_h,\theta_h-\Delta\theta_h)-z(\rho_h-\Delta\rho_h,\theta_h+\Delta\theta_h)-z(\rho_h,\theta_h+\Delta\theta_h)\right)\left(C(\rho_h,\theta_h)-C(\rho_h-\Delta\rho_h,\theta_h)\right)$$

$$+\left(z(\rho_h+\Delta\rho_h,\theta_h)+z(\rho_h+\Delta\rho_h,\theta_h+\Delta\theta_h)-z(\rho_h-\Delta\rho_h,\theta_h)-z(\rho_h-\Delta\rho_h,\theta_h+\Delta\theta_h)\right)\left(C(\rho_h,\theta_h+\Delta\theta_h)-C(\rho_h,\theta_h)\right)$$

$$+\left(z(\rho_h+\Delta\rho_h,\theta_h-\Delta\theta_h)+z(\rho_h+\Delta\rho_h,\theta_h)-z(\rho_h-\Delta\rho_h,\theta_h-\Delta\theta_h)-z(\rho_h-\Delta\rho_h,\theta_h)\right)\left(C(\rho_h,\theta_h)-C(\rho_h,\theta_h-\Delta\theta_h)\right) \qquad (29)$$

$$+\left(z(\rho_h+\Delta\rho_h,\theta_h)-z(\rho_h,\theta_h+\Delta\theta_h)\right)\left(C(\rho_h+\Delta\rho_h,\theta_h+\Delta\theta_h)-C(\rho_h,\theta_h)\right)$$

$$+\left(z(\rho_h,\theta_h-\Delta\theta_h)-z(\rho_h-\Delta\rho_h,\theta_h)\right)\left(C(\rho_h,\theta_h)-C(\rho_h-\Delta\rho_h,\theta_h-\Delta\theta_h)\right)$$

$$+\left(z(\rho_h,\theta_h+\Delta\theta_h)-z(\rho_h-\Delta\rho_h,\theta_h)\right)\left(C(\rho_h-\Delta\rho_h,\theta_h+\Delta\theta_h)-C(\rho_h,\theta_h)\right)$$

$$+\left(z(\rho_h+\Delta\rho_h,\theta_h)-z(\rho_h,\theta_h-\Delta\theta_h)\right)\left(C(\rho_h,\theta_h)-C(\rho_h+\Delta\rho_h,\theta_h-\Delta\theta_h)\right)\Bigg]$$

This equation is suitable for numerical integration.

IV. Trials

A. Description of computational method and data

In order to calculate dC/dt from (29) it is necessary to know the field of constant pressure height. The heights of certain pressure values are observed every twelve hours by several hundred stations scattered across the North American continent. The height field of constant pressure can be found by interpolating between all of these stations. The interpolation scheme used in this paper is not standard and is discussed in Appendix A.

The scheme produced fields that were realistic, sufficiently smooth and, when contoured, agreed closely with with iso-height contours that were produced on NMC analysis of the same data. In the trials tested here, the height field was artificially constructed to produce pure zonal winds. The interpolation scheme was used, but in the case of idealized winds, a generating function could have been substituted. The intent, again, was to provide the groundwork for more sophisticated trials with real wind fields.

The method of computation was quite straightforward. A 51 by 151 grid represented the North American region with a grid spacing of 1/2 degree in both latitude and longitude.

The boundaries of the grid were 30 degrees north latitude and 55 degrees north latitude and 55 degrees west longitude and 130 degrees west longitude. Since no longitudinal variation was present in the wind field or in the grid spacing that was used, the particular longitudinal boundaries of the grid were not important in the advection. The computation was initialized with a starting concentration field and an initial height field. From this initialization, the concentrations at all points were calculated by a backwards differencing scheme, also known as the Euler method:

$$C(t) = C(t-\Delta t)+ dC/dt \qquad (30)$$

This backwards differencing scheme is accurate to order Δt. The concentration field was updated each timestep, but the height field was not changed. Upper atmospheric weather systems tend to move more slowly than surface systems and much more slowly than the wind velocity field in which they are embedded. Thus, it was reasonable to neglect the time variation of the height field over sufficiently short time periods. By making this approximation, the model essentially moves particles along the streamlines of the flow. It would be simple to modify the scheme to allow for the updating of the height field at appropriate intervals

Longitudinal grid spacing varied from 48200 m at the southern boundary of the grid to 31900 m at the northern

boundary. This variation is shown below in figure 2.

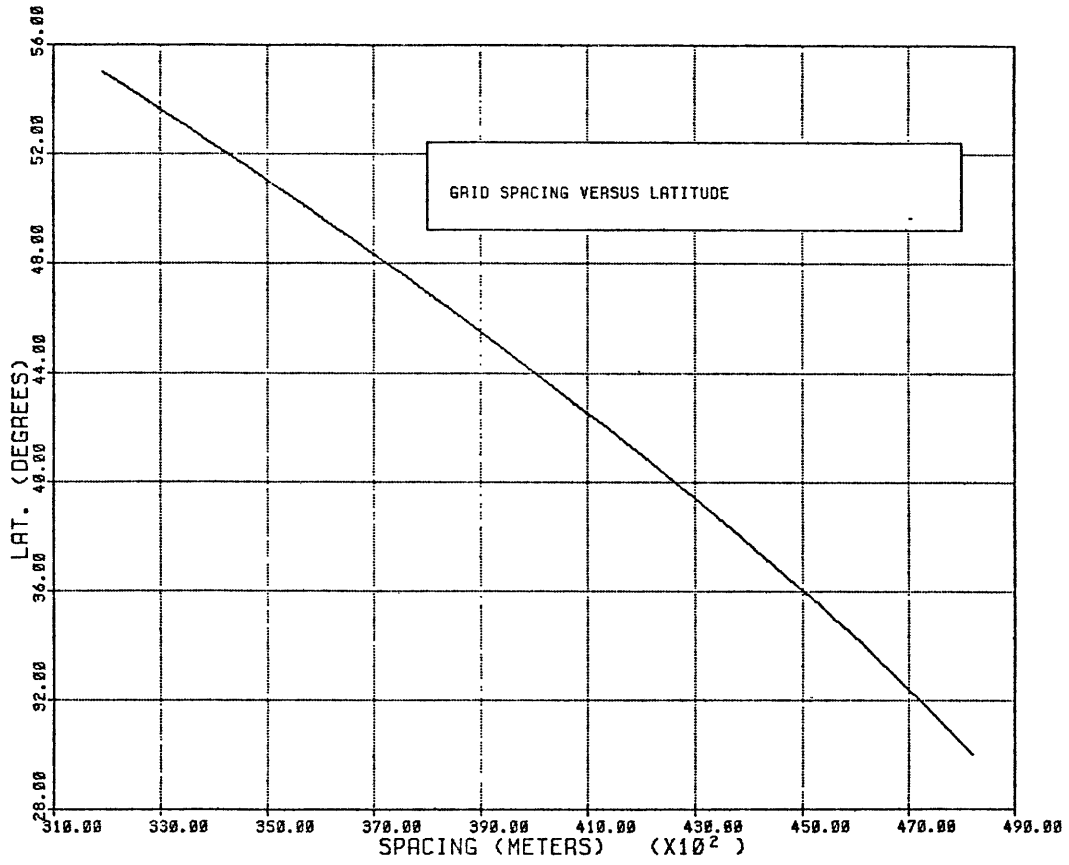

Figure 2: Longitudinal gridpoint spacing

Latitudinal grid spacing was constant and equal to 55700 meters. The result of this difference in spacing was to introduce a asymmetry into the particle advection patterns. In fact, a symmetrical concentration pattern in this grid

space would indicate an unsymmetric mass distribution in the actual cloud.

Much of the debris that is thrown up by nuclear explosions is deposited at high levels in the atmosphere corresponding to pressures of 10000 pa to 30000 Pa (Pascals) (1 Pascal = 1 kg m-1 s-2 = 0.01 mb (millibars)). At these levels the winds in the jet stream can be as high as 80 m s-1. In order to keep the computation stable according to CFL criterion the Courant number must be less than unity, thus, the time necessary for a particle to traverse one gridpoint must be much less than one time step (Roache, 1976). With a time step of one minute this condition was always satisfied in the model. In the worst case, with 80 m s-1 winds blowing zonally across the northern edge of the grid, the time that a particle would take to cross one gridpoint would be much larger than one, one minute, timestep. This is shown by the calculation below.

$$\frac{\text{time}}{\text{gridpoint}} = \frac{\text{grid spacing}}{v} = \frac{31900\ \text{m}}{80\ \text{m s-1}} = 399\ \text{s} = 6.65\ \text{timesteps} \quad (31)$$

This gives a Courant number of 1/6.65 or 0.15.

These trials were run on a Digital Equipment Corporation

PDP-11/60 computer. The computer was part of the MCIDAS computer facility in the Department of Meteorology and Physical Oceanography at the Massachusetts Institute of Technology. This computer was not extremely fast but there were many instances when the trials could be calculated without competition from other jobs on the system. The unsmoothed trials described below required about one to two days of computing time. The advection program did not calculate the concentrations for any gridpoints that were far removed from the cloud. It was not necessary to calculate concentrations for these grid boxes because (28) has a very limited spatial range. (28) only affects grid boxes that are adjacent or diagonally adjacent to a non-zero concentration. The skipping of many gridpoints allowed the smoothed trials to run much faster due to the small dimensions of the smoothed clouds. Integer arithmetic was used throughout to calculate the advection. This arithmetic saved computational time and space but resulted in truncation errors in some of the trials that were much larger than would have been present if floating point arithmetic had been used. As will be discussed in the descriptions of the trials, some of the trials were computed with integer arithmetic that used truncation rounding and some of the trials were computed with nearest integer rounding.

In order to test the properties of the Arakawa Jacobian in the advection scheme, the sum of the area-weighted concentrations and the sum of the squares of the area-weighted

concentrations was calculated. The first quantity was conserved if the scheme properly conserved mass. This was because the area weighted concentration in a grid box was just the number of particles in that grid box. This quantity is conserved exactly by the Arakawa scheme, even in its finite difference form. Variations in this quantity are a measure of arithmetic truncation error due to the integer arithmetic used in the trials studied here. The Arakawa scheme should also conserve the second quantity. This second quantity represents the resistance to spurious diffusion caused by the numeric scheme. This is not conserved exactly and is a measure of time differencing errors in the finite difference scheme.

To simplify much of the early testing a simplified height field was used. The height field that was used had no longitudinal variation and thus, by (6a) and (6b) represented a pure westerly wind. This height field is shown below in figure 3.

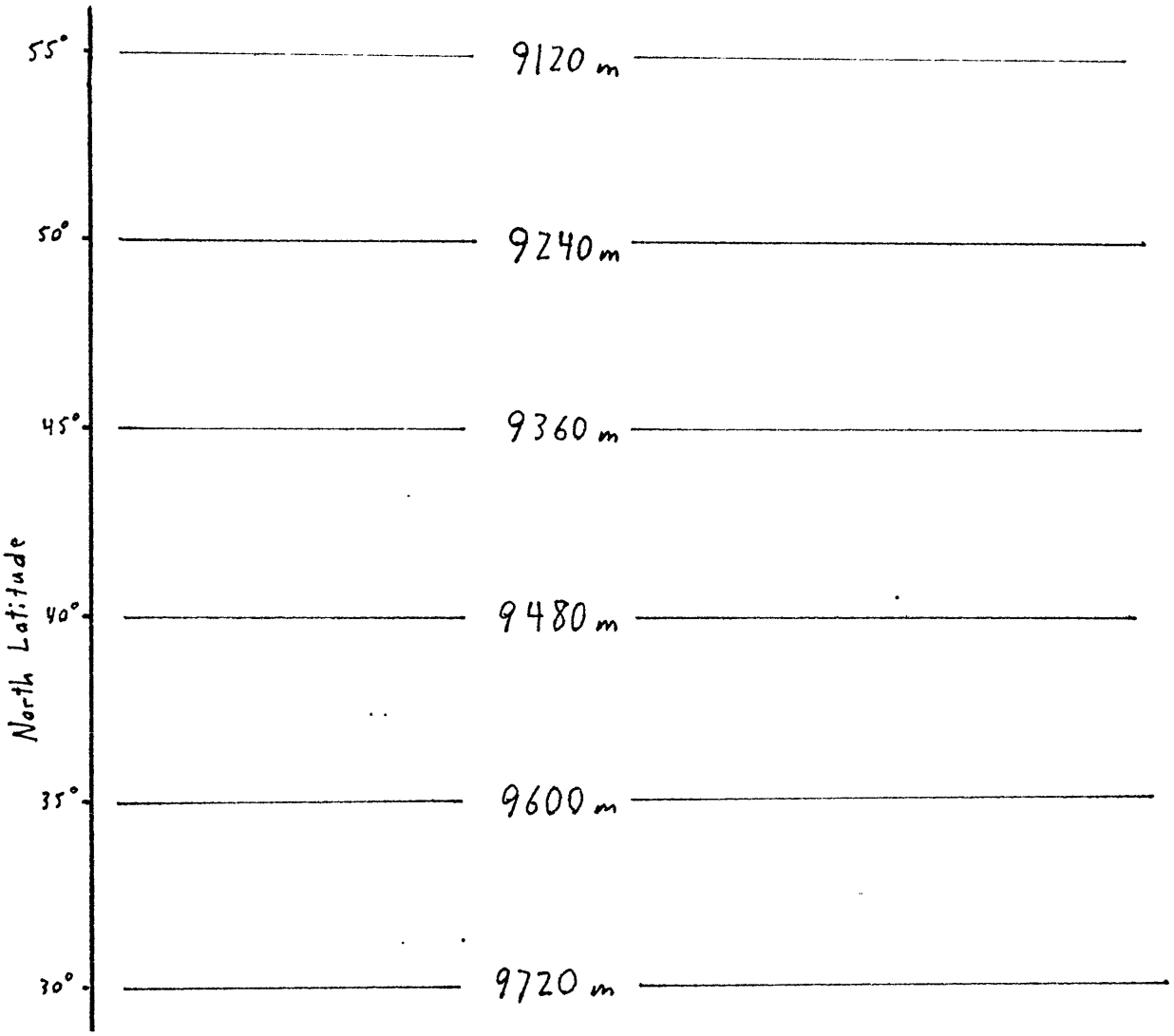

Figure 3: Height field used in the trials

The heights dropped uniformly by 240 m every 10 degrees of latitude. The combination of equations (6b), (9b), and (10) gives

$$u_g = - \frac{1}{2\ om\ \sin(th)\ R_e\ p} \frac{\partial P}{\partial (th)} \qquad (32)$$

which, assuming an ideal gas, reduces to,

$$u_g = - \frac{g}{2\ om\ R_e \sin(th)} \frac{\partial z}{\partial (th)} \qquad (33)$$

This gave a wind speed of u = 14.54/sin(th) m s-1 in the simplified field. In grid units the wind was,

$$U = - \left[\frac{g}{2\ om\ R_e \sin(th)} \right] * \left[\frac{1\ gp}{2\ pi\ R_e \cos(th)(0.5 \text{ degrees}/360 \text{ degrees})} \right] \left[\frac{\partial z}{\partial (th)} \right] \qquad (34)$$

Where gp stands for gridpoint. By substituting actual values for the physical constants in the above equation, the wind velocity was found to be:

$$U = \frac{2.613 \times 10^{-4}}{\sin(th)\ \cos(th)}\ gp\ s\text{-}1 = \frac{1.568 \times 10^{-2}}{\sin(th)\ \cos(th)}\ gp\ tstp\text{-}1 \qquad (35)$$

where tstp indicates timestep.

The wind was not independent of latitude in these coordinates, but the variation was small in the domain under study. In the grid units, the wind reached a minimum, at 45 degrees north longitude, of 5.22×10^{-4} gp s-1 and rose to 6.03×10^{-4} gp s-1 and 5.56×10^{-4} gp s-1 at the southern and northern boundaries of the grid, respectively. In the trials the cloud was initialized at the center latitude of the grid, at latitude 42.5 degrees north. In this region the latitudinal shear of the wind was only of the order of a few percent over several degrees. The longitudinal shear was, of course zero since there was only zonal wind in these trials. The latitudinal variation of the wind is shown below in figure 4 and figure 5.

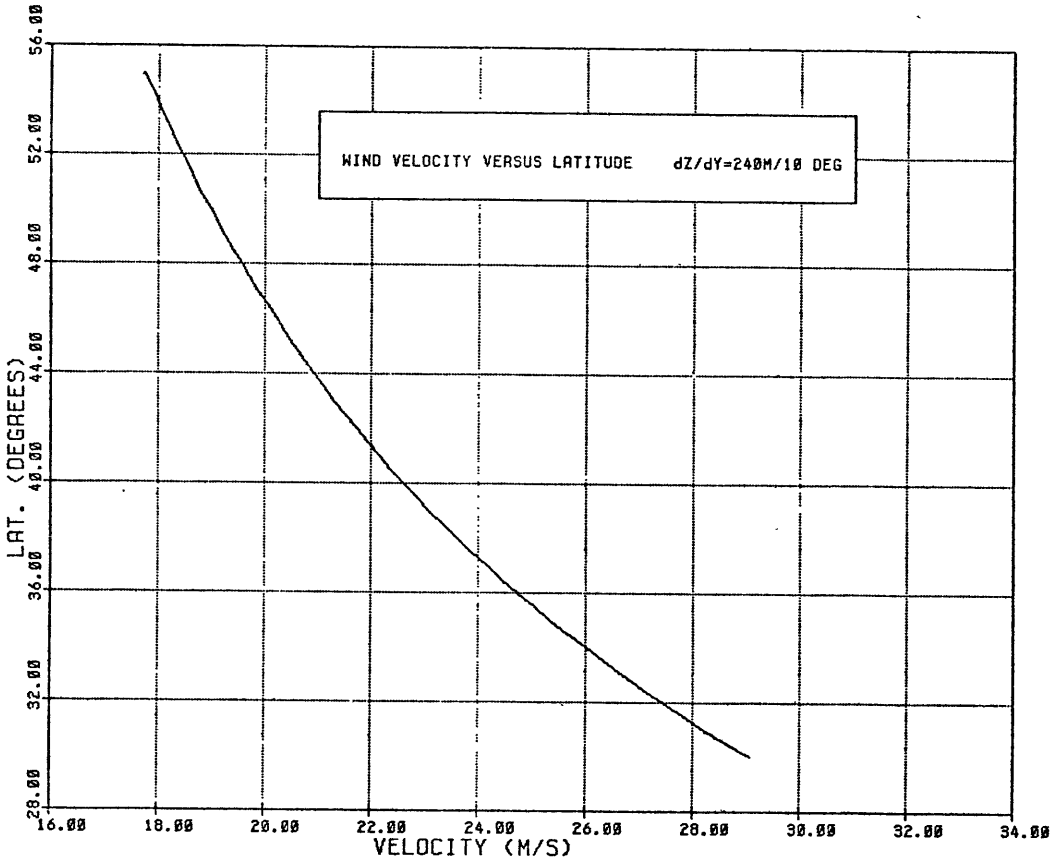

Figure 4: Wind speed versus latitude in m s-1

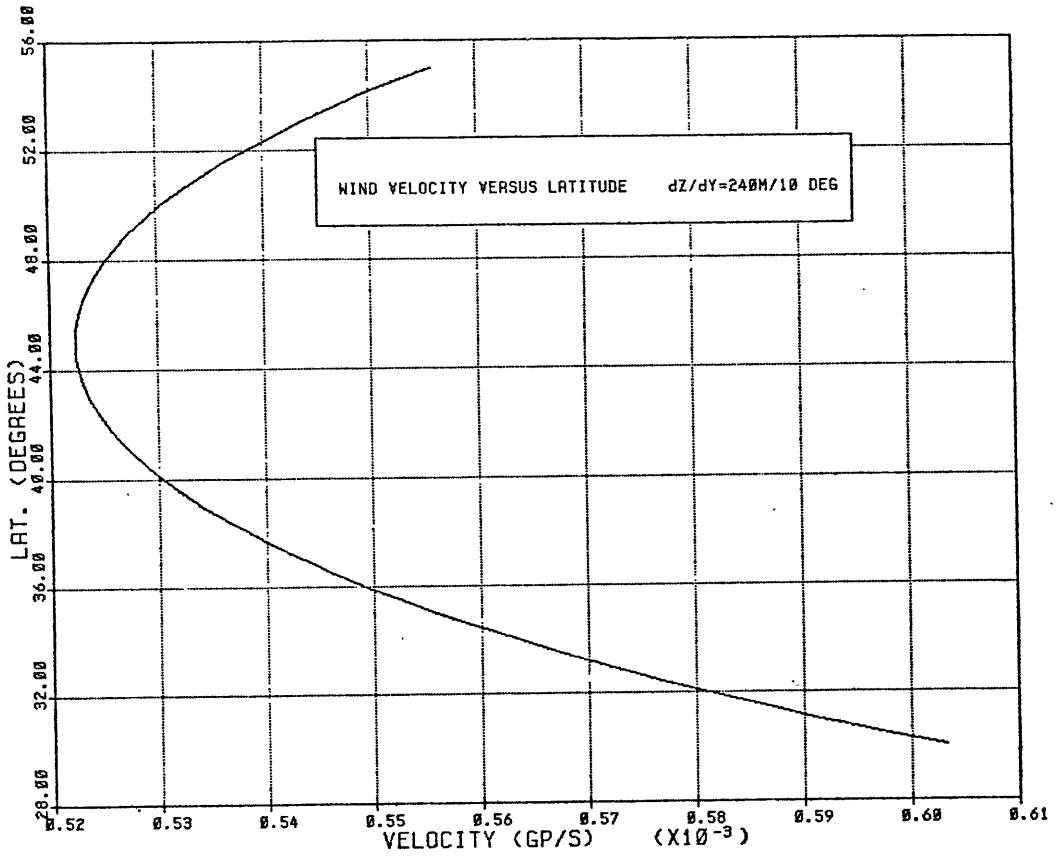

Figure 5: Wind speed versus latitude in gridpoints s-1

Using this simplified wind field a number of trials were run.

B. Individual trials

1. Unsmoothed trials

a. One point initialization

i. Description of initialization

In the first test case, a concentration of 10,000 units was placed in a grid box at a latitude of 42.5 degrees and longitude of 92.5 degrees. The location of the initialization in the model was at gridpoint (76,26) with the longitudinal gridpoint listed first, as will be the convention throughout this paper.

ii. Diagrams of the advection

The resulting model advection is shown in figures 6a through 6g.

0	0	0
0	0	0
0	10000	0
0	0	0
0	0	0

6a. One point initialization unsmoothed: advection pattern at t=0000

0	0	0	0	0
0	0	0	0	0
0	-26	0	26	0
0	-105	10000	105	0
0	-26	0	26	0
0	0	0	0	0
0	0	0	0	0

6b. One point initialization unsmoothed: advection pattern at t=0001

```
                    75
                    |
      0     0     0     0     0     0     0
      0     0     0     0     0     0     0
      0     1   -52    -1    52     1     0
      0     1  -210  9998   210     1     0
25 -  0     1   -52    -1    52     1     0
      0     0     0     0     0     0     0
      0     0     0     0     0     0     0
```

6c. One point initialization unsmoothed:

advection pattern at t=0002

```
                    75
                    |
      0     0     0     0     0     0     0
      0     0     0     0     0     0     0
      0     2   -78    -3    78     2     0
      0     3  -315  9993   315     3     0
25 -  0     2   -78    -3    78     2     0
      0     0     0     0     0     0     0
      0     0     0     0     0     0     0
```

6d. One point initialization unsmoothed:

advection pattern at t=0003

```
                          75
                          |
      0     0     0     0     0     0     0     0     0
      0     0     0     0     0     0     0     0     0
      0     0     2     0    -6     0     2     0     0
      0     0    25  -258   -49   259    25     0     0
      0    -1    55 -1044  9890  1044    55     1     0
25 -  0     0    25  -259   -49   259    25     0     0
      0     0     2     0    -6     0     2     0     0
      0     0     0     0     0     0     0     0     0
```

6e. One point initialization unsmoothed:

advection pattern at t=0010

```
                                75
                                |
      0     0     0     0     0     0     0     0     0     0     0     0     0     0     0
      0     0     0     0     0     0     0     0     0     0     0     0     0     0     0
      0     0     0     0    17   -43   -24    78    24   -43   -17     0     0     0     0
      0     5   -38    89   -94  -166   511   107  -511  -166    94    89    38     5     0
      0    24  -113   359  -811   986   441 -2759  -441   986   811   359   113    24     0
      0    35  -164   580 -1624  3439 -4738  1887  4738  3439  1624   580   164    36     0
25 -  0    25  -116   363  -816   990   448 -2765  -448   990   816   363   116    25     0
      0     6   -39    90   -95  -169   512   108  -512  -169    95    90    39     6     0
      0     0     0     0    18   -44   -26    78    26   -44   -18     0     0     0     0
      0     0     0     0     0     0     0     0     0     0     0     0     0     0     0
      0     0     0     0     0     0     0     0     0     0     0     0     0     0     0
```

6f. One point initialization unsmoothed:

advection pattern at t=0100

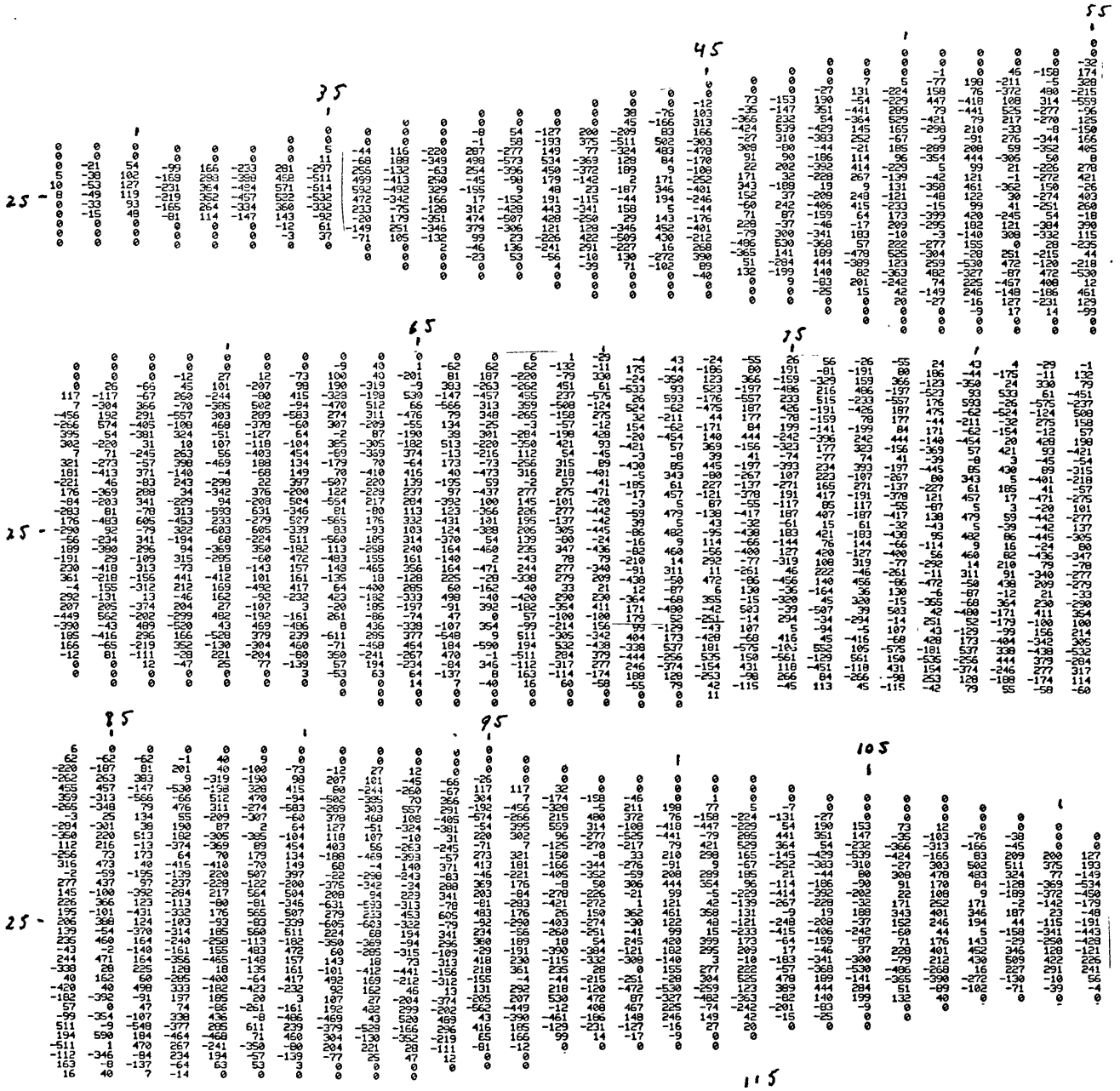

6g. One point initialization unsmoothed:

advection pattern at t=1440

iii. Description of advection

A problem developed immediately at the lee side of the cloud. The model produced a wake of negative concentrations upwind of the original burst of particles. This wake first appeared in timestep 0001. By timestep 0002 the negative wake had grown larger and had expanded to include the gridpoints north and south of the initial burst. In timestep 0002, a positive wake had developed behind the negative one. The positive and negative wakes continued to grow in magnitude and at timestep 0010, another negative wake began to develop behind the trailing positive one. In subsequent timesteps, the wakes continued to grow in a similar fashion. In timestep 0020 the first negative wake had wrapped around to the northeast and southeast of the main cloud. In addition, the first positive wake had begun to wrap around the first negative wake.

The wakes are a serious problem in this model. By timestep 0100 they had begun to dominate the advection. The gridpoints with non-zero concentrations were counted; 54 were in the wake while only 25 were in what appeared to be the real cloud. By timestep 1440, one day after the initial burst, the grid was covered by a confusing field of positive and negative concentrations with a small positive cloud at its front. The peak negative value tended to be found in the first negative wake to the southwest of the positive area. A table comparing

the peak values in the positive area to the peak values in the first lee wake is shown below in table 1.

timestep	largest positive value	maximum first wake value	ratio
0300	1749	-1821	-.96
0900	784	-666 (maximum value in any wake was a +894)	-1.17 (.88)
1200	657	-624 (maximum value in any wake was a +760)	-1.05 (.86)
1440	614	-573 (maximum value in any wake was a -631)	-1.07 (-.97)

Table 1: One point initialization unsmoothed: magnitude of wake and the forward positive area

With this single gridpoint initialization, the absolute value of the concentrations remained perfectly symmetrical about the starting latitude. The only difference between the upwind and downwind concentrations was the region of purely positive concentration at the front of the concentration distribution.

The cloud was not perfectly symmetrical about an east-west axis. Although in the early timesteps the cloud was nearly symmetrical about this axis, much of the symmetry was eventually lost. This was not unexpected since the gridpoint area and the wind were not latitude independent. These wakes appear quite similar, qualitatively, to the wakes found in the

advection study by Orzag (1971) and illustrated in figure 1.

iv. Cross-sections

Cross sections of the concentrations along a latitudinal line through the initialization latitude (42.5 degrees north or grid level (x,26)) are shown below in figures 7a through 7g for selected timesteps. These show the process of wake development along the axis of movement of the cloud.

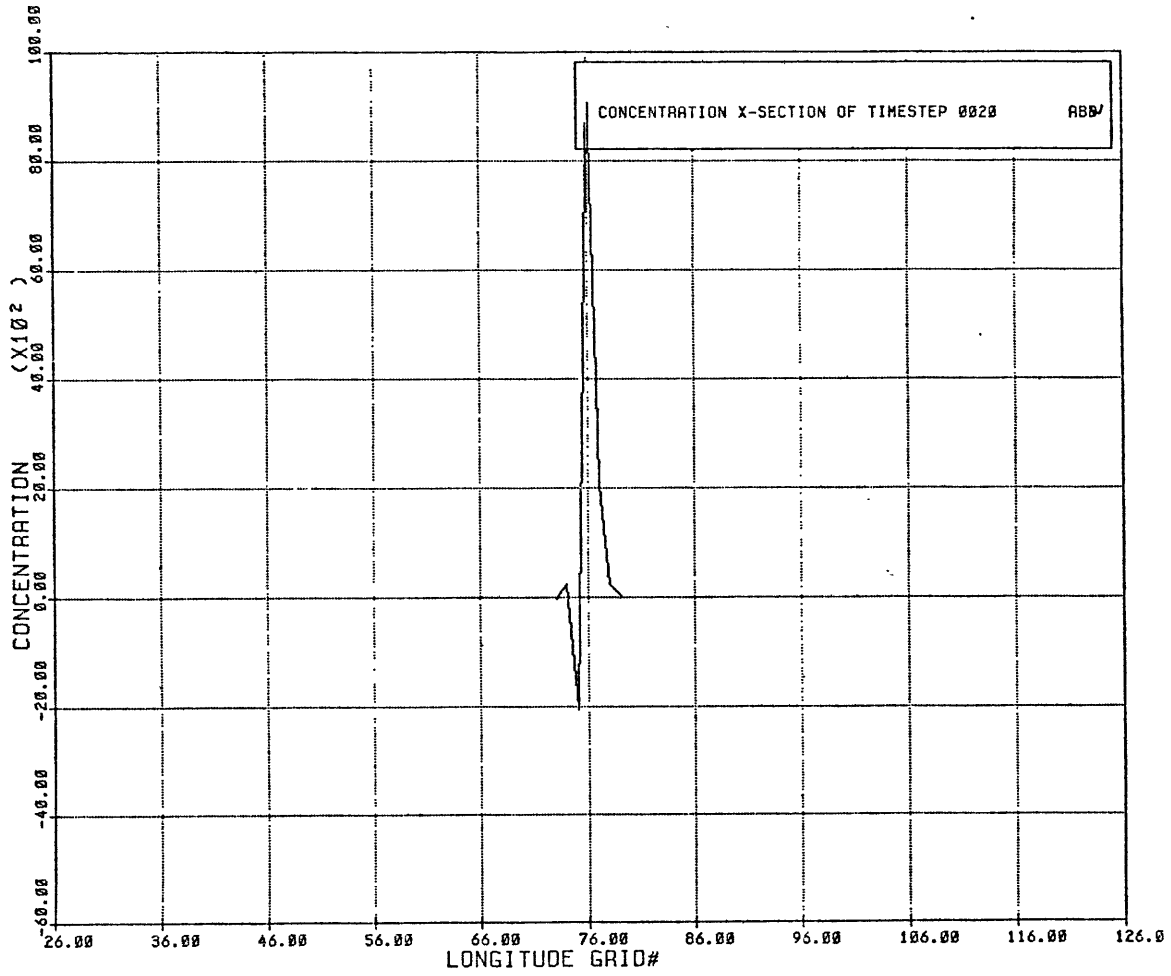

7a. One point initialization unsmoothed:

cross-section at t=0020

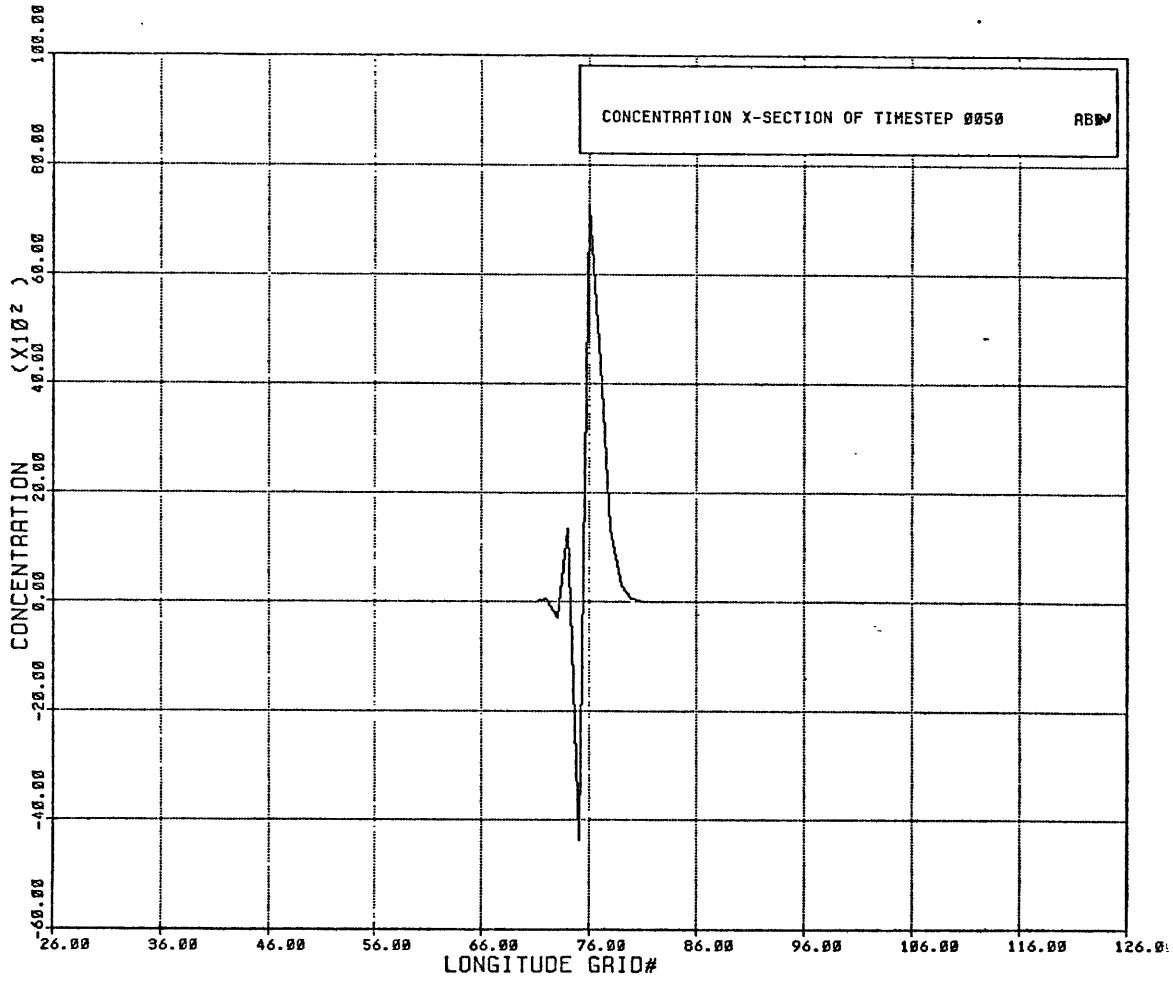

7b. One point initialization unsmoothed:

cross-section at t=0050

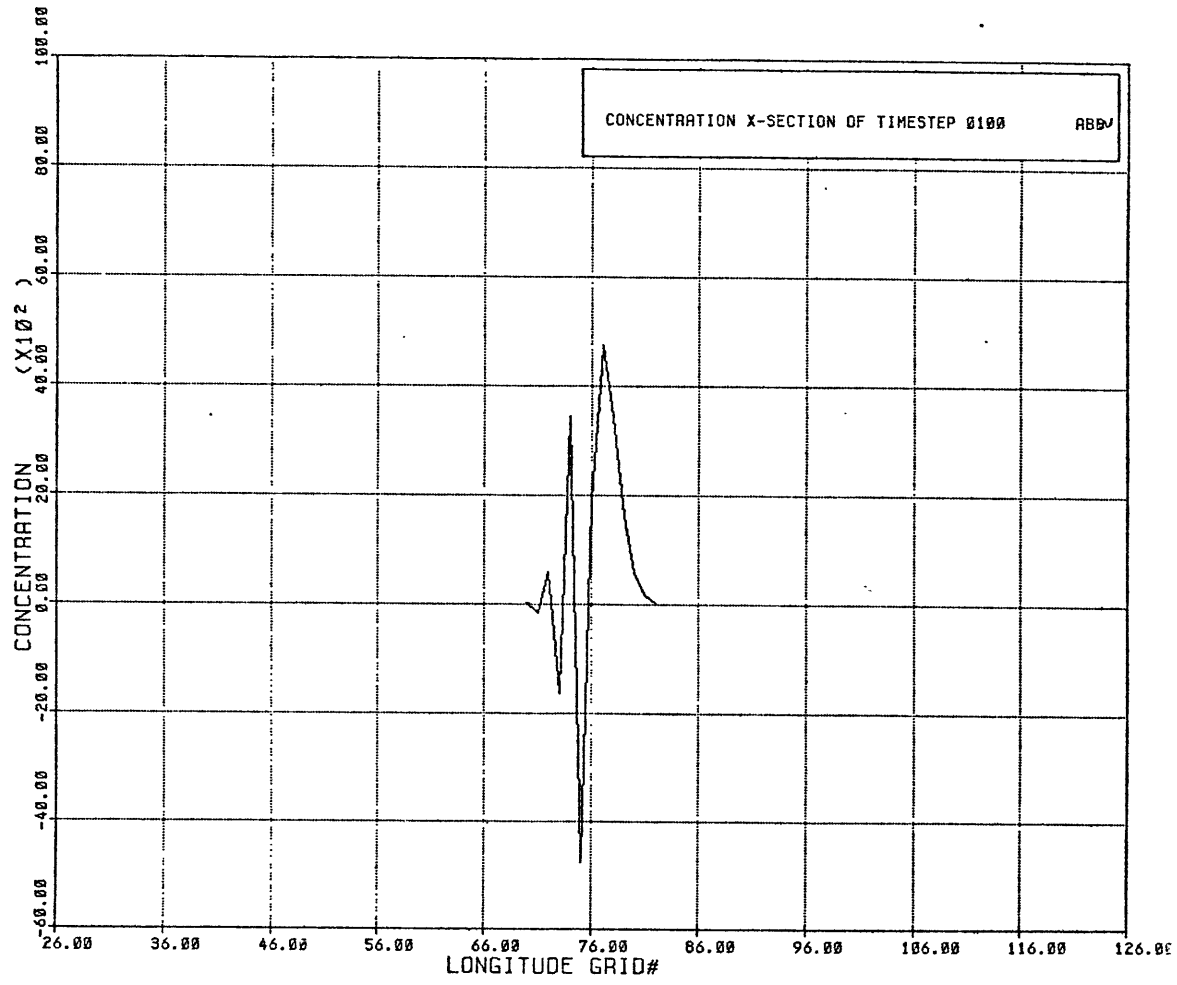

7c. One point initialization unsmoothed:

cross-section at t=0100

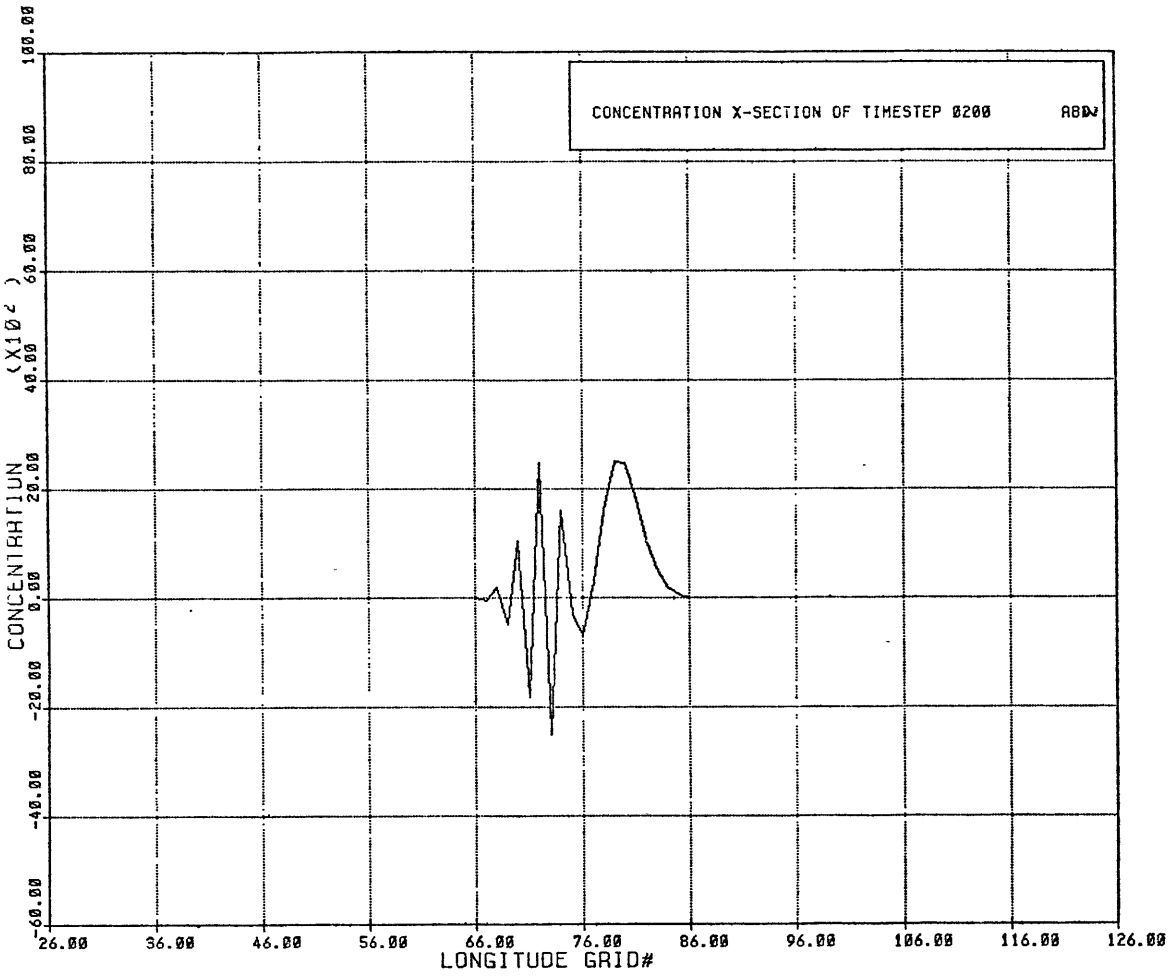

7d. One point initialization unsmoothed:

cross-section at t=0200

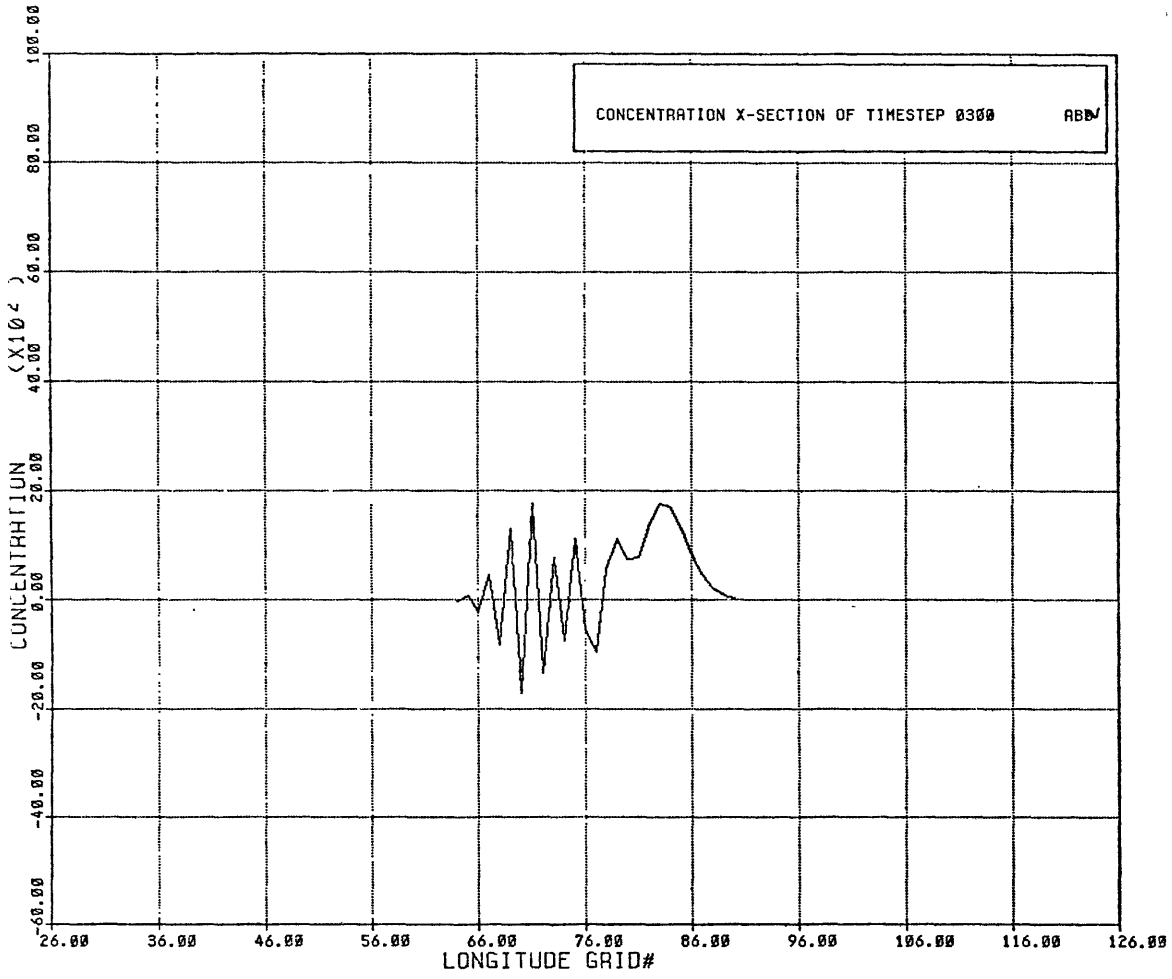

7e. One point initialization unsmoothed:

cross-section at t=0300

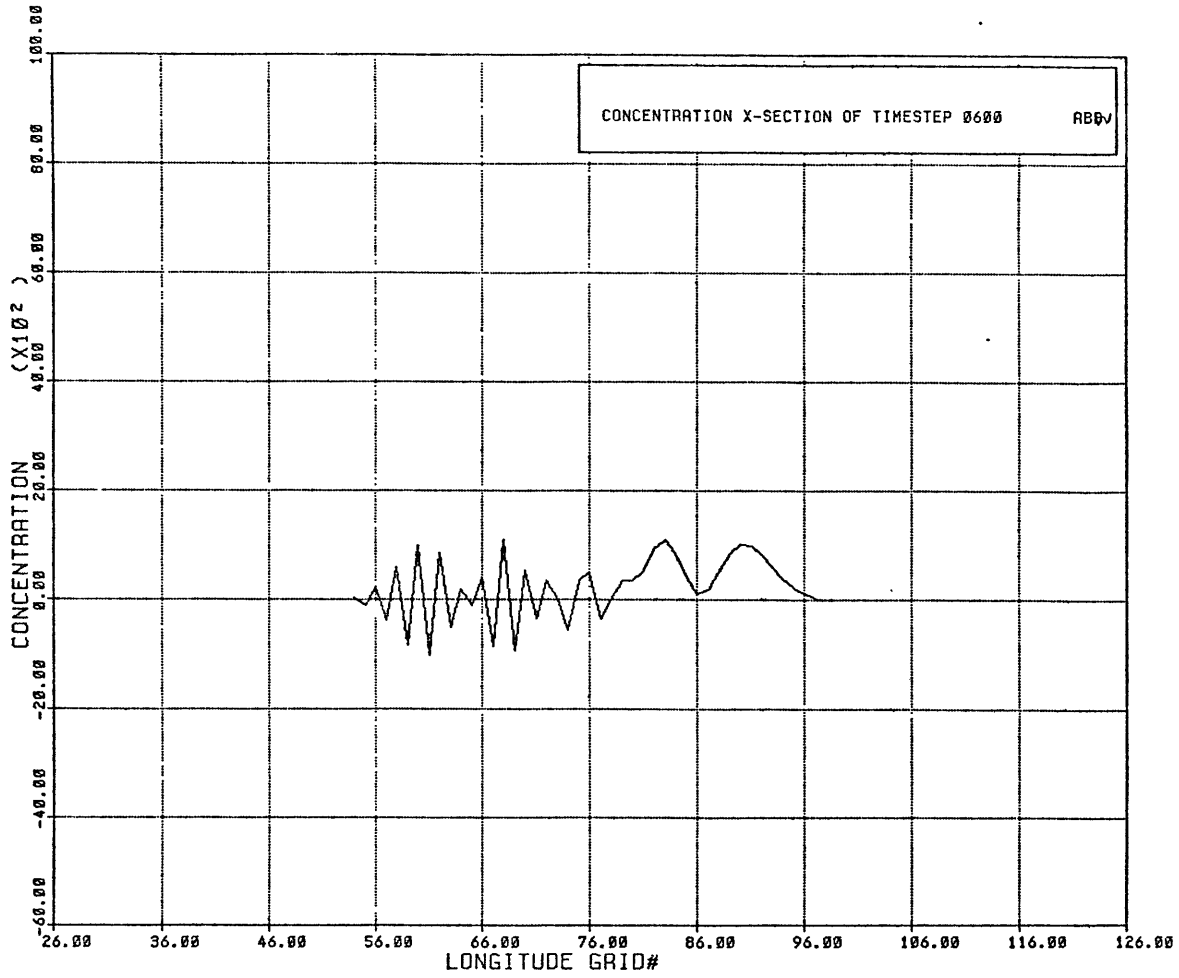

7f. One point initialization unsmoothed:

cross-section at t=0600

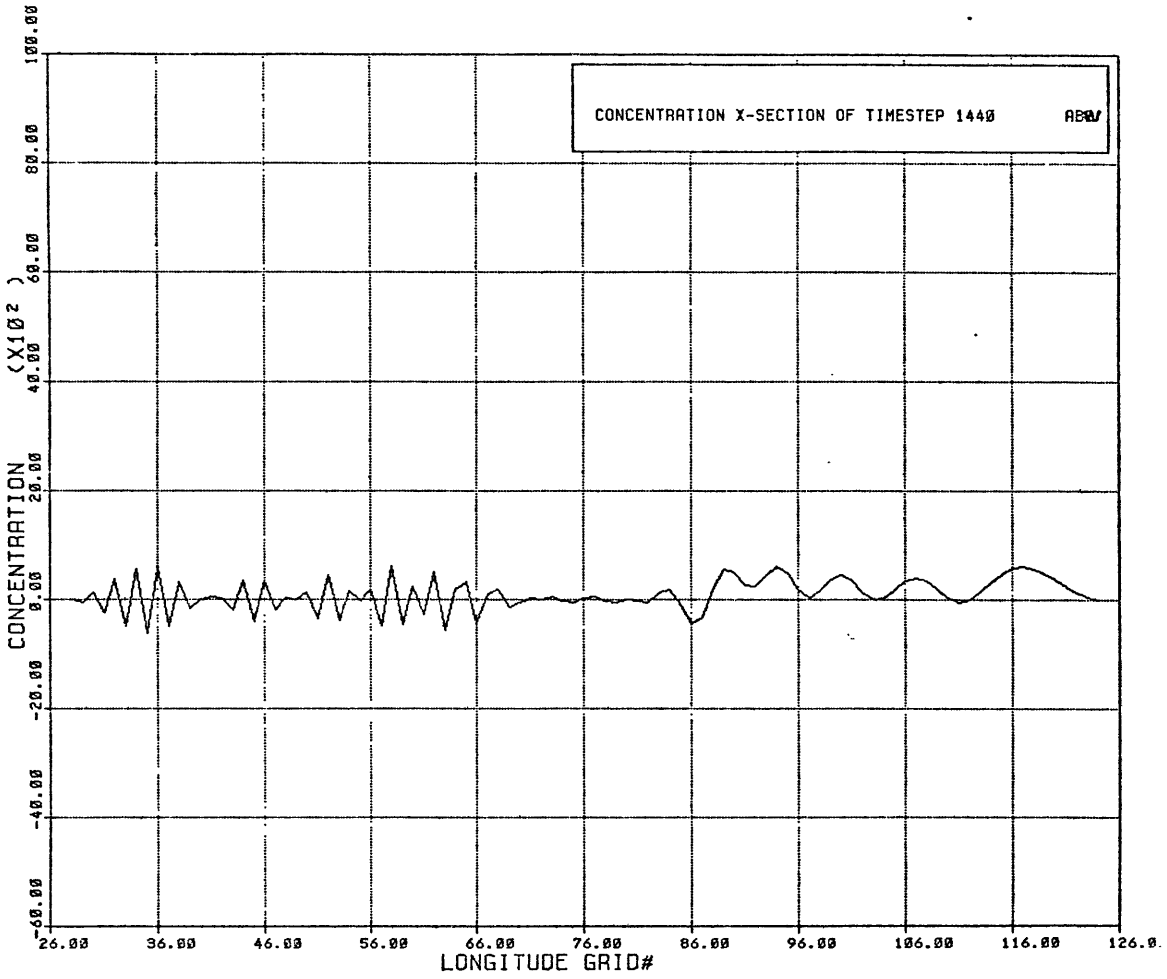

7g. One point initialization unsmoothed:

cross-section at t=1440

The graphs show the continued growth, in number and in magnitude, of the wakes. Also shown is the decrease in the peak magnitude in the forward area caused by numerical diffusion in the model.

In early timesteps, the wake was small compared to the peak positive concentration. But this was only because the peak concentration had not yet moved from its initial grid location. As soon as the cloud began to drift significantly from its starting location, the wake values became comparable and even larger than the peak values in the forward positive area. The wakes in the early timesteps were rapidly varying in the longitudinal direction. But, by timestep 0300, an interesting phenomenon occurred. The cloud began to develop a large wake to the immediate rear of the forward positive area that had a great longitudinal extent. This process continued, and by timestep 1440, a train of long period smooth wakes trailed the forward area and separated it from the rapid oscillations that were still present at the rear of the cloud. The process responsible for this smooth wake shedding was probably a reduction of the gradients in the cloud by the diffusion inherent to the finite difference approximations that were made in the numerical scheme. The model apparently reduced the gradients around the positive area over a long period of time and thus slowed the wake forming process. This may have made the pattern look more pleasing, but it did not reduce the problem introduced by the wakes. In the later

timesteps, the smooth wakes became mostly positive and comparable in magnitude to the forward area. Thus the actual boundaries of the "real" cloud were difficult to ascertain.

v. Mass in the forward positive area

It was tempting to try to interpret the forward positive area as the actual cloud and the wakes as just a spurious byproduct of the Arakawa scheme. However, this interpretation was not justified. The number of particles in the positive area grew quickly to significantly more particles than the initial burst. The table below shows the sum of the values of the concentrations in the positive area grid boxes at selected timesteps.

timestep	sum of concentrations	percentage over t=0000
0	10000	0
1	10288	3
2	10315	3
100	17527	18
1000	15918	16
1440	14532	15

Table 2: One point initialization unsmoothed:
excess concentration in the forward positive area

The mass of the entire distribution of concentrations, including the wakes, was conserved to within a few percent (see section vii). This indicates that the mass in the wakes, in the later timesteps, while nearly adding to zero, must have had a negative component representing about one half the mass of the cloud.

The sum of concentrations shown above is not area weighted and thus is not exactly a conservation of mass indicator. However, in a cloud of small north-south extent, the sum of concentrations should be closely conserved. With perfect mass conservation, the change in the sum of concentrations in a cloud that moved from 45 degrees north to 40 degrees north latitude only be minus eight percent. The concentrations would drop because the area of the grid boxes would increase but the number of particles would remain constant. The number of particles did not remain constant if the positive area was interpreted as the "real" cloud.

It is notable that, despite the fact that there were thousands of grid points filled with wake particles, the alternating positive and negative wakes did, almost, add to zero. This was evident because the model conserves mass to within 20 percent (see discussion below) and the positive region's sum of concentrations did not differ drastically from the initialization value of 10000 units of concentration.

vi. Velocity of forward positive area

Another difficulty with interpreting the positive area as the actual cloud was its velocity. At 42.5 degrees north latitude the winds should carry particles at 0.03147 gridpoints per timestep. At this speed, the cloud should have been located at gridpoint (79.1,26) by timestep 0100. By inspection, it was obvious that the bulk of the region of positive concentration was far upwind of gridpoint (79,26) at that time. By timestep 1000 the cloud should have been at gridpoint (107.5,26). It was clear again that the region of positive concentration lagged behind this location.

The wakes did have significance in the advection speed of the cloud. If the model advected the cloud at exactly the wind speed, then the centroid of the cloud would always have been at gridpoint (76+.03147*T,26)(see figure 5). If the wakes were included in a calculation of the centroid of the cloud, then the centroid did move at the predicted velocity of the cloud. For example, at timestep 0001 the centroid of the positive area was at gridpoint (76.0155,26). But the centroid of the entire cloud, including the wake, was close to the predicted gridpoint, at (76.0314,26).

vii. Conservation of mass

The Arakawa scheme should conserve both the area weighted sum of the concentrations at all gridpoints and the area-weighted sum of the squares of the concentrations at all gridpoints. The first is just a conservation of mass criteria and the model did fairly well. Truncation error was the likely cause of the drift from perfect conservation. The model lost about one fifth of the particles by timestep 1200 but began to regain them by timestep 1600. Though the loss of particles appears systematic, it is possible that the first 1600 timesteps are just representative of the first portion of a random walk about pure conservation. The version of the program that performed this particular trial was lost and it is not known whether it used truncation rounding or nearest integer rounding in its integer arithmetic. A graph of the time history of the mass of the cloud is shown below in figure 8.

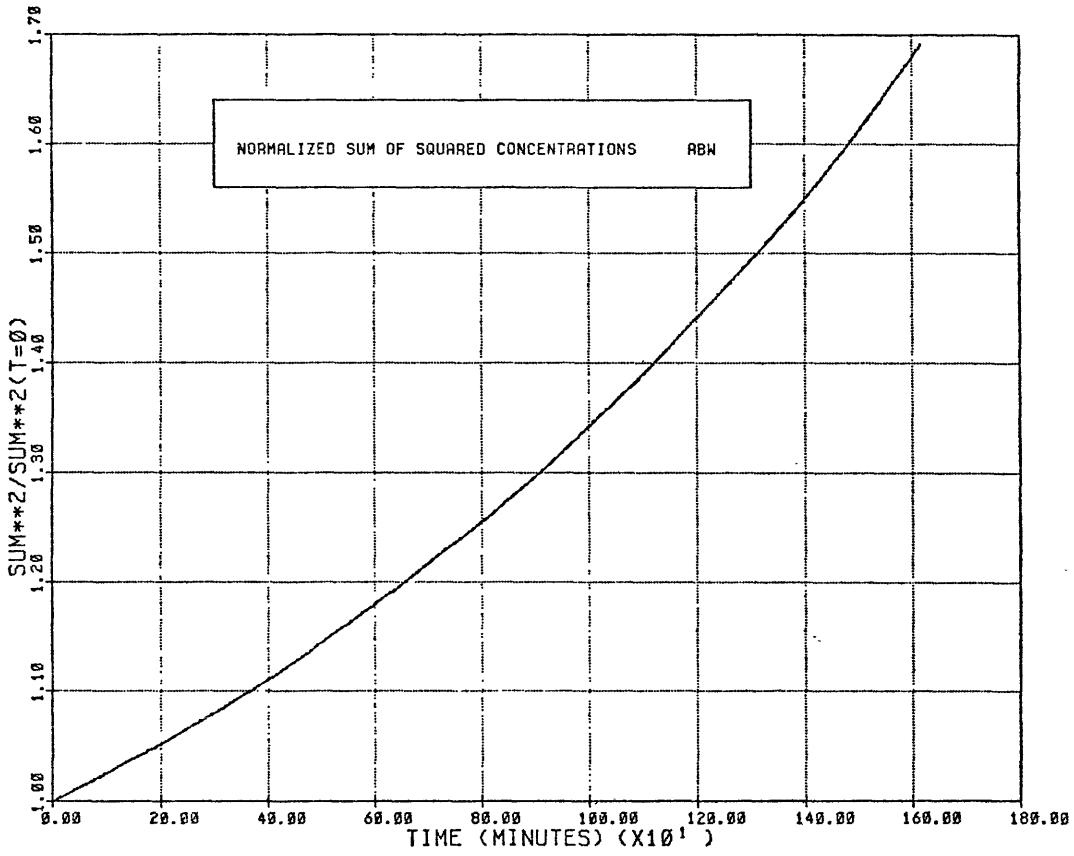

Figure 8: One point initialization unsmoothed: normalized mass

viii. Conservation of squared mass

The sum of the area weighted squares of concentrations presented more of a problem. This quantity grew smoothly and systematically to a value that was 69 percent higher than its initialization value. This monotonic growth cannot be explained by arithmetic truncation error and its origin was rooted in spurious numerical diffusion. The mechanism responsible for this growth is discussed in detail in section IV.B.2.a.vii. Very roughly, diffusion of totally positive quantities would result in a decrease in this quantity. When negative values are produced by diffusion into the wakes, however, the sum of the squares of the masses may go up while the sum of the masses is conserved. While the increase of 69 percent that occurred over the first day of advection was not desirable, it represents an increase of only .05 percent per timestep. A graph showing the time history of the sum of the squares of the area weighted concentrations is shown below in figure 9.

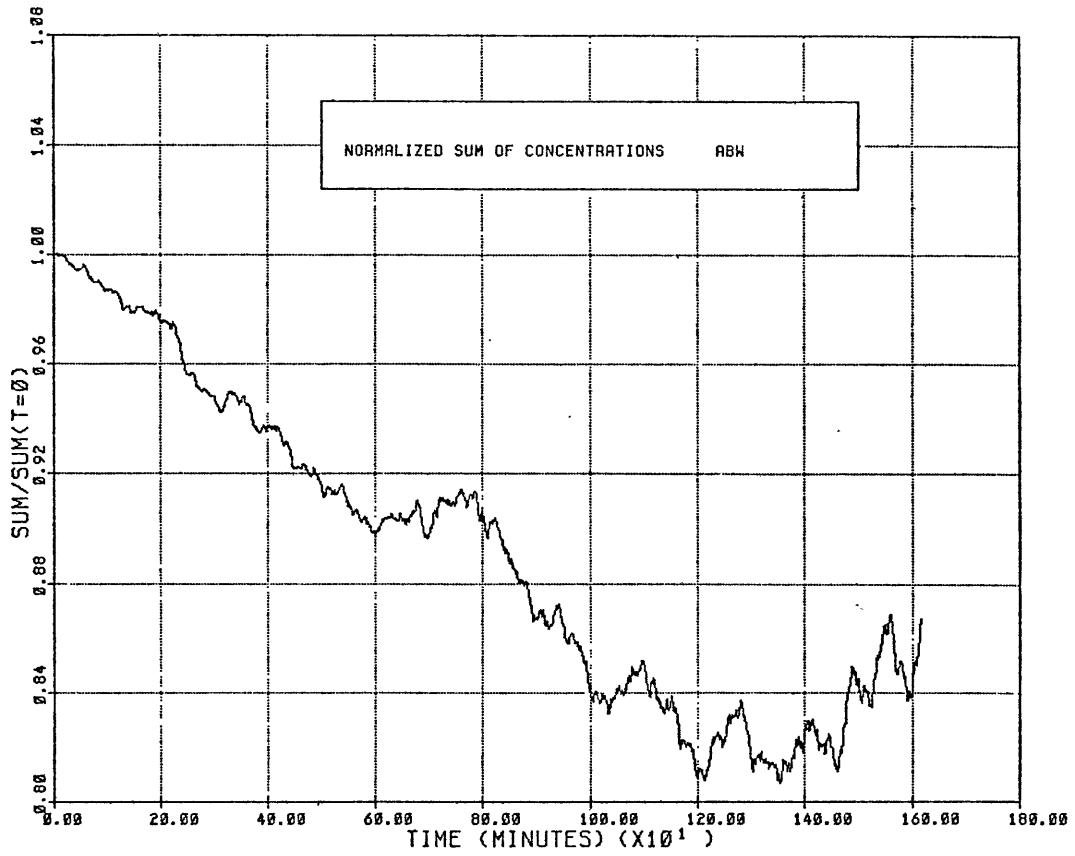

Figure 9: One point initialization:
normalized mass squared

ix. Discussion

The wakes make this model clearly unsatisfactory for calculating advection with the one gridpoint initialization. This failure stems from the errors introduced by the strong gradients of concentration that were present at the initialized gridpoint. Since the model produced alternating positive and negative wakes, the gradients were only slowly reduced. Thus, the wakes continued to grow to the rear of the cloud. The only reduction in wake frequency arose after a large number of iterations had reduced the gradients by numerical diffusion. Even this did not reduce the amplitude of the wakes; the only reduction was in their frequency.

b. Nine point initialization

i. Description of initialization

In order to reduce the wake by reducing the gradients of concentration, a multi-point initialization was attempted. In this initialization, a three by three gridpoint region was initialized with 1111 units of concentration in each gridpoint. The center of the area was, again, at 42.5 degrees north latitude and 92.5 west longitude, or at gridpoint (76,26).

ii. Diagrams of advection

The results of the advection are shown below in figures 10a through 10f.

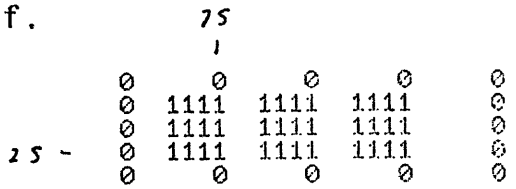

10a. Nine point initialization unsmoothed:

advection pattern at t=0000

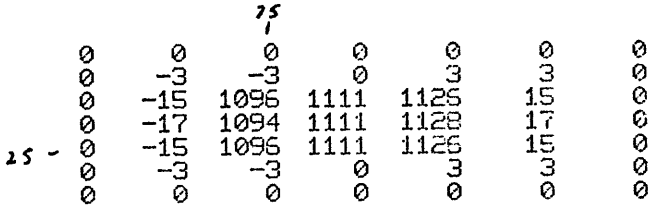

10b. Nine point initialization unsmoothed:

advection pattern at t=0001

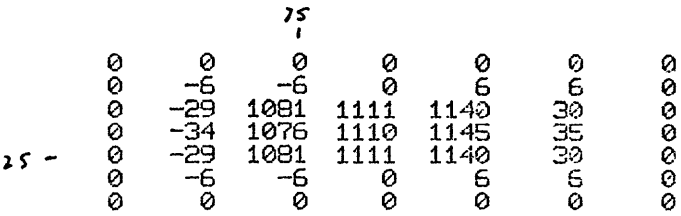

10c. Nine point initialization unsmoothed:

advection pattern at t=0002

75

0	0	0	0	0	0	0	0	0
0	0	-9	-9	0	9	9	0	0
0	0	-43	1066	1110	1154	43	0	0
0	1	-51	1058	1102	1152	50	1	0
25- 0	0	-43	1066	1110	1154	43	0	0
0	0	-9	-9	0	9	9	0	0
0	0	0	0	0	0	0	0	0

10d. Nine point initialization unsmoothed:

advection pattern at t=0003

75

0	0	0	0	0	0	0	0	0
0	0	0	0	0	0	0	0	0
0	2	-26	-30	-6	26	30	2	0
0	9	-135	957	1093	1246	155	10	0
0	11	-162	927	1086	1272	185	12	0
25- 0	9	-136	956	1093	1246	155	10	0
0	2	-26	-30	-6	26	30	3	0
0	0	0	0	0	0	0	0	0
0	0	0	0	0	0	0	0	0

10e. Nine point initialization unsmoothed:

advection pattern at t=0010

75

0	0	0	0	0	0	0	0	0	0	0	0	0	0
0	0	0	0	0	0	0	0	0	0	0	0	0	0
0	0	0	-10	17	41	26	-56	-64	-8	0	0	0	0
-6	37	-66	37	95	-98	-286	-301	83	245	173	71	19	0
-24	83	-191	312	-224	-32	-83	812	1174	869	433	160	43	4
-30	110	-259	385	-190	-224	-404	624	1388	1106	552	201	54	8
25- -24	86	-198	312	-223	-35	-90	806	1173	872	436	162	44	5
-6	37	-66	35	96	-97	-289	-305	81	246	175	73	19	0
0	0	0	-12	18	43	27	-56	-64	-9	0	0	0	0
0	0	0	0	0	0	0	0	0	0	0	0	0	0
0	0	0	0	0	0	0	0	0	0	0	0	0	0

10f. Nine point initialization unsmoothed:

advection pattern at t=0100

iii. Description of advection

The wakes, as expected, developed more slowly. The first negative wake developed immediately, but it took until timestep 0003 until the first positive wake developed. Even at timestep 0100 the initial cloud area still dominated the concentration pattern. However, the wakes were still a serious problem. At timestep 0100 the number of grid boxes occupied with wake was 51, compared with 31 occupied by the leading positive area. This was better than the one point start, but was still unsatisfactory. By timestep 1000 the grid was filled with a huge array of positive and negative wakes trailing a small positive region.

The wakes near the front of the cloud eventually became smoothly varying and of a longer period than the rapid early oscillations. The ratio of the highest wake value to the highest forward peak value is shown to decrease to near unity in the table below. The highest wake value was not found on the axis chosen for the cross sectional graphs and thus the table indicates, perhaps more realistically than the cross sections, the scale of the wake problem.

timestep	largest forward positive value	maximum wake value	ratio
0000	1111	no wake	N.A.
0001	1128	-17	-66.4
0002	1145	-34	-33.7
0010	1272	-162	-7.9
0050	1483	-464	-3.2
0100	1388	-404	-3.4
0300	1075	-628	-1.7
0600	772	-489	-1.6
0900	612	-430	-1.4
1200	561	-421	-1.3
1440	533	-400	-1.3

Table 3: Nine point initialization unsmoothed: magnitudes of wake and the forward positive area

The symmetry that was present in the one point initialization was not evident here. The values in the windward side of the cloud tended to be larger in absolute value. The largest values of concentrations (positive or negative) were always found in the forward positive area, and were, of course, positive. There was not a mirror image of high alternating positive and negative values at the rear.

iv. Cross-sections

Cross sections through the cloud at selected timesteps are shown below in figures 11a through 11f.

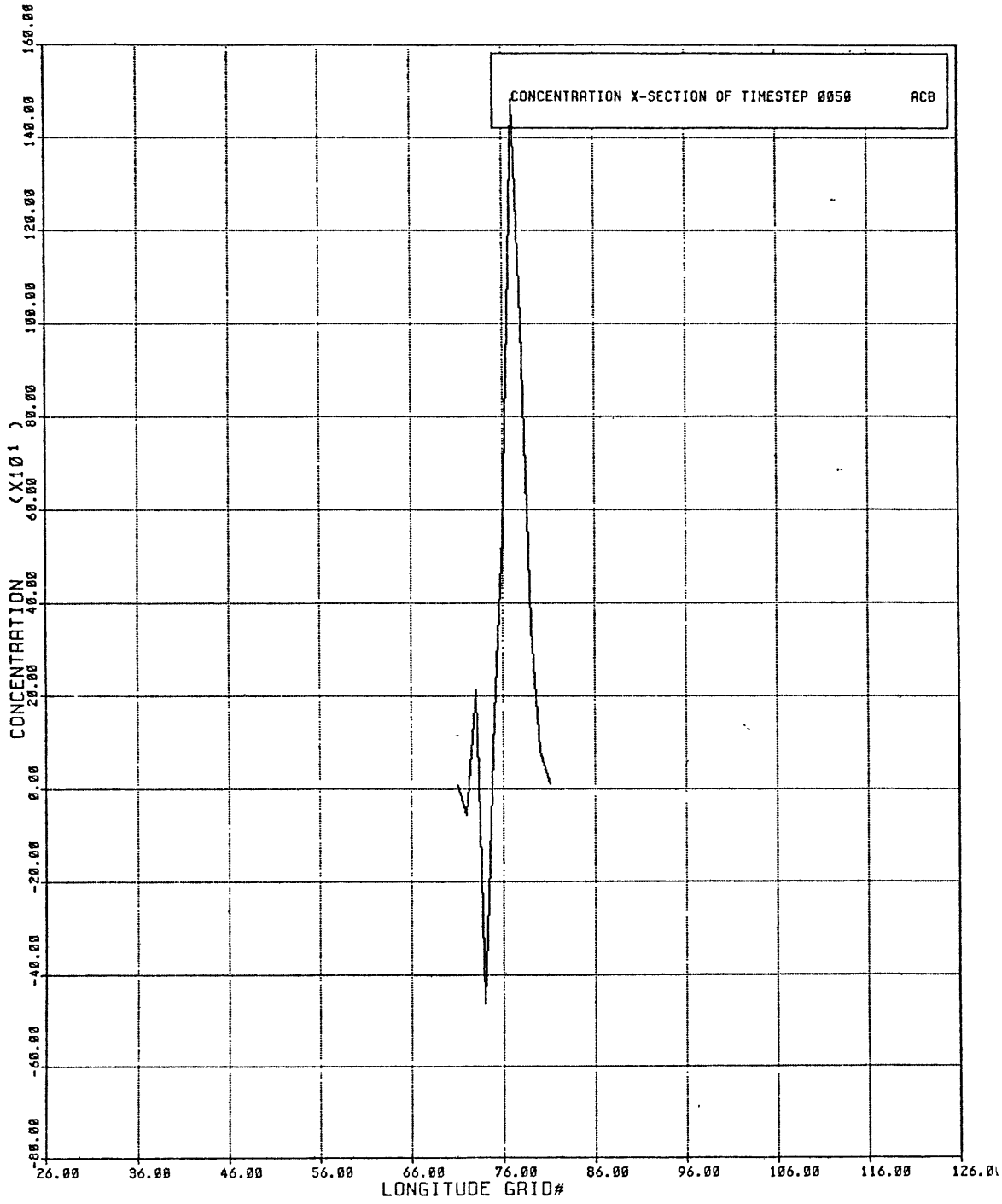

11a. Nine point initialization unsmoothed:

cross-section at t=0050

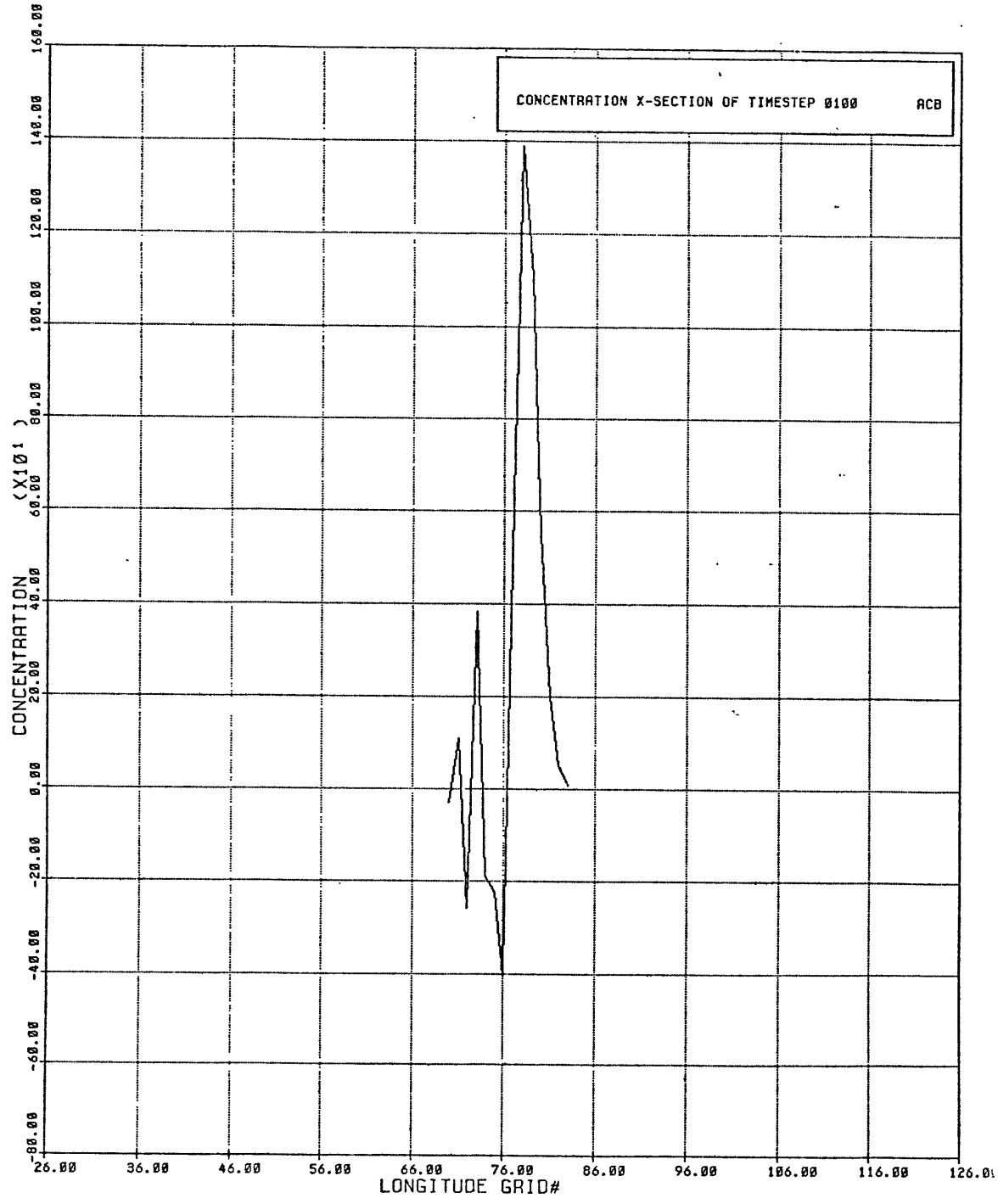

11b. Nine point initialization unsmoothed:

cross-section at t=0100

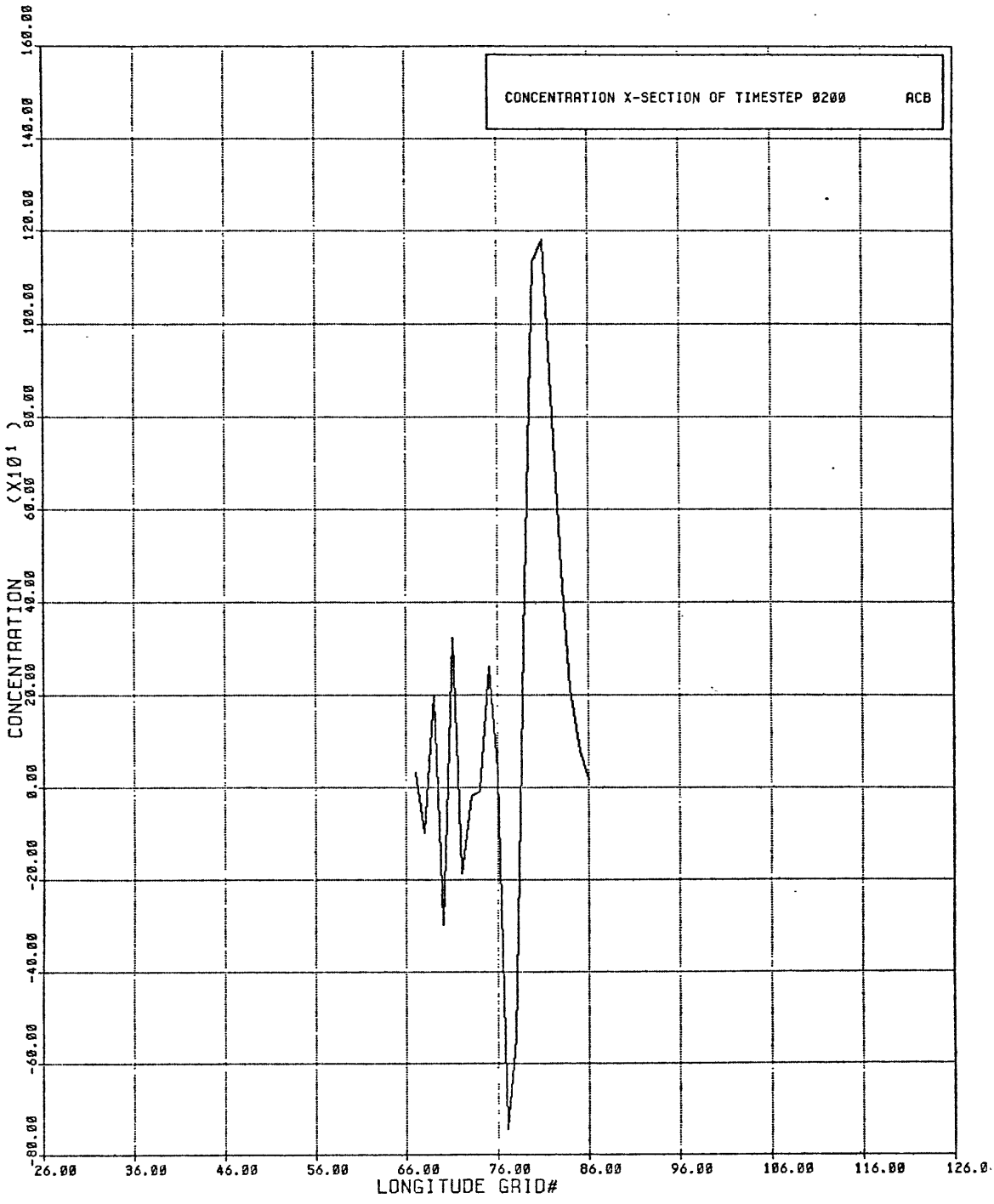

11c. Nine point initialization unsmoothed:

cross-section at t=0200

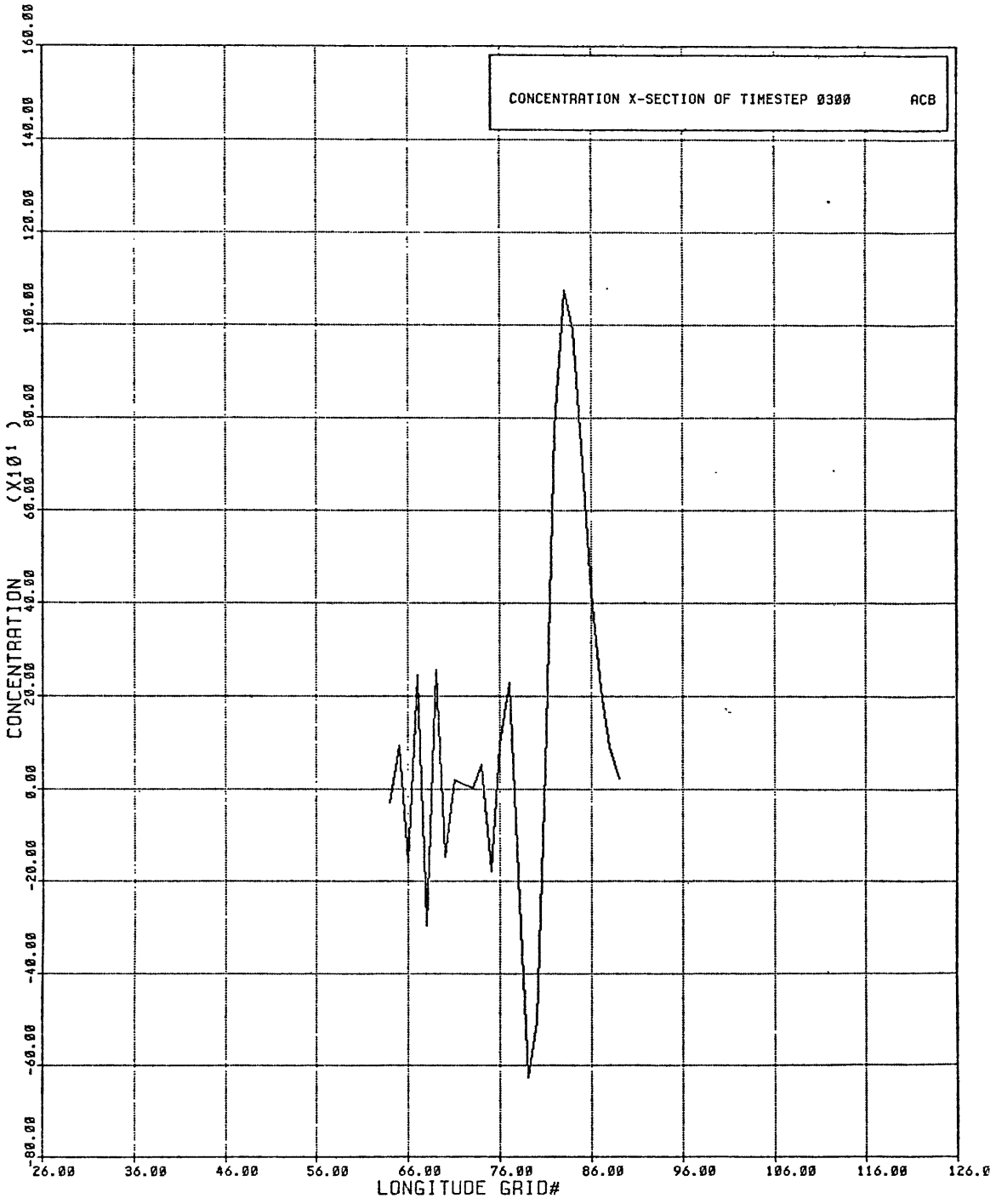

11d. Nine point initialization unsmoothed:

cross-section at t=0300

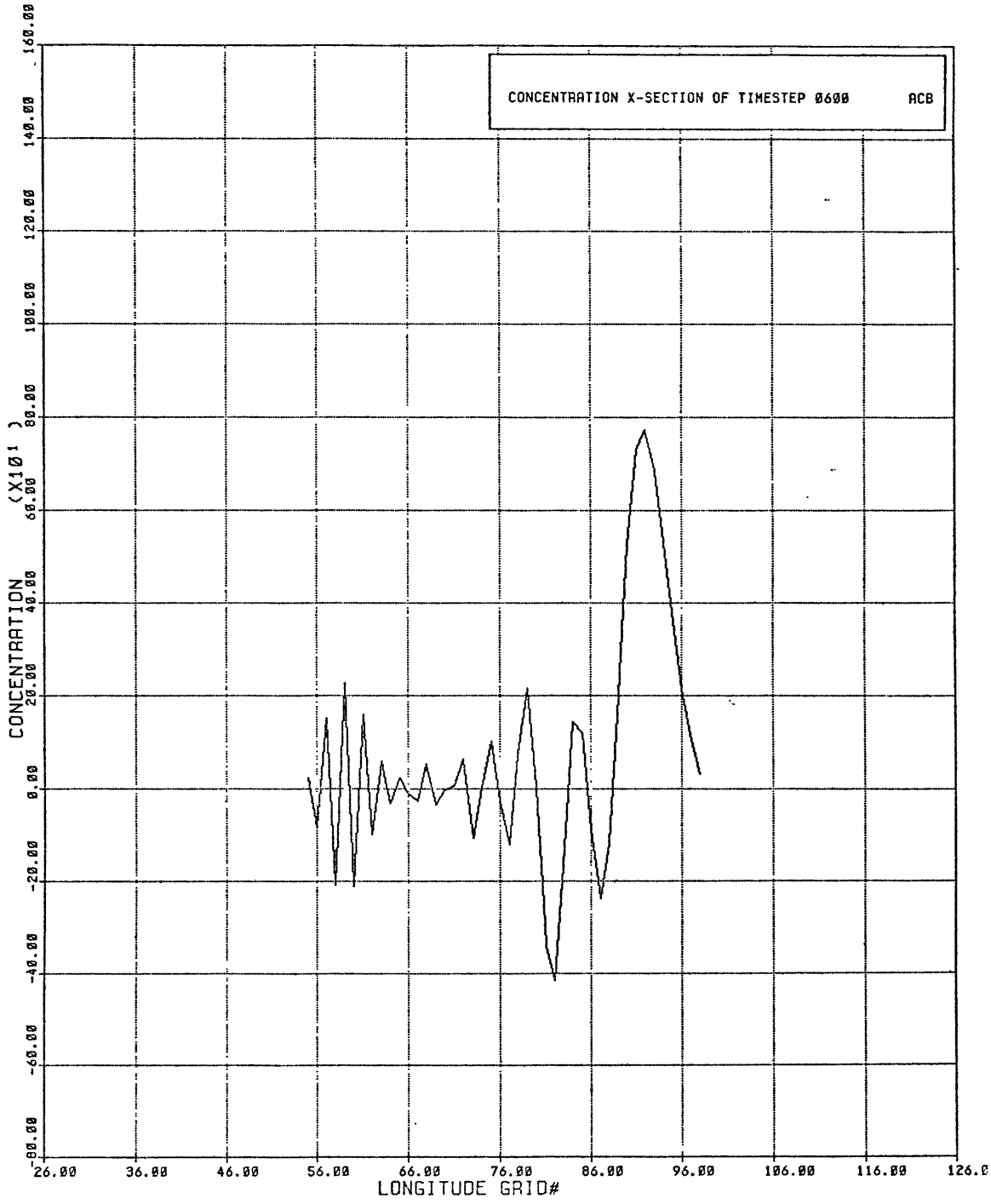

11e. Nine point initialization unsmoothed:

cross-section at t=0600

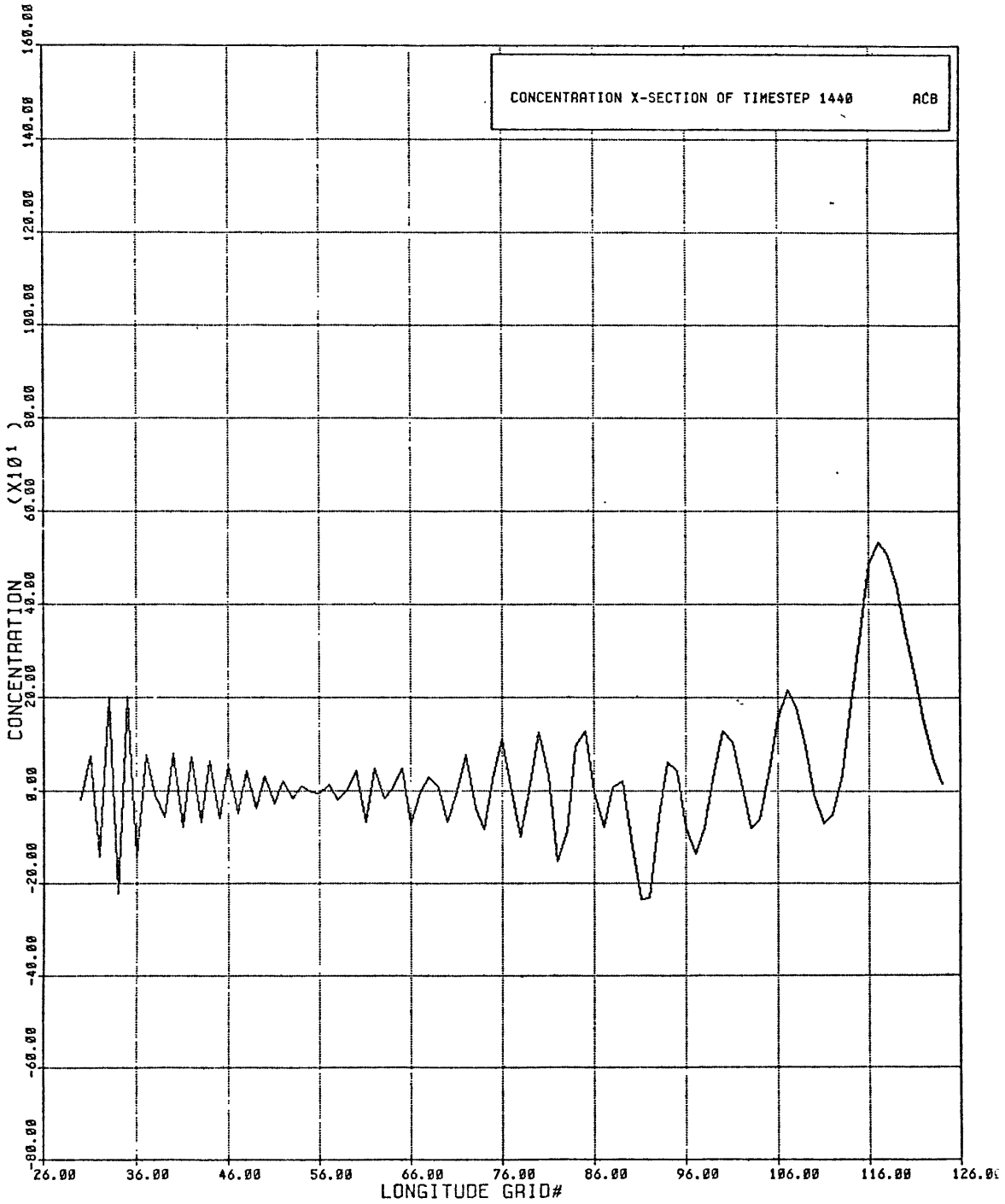

11f. Nine point initialization unsmoothed:

cross-section at t=1440

These cross sections indicate better results than were indicated in the one point initialization. The forward peak was the dominant feature throughout the first day of advection. Towards the end of one day, however, the wakes were growing relative to the forward peak. As with the one point initialization, the model seemed to have reduced the destablizing gradients, somewhat, by the later timesteps.

v. Mass of forward positive area

With this initialization, the positive area became slightly more like what was expected of a "real" cloud of particles. As discussed above, it was the dominant feature in terms of the magnitude of its concentrations. But, there were still problems with this interpretation. As in the previous case, the region contained too much concentration. A chart of the sum of the concentrations is shown below in table 4.

timestep	sum of concentrations	percent over t=0000
0	10000	0.0
1	10058	0.6
2	10114	1
10	10520	5
100	12111	12
500	14181	14
1000	14391	14
1440	14155	14

Table 4: Nine point initialization unsmoothed: excess concentration in the forward positive area

The magnitude of the excess was a bit smaller than that of the one point initialization, but it was still very large. It should be noted again that the sum of the concentrations was not area weighted and is thus not a perfect measure of conservation of mass.

vi. Velocity of the forward positive area

The velocity of the positive region was closer to that expected of an actual cloud. The centroid of the positive region at timestep 0001 was at gridpoint (76.0202,26) which was closer to the desired gridpoint, (76.03147,26) than than

in the one point initialization. The location of the highest concentrations at timestep 0100 was at gridpoint (78,26) which was near the predicted gridpoint (79.1,26), and at timestep 1000 the peak concentration was at gridpoint (104,26). This means that the positive region only lagged behind the predicted position by about ten percent in the later timesteps.

vii. Conservation of mass

The area-weighted sum of the concentrations was much more closely conserved in this trial. The maximum deviation was only about 5 percent. The model, in this case, did not preferentially lose particles, but seemed to waver back and forth around approximate conservation of mass. Nearest integer rounding was used in the integer arithmetic in this trial. The variation here was consistent with a random walk about perfect conservation. The time history of the sum of the area weighted concentrations is shown below in figure 12.

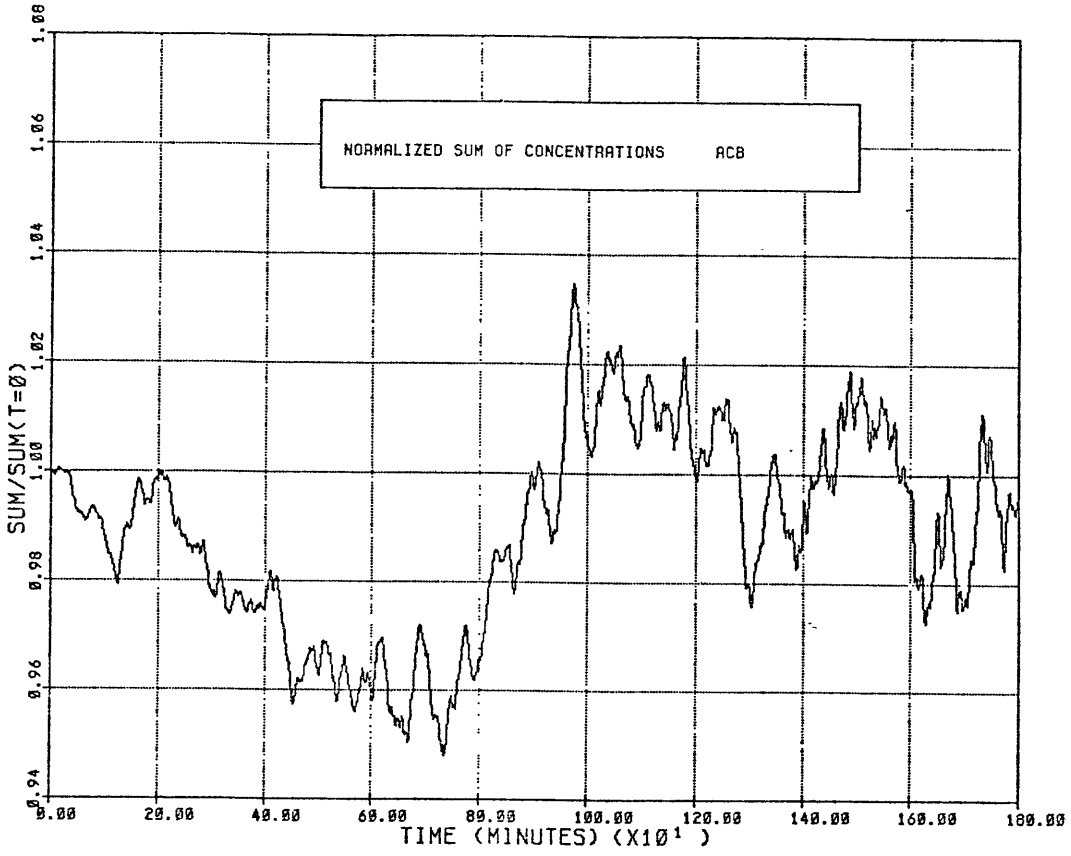

Figure 12: Nine point initialization unsmoothed: normalized mass

viii. Conservation of squared mass

As with the one point initialization, the area weighted sum of the squares of the concentrations grew monotonically. As stated before, an explanation for this increase is discussed in section IV.B.2.a.viii. The time history of the area weighted squares of the concentrations is shown below in figure 13.

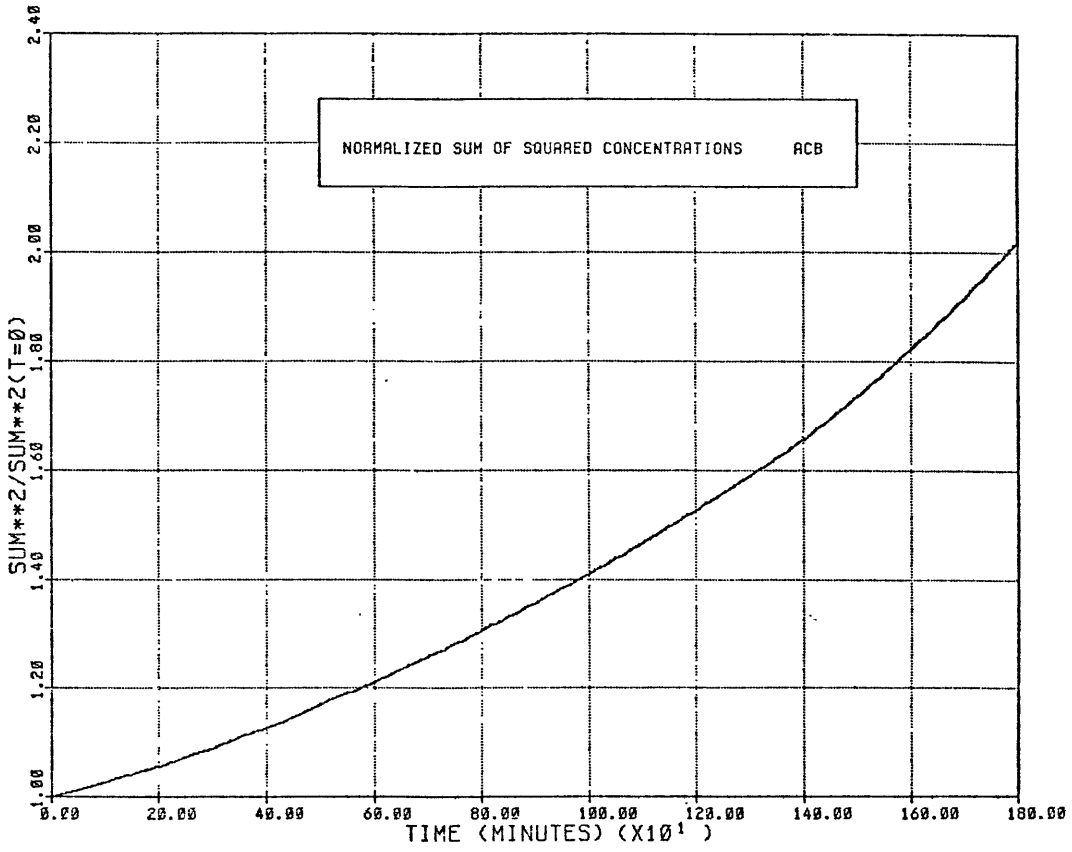

Figure 13: Nine point initializion unsmoothed: normalized squared mass

c. Sixty-nine point initialization

i. Description of initialization

The results of the nine point initialization were an improvement over the one point initialization. In an attempt to further reduce the sharp gradients at the edge of the cloud and thus reduce the wake, a much smoother initialization was used. This initialization consisted of a 69 point grid illustrated as timestep 0000 below. The concentrations were determined by calculating the value of a normal distribution that was centered on a certain gridpoint and dropped off evenly in all directions. The variance of the distribution was defined to be the distance between adjacent gridpoints. No distinction was made between longitudinal and latitudinal grid spacing. Thus, the concentration was symmetric in gridpoint units but the actual mass distribution was slightly skewed. The cloud contained more mass at its southern edge than in the north due to the greater grid box area in the south. In addition, the cloud was longer latitudinally than longitudinally due to the greater latitudinal grid spacing. All calculated values were multiplied by 30000 in order to produce integers large enough so that they would be relatively resistant to truncation error. Thus, the central gridpoint contained 11,968 units of concentration or 30000*normal(0). The gridpoints immediately to the north, south, east and west

of this center had concentrations of 7259 units of concentration which was 30000*normal(1). The gridpoints immediately to the northeast, northwest, southeast, and southwest, at a distance of V2 gridpoints from the center, contained 4403 units of concentration which is 30000*normal(1.414 = V2). All boxes with calculated values above .5 units were initialized so that the gradients at the edge of the cloud were very small. The total amount of concentration in this cloud was 75196, so errors in this trial seemed larger by absolute standards than in the previous trials. The cloud center was initialized at the same location as the previously described trials.

In this trial the cloud began advecting when it was already quite large, covering most of a nine by nine gridpoint box. In real units this indicated a cloud that had a north-south dimension of 501000 meters and an east-west dimension of 369000 meters.

ii. Diagrams of advection

The results of the advection are shown below in figures 14a through 14f.

```
                                  75
                                  1
     0    0    0    0    0    0    0    0    0    0    0
     0    0    0    1    2    4    2    1    0    0    0
     0    0    1   18   81  133   81   18    1    0    0
     0    1   18  219  982 1620  982  219   18    1    0
     0    2   81  982 4403 7259 4403  982   81    2    0
     0    4  133 1620 7259 11968 7259 1620  133    4    0
25 - 0    2   81  982 4403 7259 4403  982   81    2    0
     0    1   18  219  982 1620  982  219   18    1    0
     0    0    1   18   81  133   81   18    1    0    0
     0    0    0    1    2    4    2    1    0    0    0
     0    0    0    0    0    0    0    0    0    0    0
```

14a. Sixty-nine point initialization unsmoothed:

advection pattern at t=0000

```
                                  75
                                  1
     0    0    0    0    0    0    0    0    0    0    0
     0    0    0    1    2    4    2    1    0    0    0
     0    0    0   15   76  133   86   21    2    0    0
     0    1   13  197  951 1620 1013  241   23    1    0
     0    1   66  916 4307 7259 4499 1048   96    3    0
     0    2  111 1523 7118 11968 7400 1717  155    6    0
25 - 0    1   66  915 4306 7259 4500 1049   96    3    0
     0    1   13  197  950 1620 1014  241   23    1    0
     0    0    0   15   76  133   86   21    2    0    0
     0    0    0    1    2    4    2    1    0    0    0
     0    0    0    0    0    0    0    0    0    0    0
```

14b. Sixty-nine point initialization unsmoothed:

advection pattern at t=0001

```
                                  75
                                  1
     0    0    0    0    0    0    0    0    0    0    0
     0    0    0    1    2    4    2    1    0    0    0
     0    0   -1   12   71  133   91   24    3    0    0
     0    1    9  176  919 1619 1044  263   28    1    0
     0    0   52  851 4209 7256 4594 1116  112    4    0
     0    0   90 1427 6975 11964 7540 1816  178    8    0
25 - 0    0   52  850 4208 7256 4596 1117  112    4    0
     0    1    8  176  918 1619 1045  263   28    1    0
     0    0   -1   12   71  133   91   25    3    0    0
     0    0    0    1    2    4    2    1    0    0    0
     0    0    0    0    0    0    0    0    0    0    0
```

14c. Sixty-nine point initialization unsmoothed:

advection pattern at t=0002

```
                                        75
                                        |
      0    0    0    0    0    0    0    0    0    0    0
      0    0    0    1    2    4    2    1    0    0    0
      0    0   -2    9   66  132   96   28    4    0    0
      0    1    5  155  887 1617 1075  286   34    2    0
      0   -1   39  787 4111 7250 4688 1185  129    6    0
      0   -1   71 1333 6831 11956 7679 1917  203   10    0
25 -  0   -1   39  786 4129 7250 4691 1186  129    6    0
      0    1    4  155  886 1617 1076  286   34    2    0
      0    0   -2    9   66  132   96   29    4    0    0
      0    0    0    1    2    4    2    1    0    0    0
      0    0    0    0    0    0    0    0    0    0    0
```

14d. Sixty-nine point initialization unsmoothed:

advection pattern at t=0003

```
                                        75
                                        |
      0    0    0    0    0    0    0    0    0    0    0
      0    0    0    1    2    4    2    1    0    0    0
      0    0   -2  -10   31  121  125   56   13    0    0
      0    1  -14   26  653 1567 1274  457   86    9    0
      0   -2  -26  377 3401 7128 5314 1696  276   26    0
      0   -3  -30  726 5795 11788 8601 2664  416   38    0
25 -  0   -2  -26  376 3396 7126 5318 1702  277   27    0
      0    1  -15   26  651 1566 1276  458   86   10    0
      0    0   -3  -10   31  121  125   57   13    0    0
      0    0    0    1    2    4    2    1    0    0    0
      0    0    0    0    0    0    0    0    0    0    0
```

14e. Sixty-nine point initialization unsmoothed:

advection pattern at t=0010

```
                                        75
                                        |
      0    0    0    0    0    0    0    0    0    0    0    0    0    0    0    0    0
      0    0    0    0    0  -33   44   91  -16 -103  -66  -13   19   22    4    0    0
      0    0    0   23  -79   38  284  -50 -503 -342  123  345  281  153   58   15    0
      0  -18   46  -19 -204  449  236 -1262-1167  634 1868 1747 1048  467  166   44    6
      0  -31   94 -113 -183  989 -765 -2357 1023 5367 6238 4390 2242  902  297   79   14
      3  -41  116 -178 -120 1179-1525 -2158 3843 9219 9181 5971 2898 1122  359   95   17
25 -  0  -31   93 -113 -186  992 -754 -2378  985 5346 6250 4414 2261  909  298   81   14
      0  -19   45  -14 -210  451  252 -1254-1205  610 1866 1762 1062  476  169   46    6
      0    0    0   23  -80   35  290  -40 -510 -359  116  346  284  157   61   15    0
      0    0    0    0    0  -34   44   94  -12 -104  -73   -9   29   28    8    0    0
      0    0    0    0    0    0    0    0    2    0    0    0    0    0    0    0    0
                                        0    0    0
```

14f. Sixty-nine point initialization unsmoothed:

advection pattern at t=0100

iii. Description of advection

The first thing that was immediately obvious was that the first negative wake developed much more slowly than in the previous trials. In timestep 0001 there was no negative wake. In timestep 0002 there were two grid points with negative concentrations. These wake values were both much smaller than with the nine point initialization, this difference was especially marked since this trial had a larger total concentration. In timestep 0002, at the lee end of the cloud, two grid boxes contained a single unit of positive concentration. These boxes were relatively isolated from any large concentrations and were, as a result, trapped. Without significant gradients of concentration, no advection could occur at all in this model. The terms in (29) round to zero in the integer arithmetic if large gradients are absent. The result here was that cloud started to leave the two boxes behind and the first negative wake actually developed between the isolated boxes and the remaining bulk of the cloud. This was seen first in timestep 0003. The two boxes were totally isolated by timestep 0005. The first positive wake formed by timestep 0015. It was composed of both a positive wake produced by the large negative concentrations to its windward side, and the two isolated boxes just discussed. From this time on, the advection followed the same general pattern as in the other trials. By timestep 1440, the grid was, again,

filled with a confusing array of alternating positive and negative wakes that extended to the rear and wrapped around to the front of the location of the cloud's forward positive area.

The decrease in the ratio of the largest forward positive value to the maximum wake value was slower than the decrease with the other initializations. This is shown in the table below.

timestep	largest forward positive value	maximum wake value	ratio
0000	11968	no wake	N.A.
0001	11968	0	infinite
0002	11964	-1	-11964.0
0010	11788	-30	-392.9
0050	11303	-526	-21.5
0120	9219	-1525	-6.0
0300	7243	-2976	-2.4
0600	5365	-3206	-1.7
0900	4364	-2789	-1.6
1200	3747	-2488	-1.5
1440	3421	-2394	-1.4

Table 5: Sixty-nine point initialization unsmoothed: magnitude of wake and forward positive area

The distribution of concentrations was not symmetric.

The positive cloud dominated the concentration pattern. In the early timesteps the positive area concentrations were much larger than the largest wake values, but, the wakes grew in relative magnitude as the advection continued.

The relative number of grid boxes in the wake grow more slowly, but was still unacceptable. In timestep 0120, 40 boxes were in the wake and 48 were in the forward positive area. This small difference in favor of the positive area was erased soon after this timestep as the wakes continued to grow

iv. Cross-sections

Cross sections through the cloud are shown below in figures 15a through 15e.

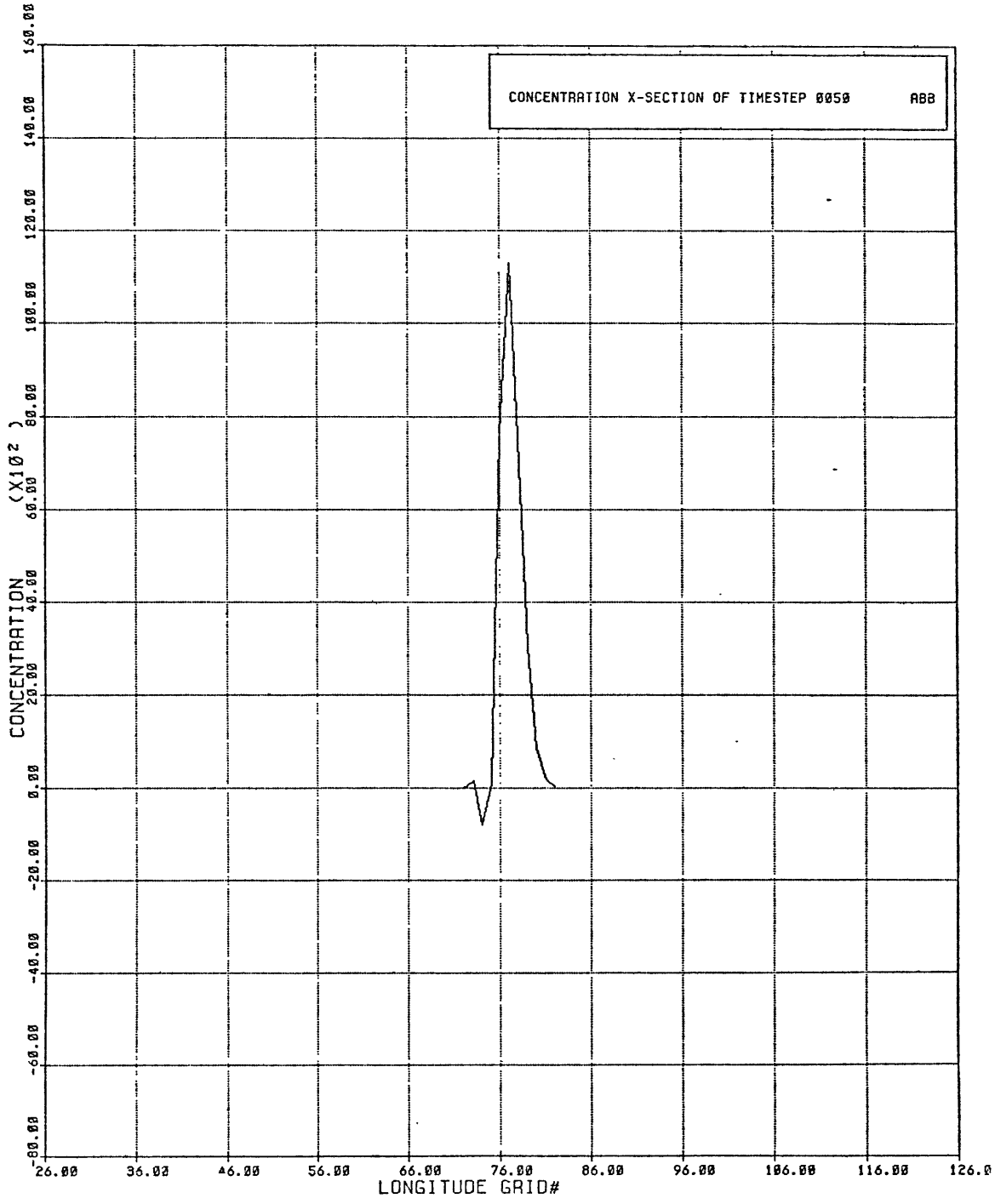

15a. Sixty-nine point initialization unsmoothed:

cross-section at t=0050

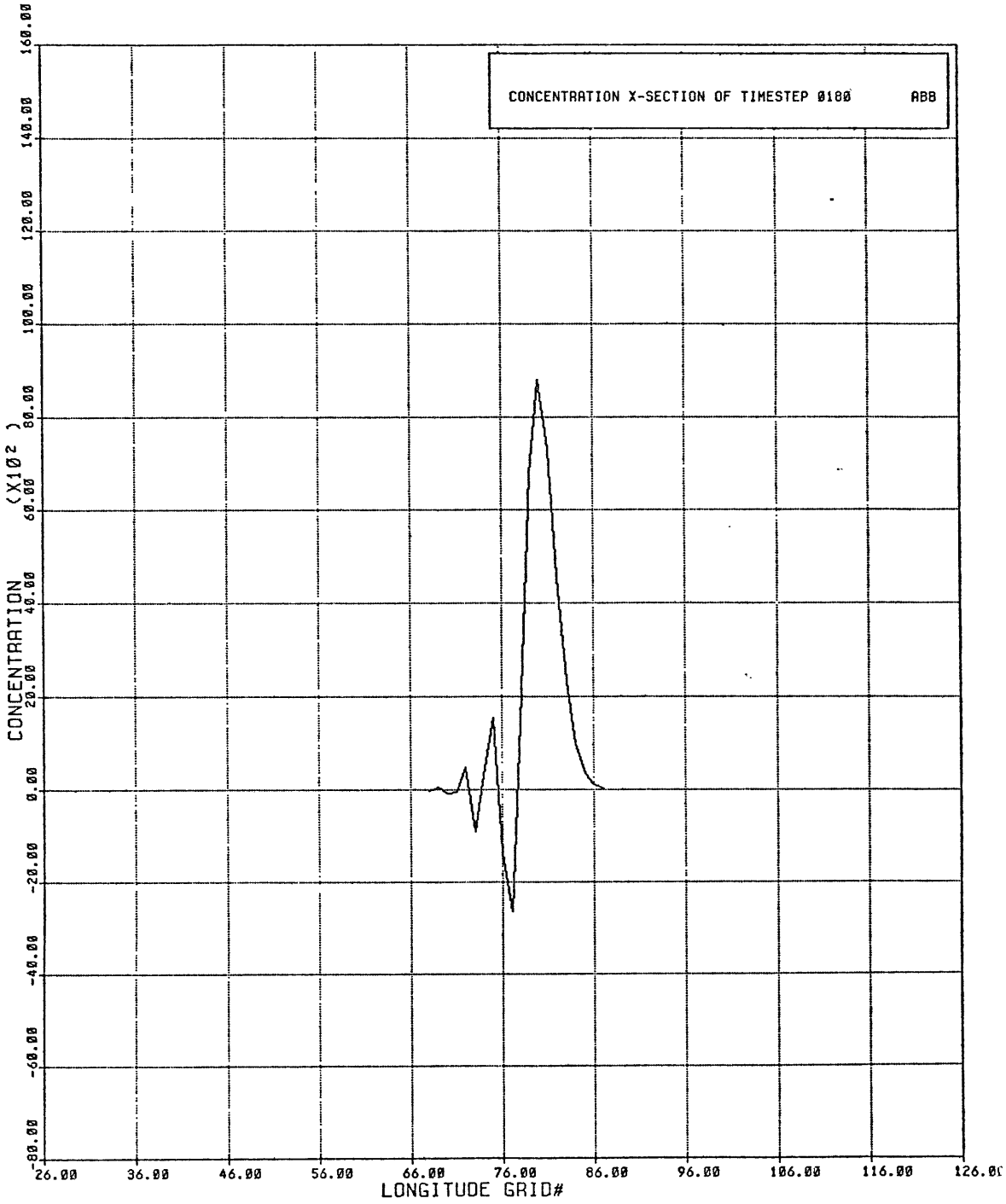

15b. Sixty-nine point initialization unsmoothed:

cross-section at t=0180

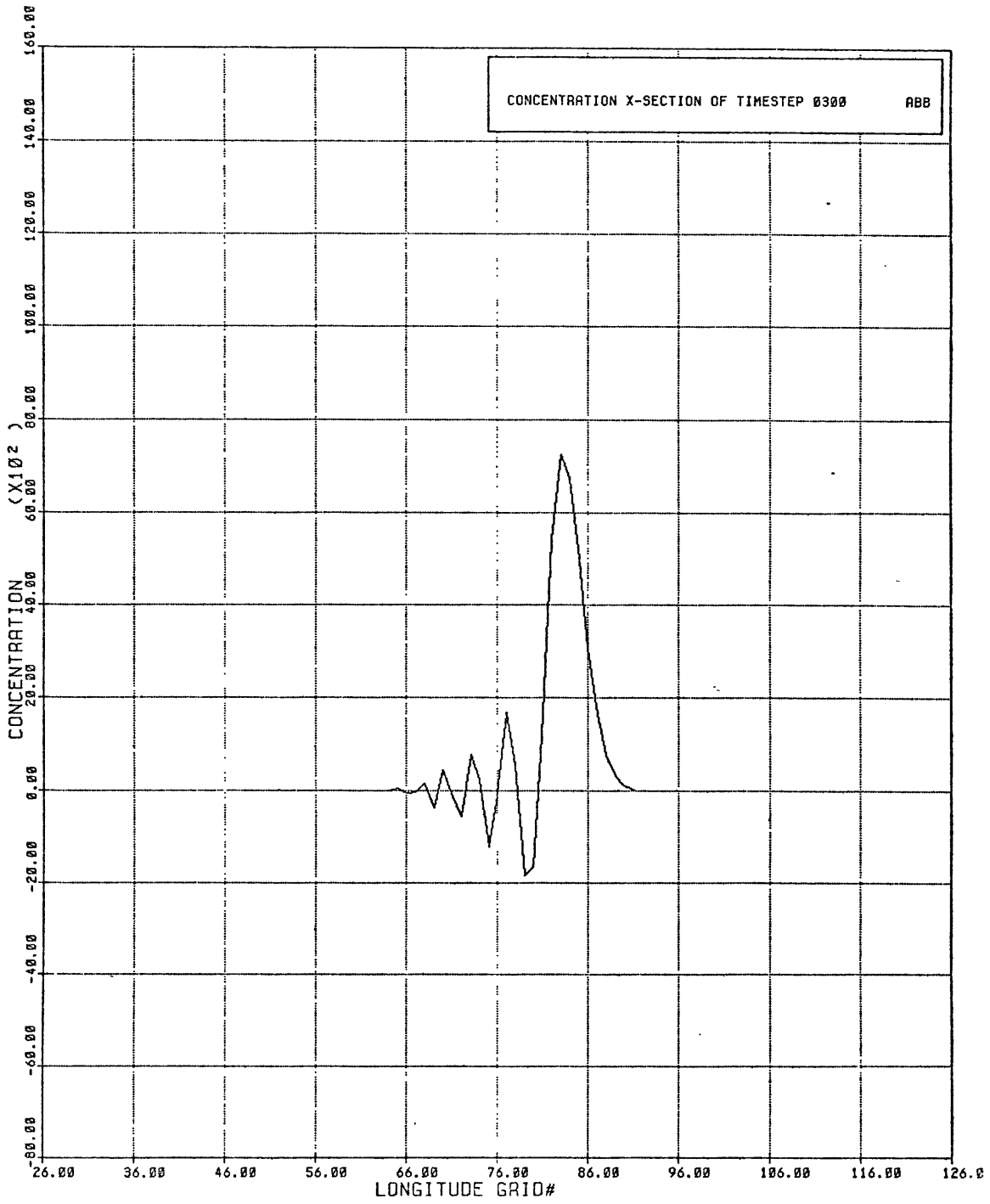

15c. Sixty-nine point initialization unsmoothed:

cross-section at t=0300

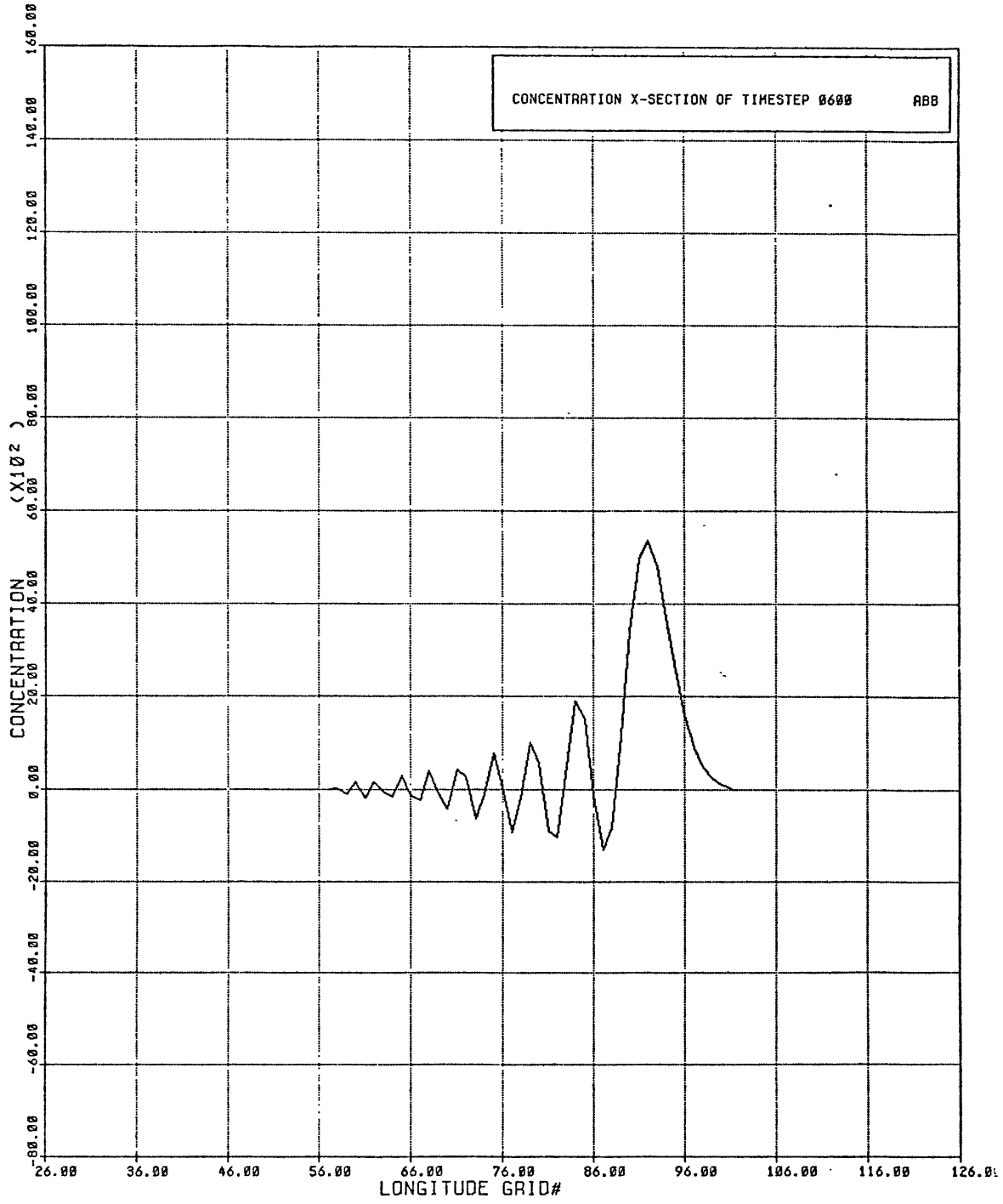

15d. Sixty-nine point initialization unsmoothed:

cross-section at t=0600

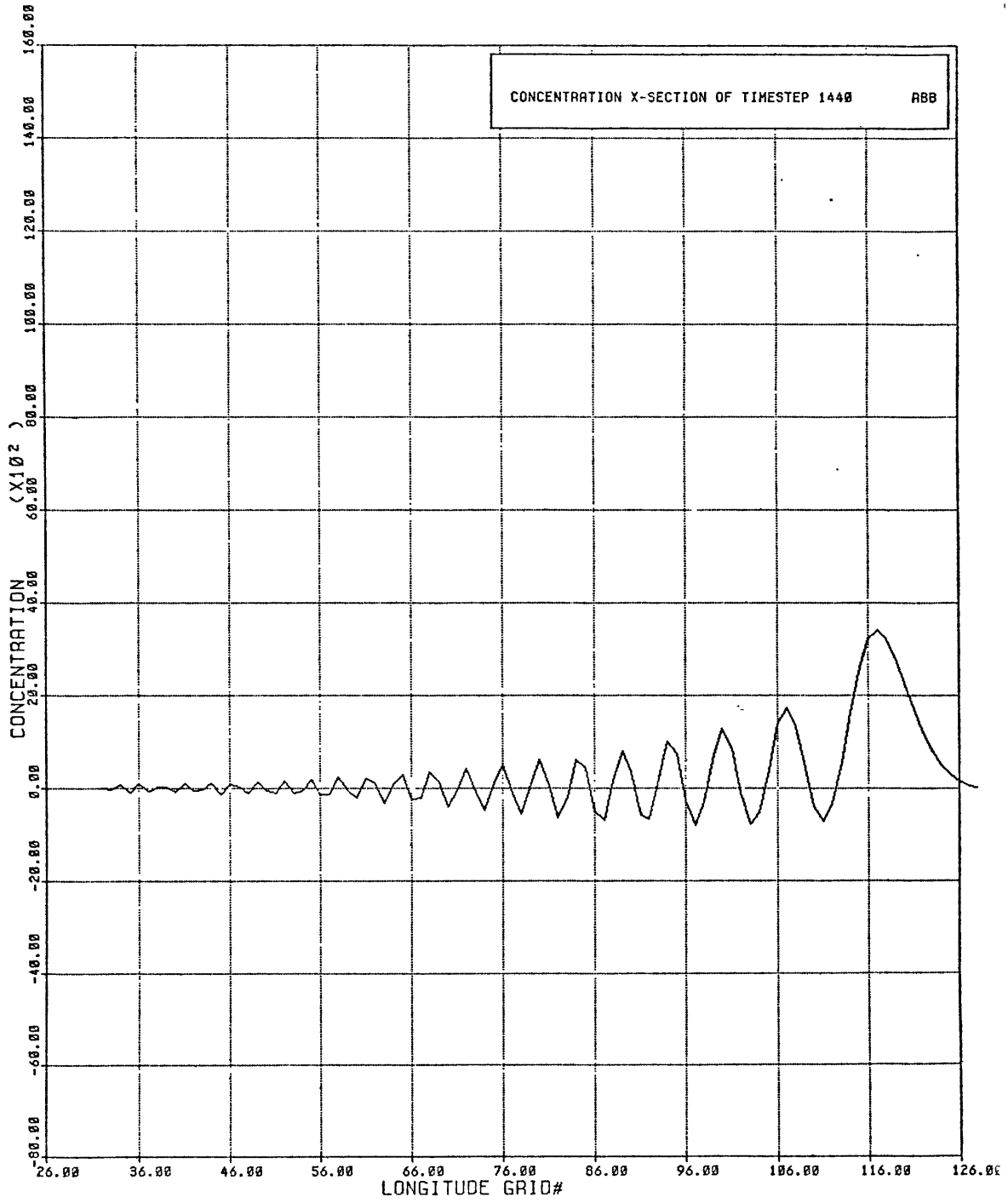

15e. Sixty-nine point initialization unsmoothed:

cross-section at t=1440

The cross sections show the well ordered pattern of wakes that developed, more slowly, behind the cloud. The reduction of the large gradients in the cloud had successfully suppressed the rapidly oscillating, chaotic pattern that was evident in the other initializations. The slowly varying oscillation was still present and, by timestep 1440 began to be comparable in amplitude to the forward positive area.

v. Mass of the forward positive area

The problems in interpreting the forward area as the "real" cloud that were present in the previous initializations were still present in this trial. The sum of the concentration in the forward area is shown in the table below for selected timesteps.

timestep	sum of concentrations	% over timestep 0000
1	75196	0.0
10	75326	0.2
120	87856	16.8
1020	109231	45.3

Table 6: Sixty-nine point initialization unsmoothed: excess concentration in the forward positive area

The excess was in about the same proportion as the other initializations.

v. Velocity of forward positive area

The location of the forward area approached, very closely, the desired location of (76+.03147*T,26). In timestep 0010 the location of the centroid of the positive area was at gridpoint (76.307,26). The centroid of the entire cloud, including the wake was at (76.313,26), very close to the predicted value of (76.3147,26). The centroid of the positive area was, thus, only 2 percent behind the predicted location. At timestep 0120, the centroid of the positive area was at gridpoint (79.307,26). The predicted location was gridpoint (79.776,26), so the positive area lagged the prediction by about 12 percent. By timestep 1020, the predicted location was at gridpoint (110.1,26). The positive area was mostly behind this point. By inspection, it was clear that the centroid of the cloud still lagged about ten percent behind the predicted location of the actual cloud.

vii. Conservation of mass

The graphs of the time history of the area-weighted sum of the concentrations is shown below in figure 16.

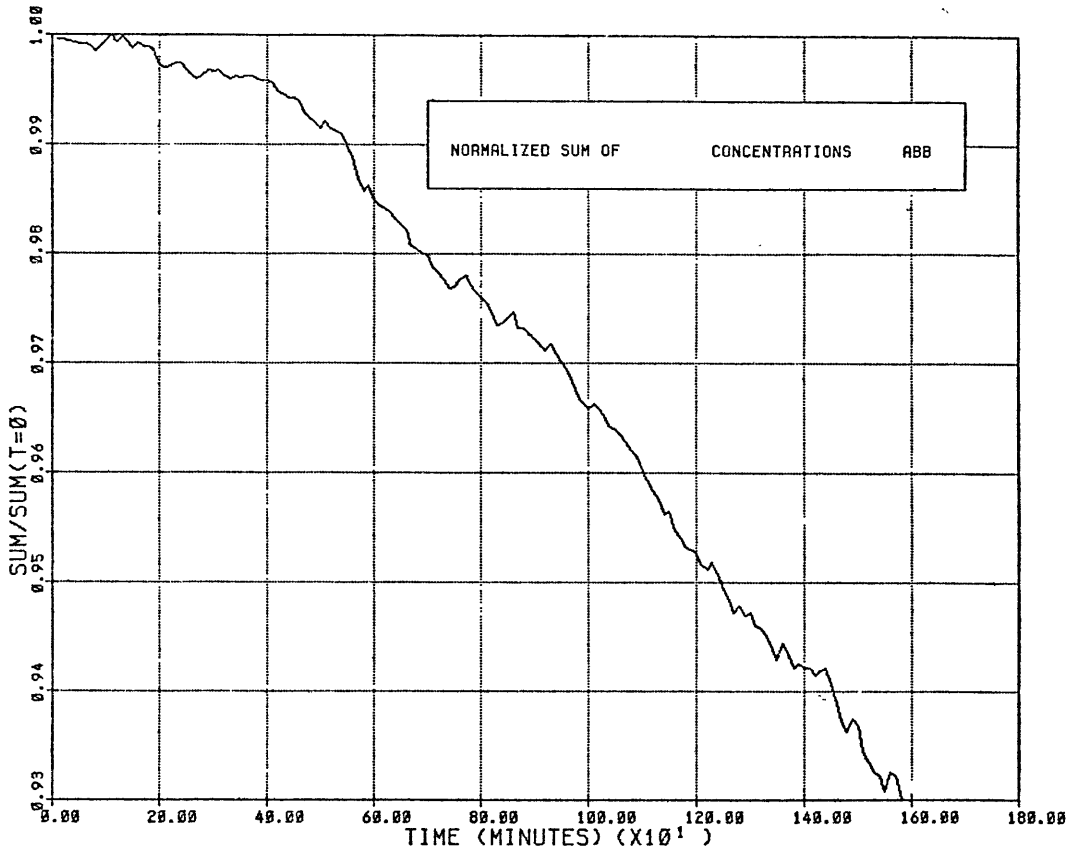

Figure 16: Sixty-nine point initialization unsmoothed: normalized mass

The graph shows similar results as previous cases. In this case the mass in the model seemed to drop more systematically. It would be hard to argue that the drop in mass that was indicated is that first part of a random walk as was possible with the nine point initialization. This drop was the result of the accumulation of thousands of truncation errors. The integer arithmetic used in this trial used truncation rounding. The drop was very small, only amounting to about a few percent of the total mass over the first day of advection. The drop appears to have been more smooth than the variation in the other initializations. This was probably due to the fact that the data was only sampled every ten timesteps in this case and every timestep in the other, rougher cases. With this sampling frequency, random, short period variations were, probably, filtered out and the resulting graph was dominated by the general downward trend.

viii. Conservation of squared mass

A graph showing the time history of the area weighted sum of the squares of the concentrations is shown below in figure 17.

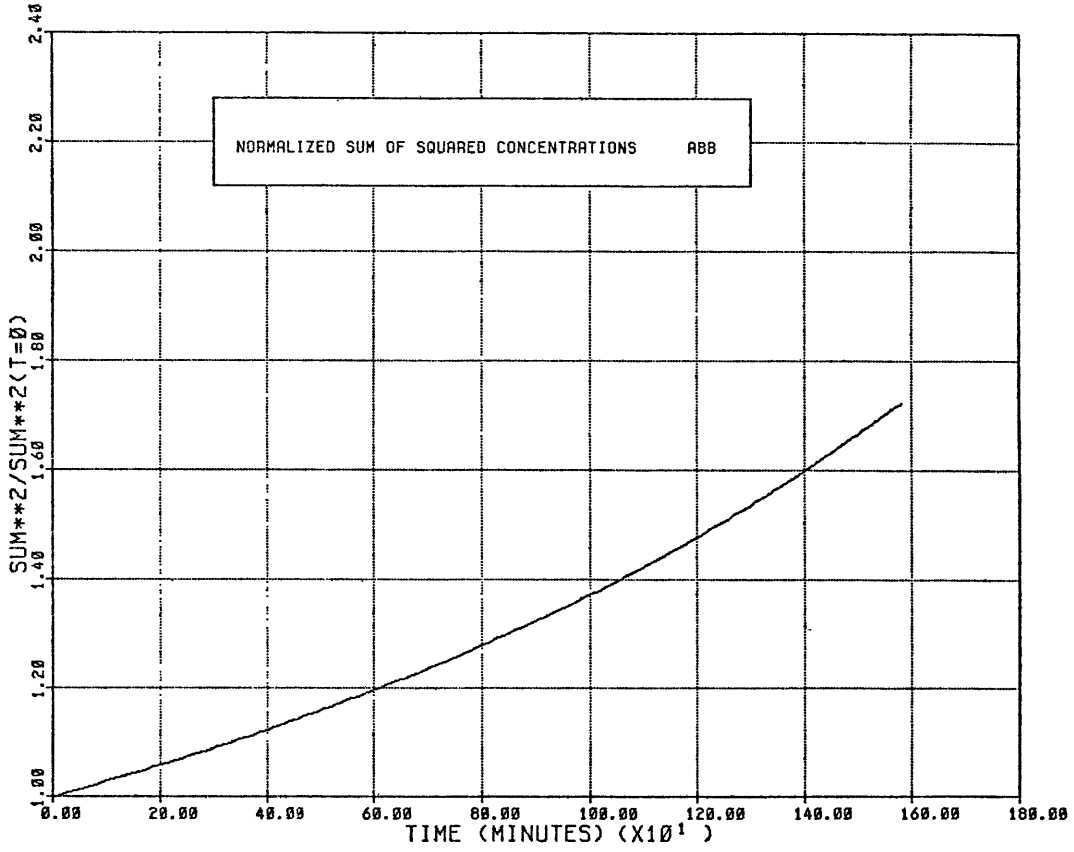

Figure 17: Sixty-nine point initialization unsmoothed: normalized squared mass

The growth of the sum of the squares of the mass in each grid box was very similar to that in the other initializations. The quantity grew slowly to about 60 percent over its initial value. This again represented a very small average increase per timestep.

2. Smoothed advection

a. Discussion

While the pure Arakawa scheme was designed to conserve certain properties of a particle field, it did not do this well and it produced quite unrealistic results. The wakes which inevitably dominated the cloud pattern were an undesirable and spurious byproduct of this scheme. In order to eliminate this problem, a method of smoothing was developed that prevented a wake from ever forming at the lee side of the cloud. Very roughly, the smoothing scheme prevented the first wake from forming to the lee of the cloud. It did this before the negative wake grew large enough to form a positive wake to its rear, and, thus, prevented the myriad of wakes from forming. It subtracted the value of the eliminated wake from the concentrations in the rear of the cloud in order to obey mass conservation. The particular method of smoothing was not standard and detailed description of its mode of action is given in Appendix B.

b. One point initialization

i. Description of initialization

To compare the smoothed advection with the pure Arakawa advection, the same one, nine, and 69 point initializations were attempted. The one point trial was initialized with 10000 units of concentration at gridpoint (10,26). This location was chosen to permit the cloud to advect for the maximum time across the grid. The cloud did not have to be centered as was necessary with the unsmoothed advections because the smoothing eliminated the backwardly propagating wakes. The smoothed trials, described here in sections c and d, were iterated for a much longer time than was possible with the unsmoothed trials. In the unsmoothed trials, the wakes would reach the edge of the grid in approximately 1600 timesteps. The unsmoothed trials lasted approximately 4200 timesteps, stopping only when the cloud reached the eastern boundary of the grid. Only the first day (1440 timesteps) of advection has been considered in this paper.

ii. Diagrams of advection

The results of the advection are shown below in figures 18a through 18h.

```
                10
                 |
        0       0       0       0
        0       0      26       0
        0    9843     105       0
25 -    0       0      26       0
        0       0       0       0
```

18a. One point initialization smoothed:

advection pattern at t=0001

```
                10
                 |
          0      0      0      0      0
          0      0     52      1      0
          0   9685    208      1      0
25 -      0      0     52      1      0
          0      0      0      0      0
```

18b. One point initialization smoothed:

advection pattern at t=0002

```
                10
                 |
          0      0      0      0      0
          0      0     77      2      0
          0   9529    310      3      0
25 -      0      0     77      2      0
          0      0      0      0      0
```

18c. One point initialization smoothed:

advection pattern at t=0003

```
                10
                 |
          0      0      0      0      0      0
          0      0      0      2      0      0
          0      0    240     25      0      0
          0   8436    973     52      1      0
25 -      0      0    241     25      0      0
          0      0      0      2      0      0
```

18d. One point initialization smoothed:

advection pattern at t=0010

```
                10                                    15
                 |                                    |
          0      0      0      0      0      0      0      0      0
          0      0      0     16    102     82     29      2      0
          0      0    180    641    588    282     92     19      0
          0    405   1698   2039   1137    442    132     28      0
25 -      0      0    180    643    589    282     92     19      0
          0      0      0     16    102     83     30      2      0
          0      0      0      0      0      0      0      0      0
```

18e. One point initialization smoothed:

advection pattern at t=0100

15

	0	0	0	0	0	0	0	0	0	0	0	0
	0	0	0	0	8	130	203	197	122	57	19	0	0
	0	0	0	0	264	581	554	425	250	121	43	5	0
	0	1	42	281	776	955	924	557	315	149	55	10	0
25 -	0	0	0	0	261	583	598	427	252	123	44	5	0
	0	0	0	0	8	128	207	188	124	60	20	0	0
	0	0	0	0	0	0	0	0	0	0	0	0	0

18f. One point initialization smoothed:

advection pattern at t=0300

30

	0	0	0	0	0	0	0	0	0	0	0	0
	0	0	27	136	226	242	194	127	60	26	0	0
	0	25	205	424	498	460	359	221	117	45	8	0
	0	24	367	570	627	530	401	266	144	60	13	0
25 -	0	25	201	422	499	465	364	227	122	48	9	0
	0	0	24	130	222	244	198	131	64	27	0	0
	0	0	0	0	0	0	0	0	0	0	0	0

18g. One point initialization smoothed:

advection pattern at t=0600

50

	0	0	0	0	0	0	0	0	0	0	0	0
	0	6	93	178	228	242	222	188	120	62	28	0
	0	0	145	291	377	400	376	312	213	117	49	10
	0	0	144	311	414	445	419	344	243	142	61	13
25 -	0	0	146	292	380	405	381	317	218	117	49	10
	1	12	93	180	233	250	231	195	128	62	29	0
	0	0	0	0	0	0	0	0	0	0	0	0

18h. One point initialization smoothed:

advection pattern at t=1440

iii. Description of advection

The results of the advection using the smoothed version of the Arakawa scheme were much more pleasing than the unsmoothed trials. After the early timesteps, when most of the concentration was in the initialized grid box, the pattern rapidly developed into an elliptical cloud. The model cloud exhibited features expected of a real cloud of particles. The concentration was highest in the center of the cloud and dropped monotonically towards the edges. The cloud rapidly grew to five gridpoints in length in the latitudinal direction The clouds latitudinal extent remained at five gridpoints throughout the rest of the trial. The longitudinal growth to five gridpoints was almost as rapid and the growth continued slowly thereafter so that the cloud was 11 gridpoints long by the end of the first day. Apparently, the Arakawa Jacobian strongly favors diffusion in the direction of motion of the cloud. It was in the direction of motion where large concentration gradients can couple with large gradients in the height field and produce a large Jacobian value at the edge of the model cloud.

One unrealistic feature in the cloud was noticeable in the later timesteps. At the lee end of the cloud there were, occasionally, trailing grid boxes with small concentrations. If these trailers grew too long or separated from the the

cloud, then the smoothing algorithm eliminated them. However, some trailers were still extant at the edge of cloud after timestep 1000. Since they contained only small concentrations they were not a serious problem and a more aggressive smoothing algorithm could have eliminated them altogether.

iv. Cross-sections

Cross sections through the cloud at selected timesteps are shown below in figures 19a through 19d.

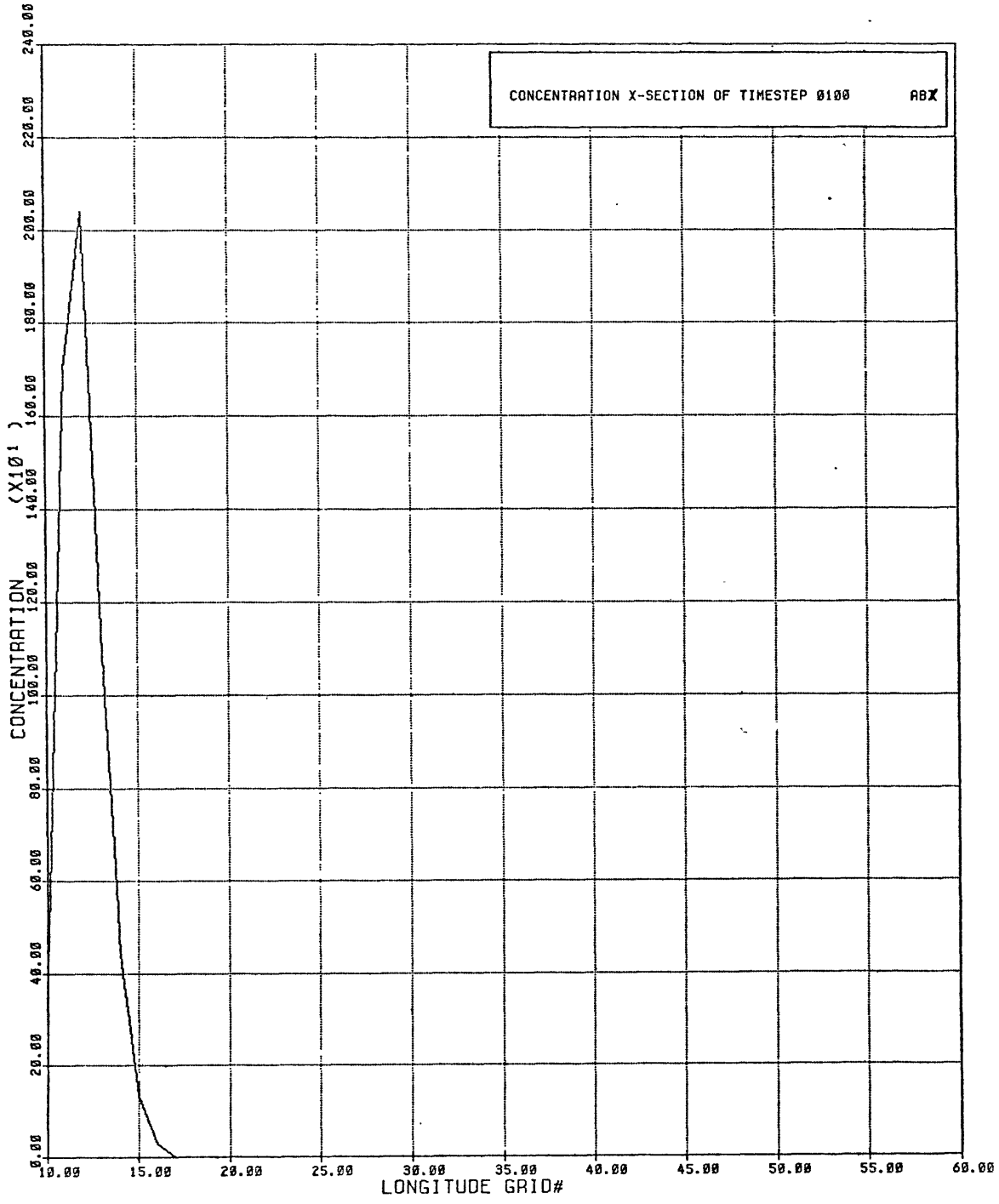

19a. One point initialization smoothed:

cross-section at t=0100

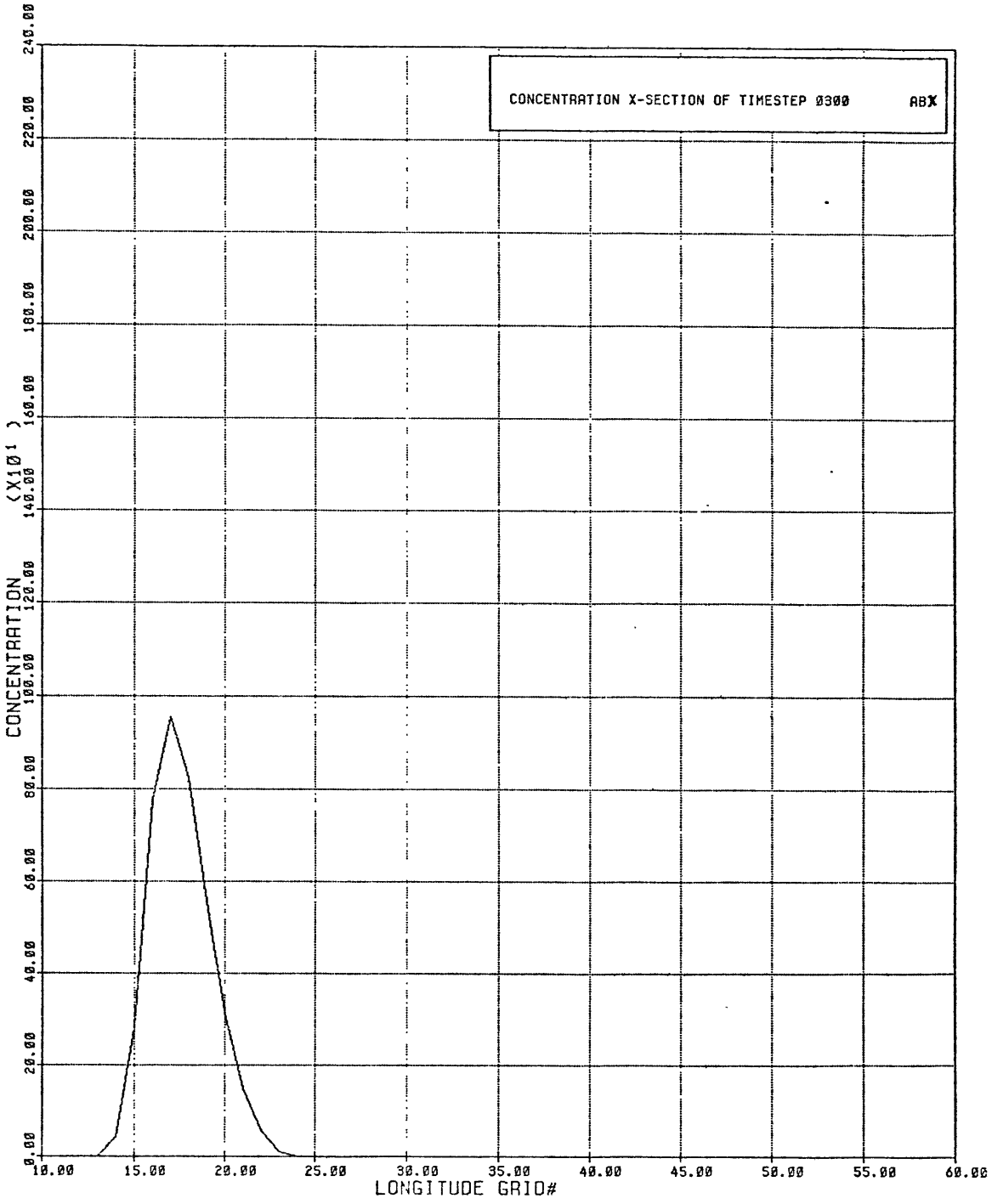

19b. One point initialization smoothed:

cross-section at t=0300

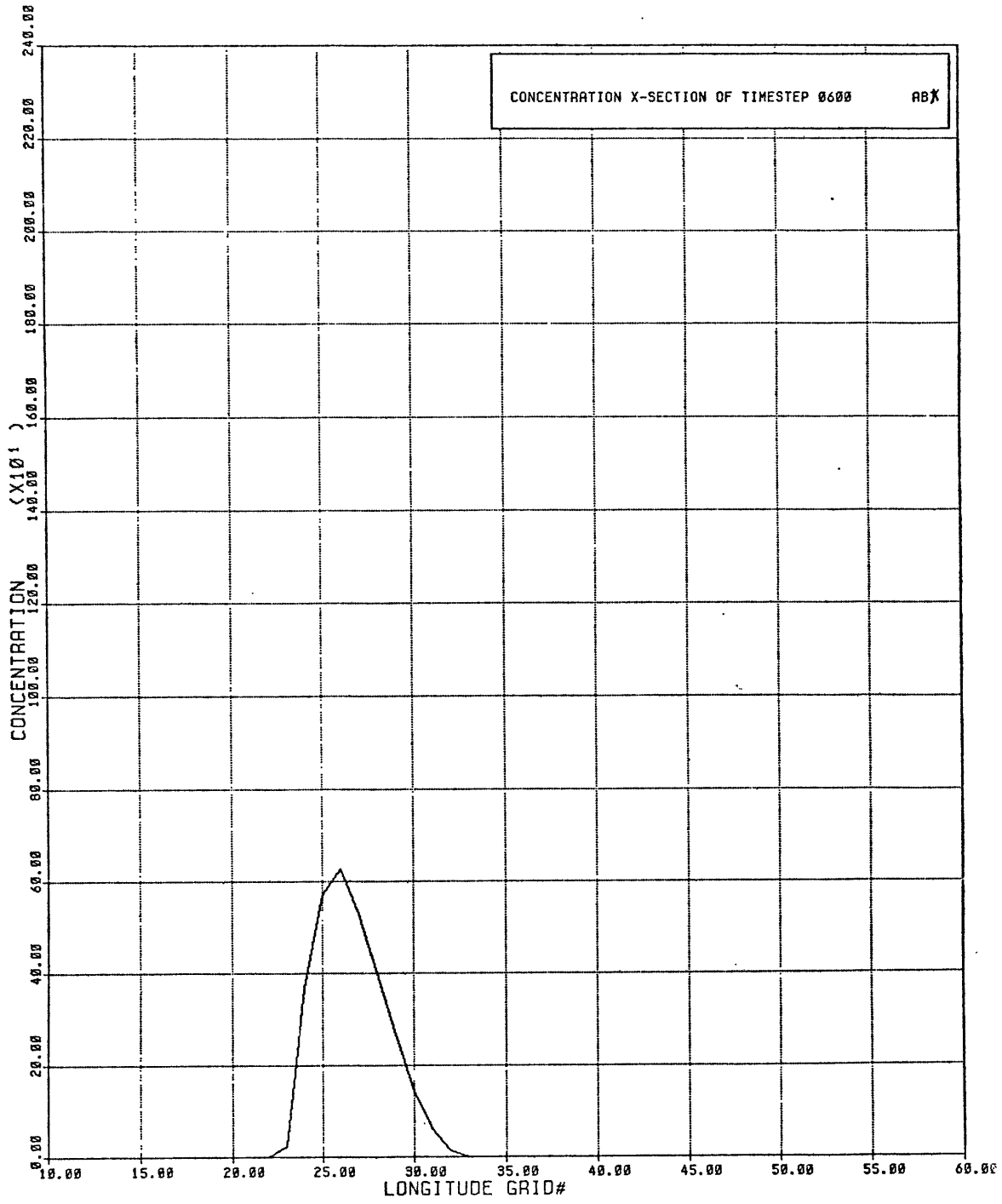

19c. One point initialization smoothed:

cross-section at t=0600

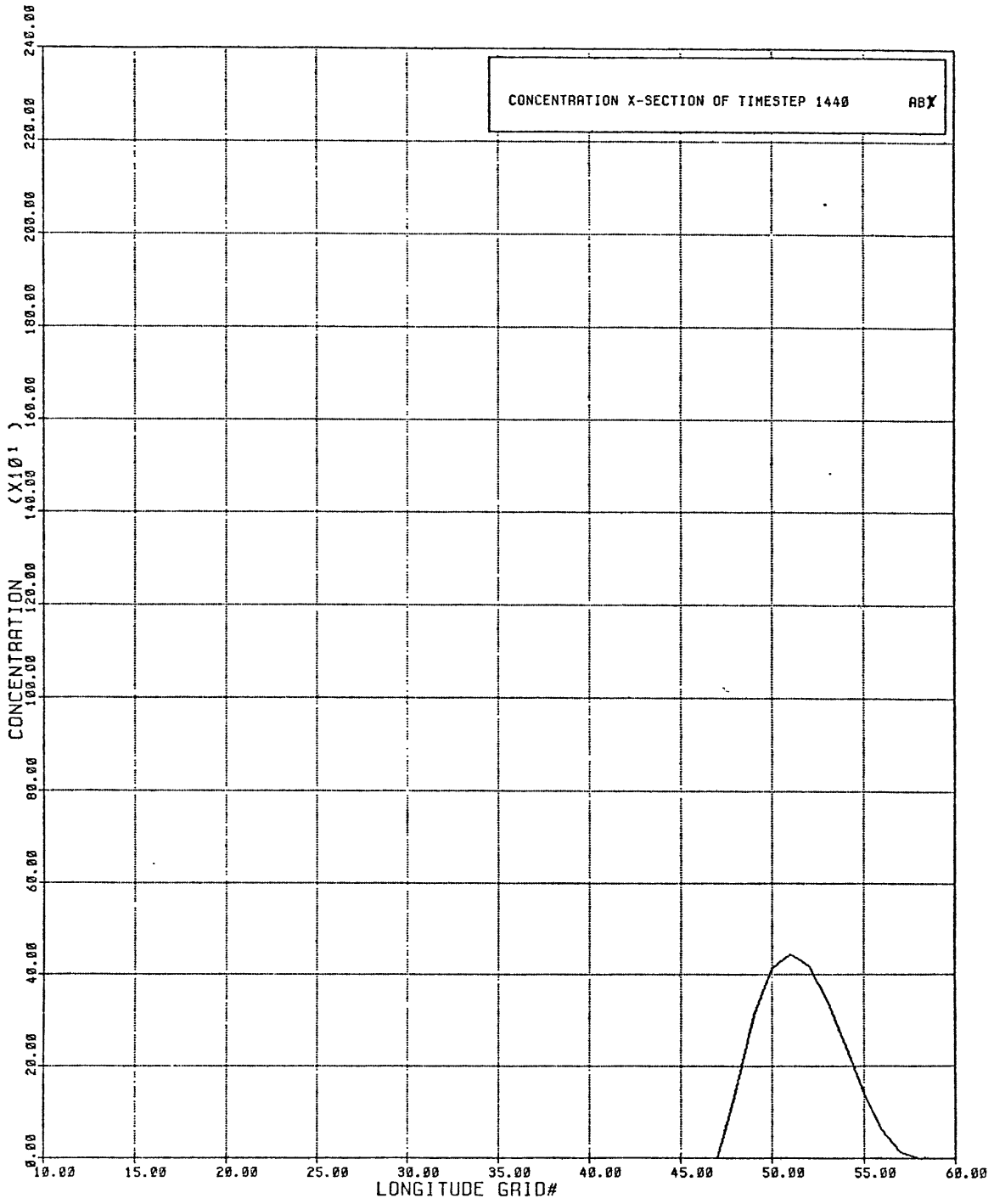

19d. One point initialization smoothed:

cross-section at t=1440

The cross-sections through the cloud show none of the complicating structure was present without the smoothing. The cloud concentrations quickly formed a smooth bell shaped distribution that advected downwind of its original location. The peak concentration dropped as numerical diffusion spread the cloud. The peak values in the cloud were smaller than in the unsmoothed cloud's forward positive area. This was not unexpected since the total concentration in the smoothed cloud was also smaller than the inflated value present in the unsmoothed forward positive area.

v. Velocity of the cloud

The cloud still moved more slowly than the wind. At first this difference was very large, but the cloud velocity approached the wind velocity in the later timesteps. A table showing the predicted longitudinal gridpoint location of the centroid of the cloud and its actual location is shown below in table 7.

timestep	predicted location of centroid	actual location of centroid	percentage lag of centroid
0001	10.03147	10.0157	50
0010	10.3147	10.1670	47
0100	13.147	12.34	26
1000	41.47	38.5	9

Table 7: One point initialization smoothed: lag in the centroid

While the centroid was not explicitly calculated for the unsmoothed case, inspection will show that the smoothed cloud was closer to the predicted location than the positive area was in the unsmoothed trials. The lag in the centroid in the forward positive area in the unsmoothed trials was due to the fact that the positive area, alone, could not have been properly interpreted as the "real cloud". The centroid in the unsmoothed trials was moved forward of the positive area by the negative concentrations in the wake. The lag in the location of the centroid of the smoothed cloud was due to the smoothing process. The specific mechanism is detailed below in figure 20. In this figure, the result of one time step of advection on a single gridpoint is shown. a is the value at the gridpoint and b is the value produced at a neighboring gridpoint by the Jacobian.

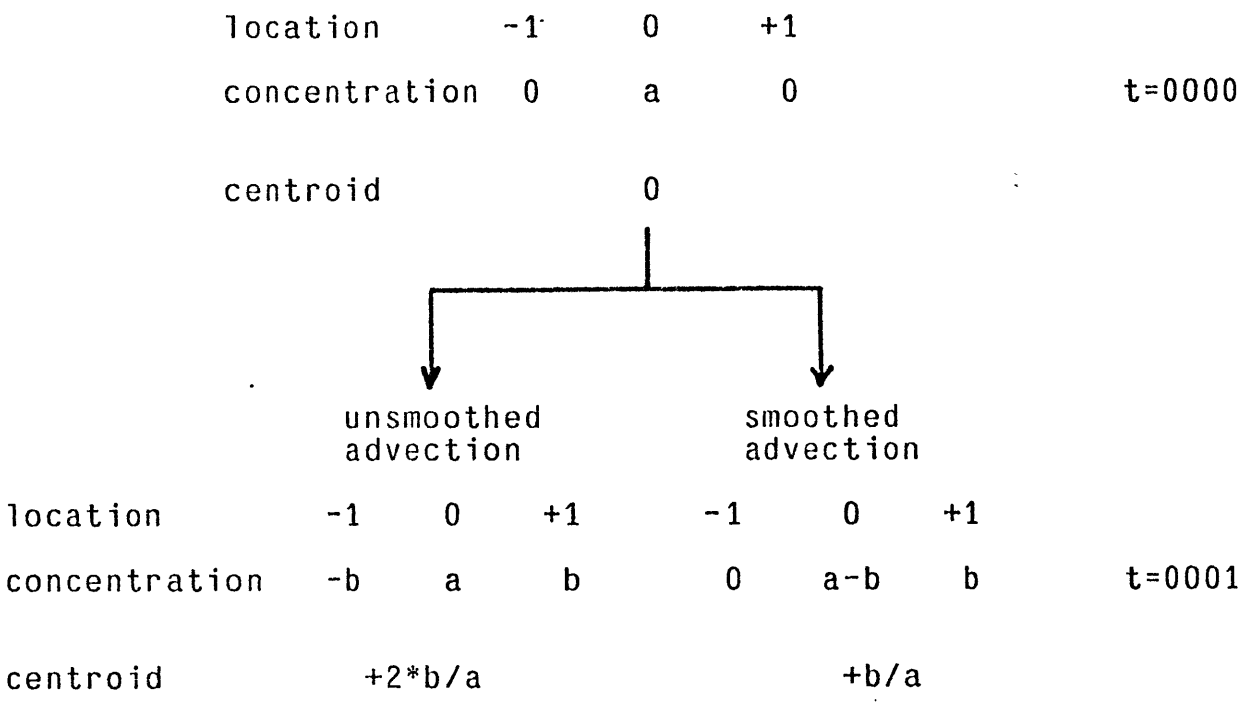

Figure 20: Cause of the centroid lag in smoothed advection

Essentially, the smoothing removed the negative concentration that would have helped move the cloud centroid forward. The negative value was added to an adjacent cloud grid box but the distance of this negative value (or reduced positive value) to the cloud centroid was reduced. In the simple example presented in figure 20, the distance was reduced from one to zero. Thus the distance weighting used in calculating the centroid weighed this negative value less and the centroid lagged behind the location that it would, otherwise, have occupied. The example shown above explains why the centroid in this trial, initialized with only one gridpoint, had moved only one half of the predicted distance

in the first timestep. The relative lag decreased as the cloud became larger in longitudinal extent and most of the diffusion acted on internal and forward portions of the cloud. In these forward portions, the addition of the negative value to a rearward gridpoint did not result in that gridpoint having a negative concentration. Thus, the smoothing scheme was not activated and the advection scheme was not affected by the lag mechanism introduced by the elimination of negative concentrations.

vi. Conservation of mass

The model preserved the mass of the cloud quite well as is shown below in figure 21. Nearest integer rounding was used in the integer arithmetic that was used in this calculation.

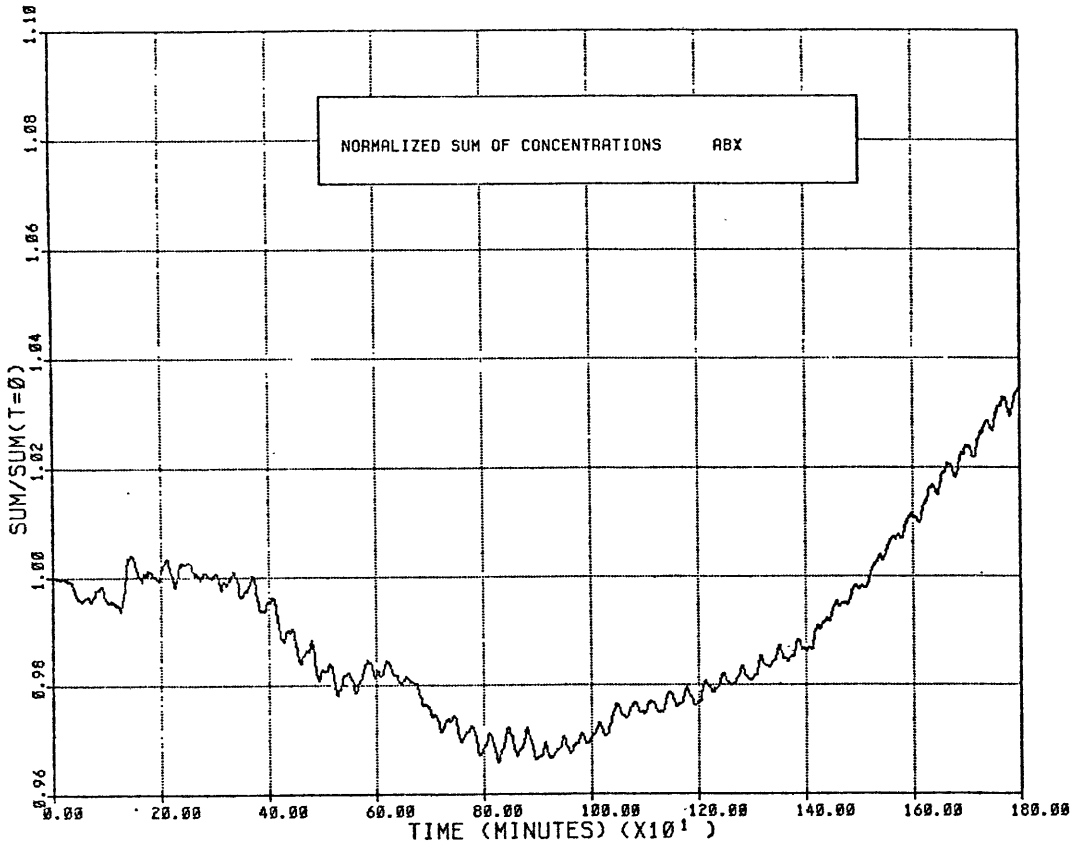

Figure 21: One point initialization smoothed: normalized mass

The fluctuations in the mass of the cloud were much less erratic than in this trial's unsmoothed analogue. The regular oscillations with a very short period were due to the smoothing scheme.

vii. Conservation of squared mass

The time history of the area weighted sum of the squares of the concentrations is shown below in figure 22.

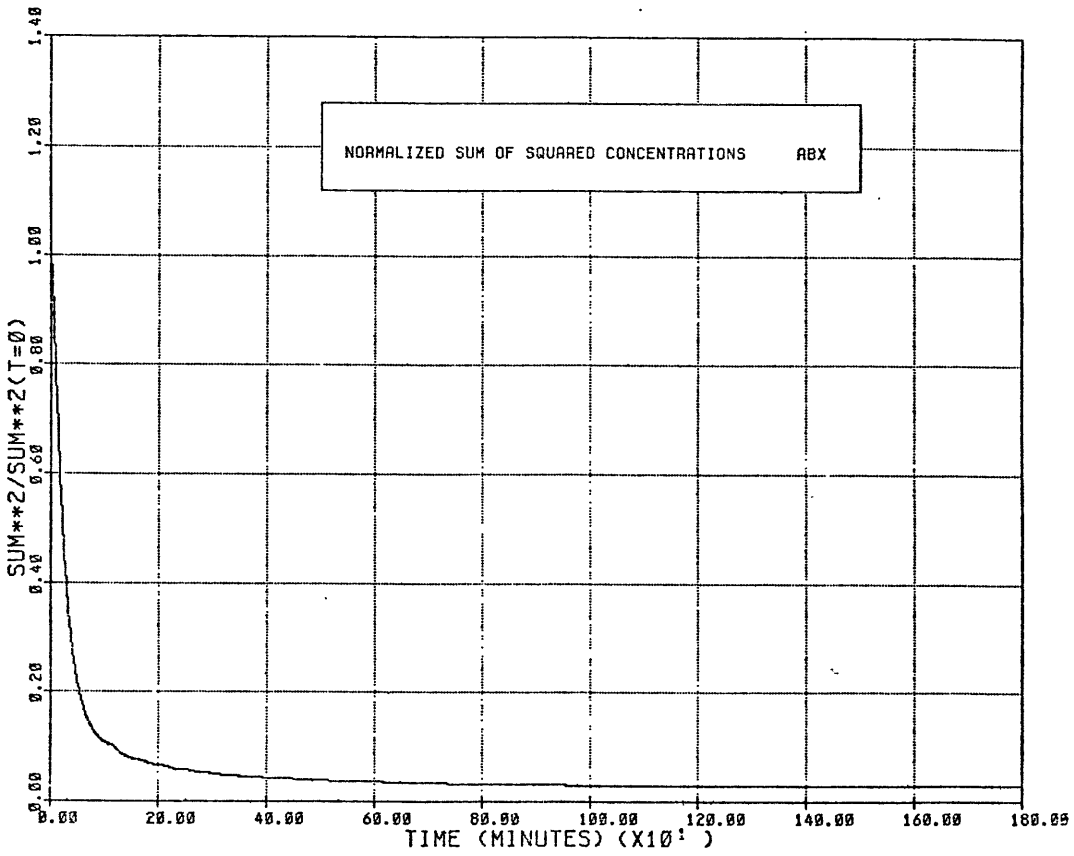

Figure 22: One point initialization smoothed normalized squared mass

The sum of the squares of the mass in each gridbox decreased sharply during the advection. The decrease slowed with time and eventually the sum of the squares of the masses became nearly constant. The process that caused this reduction is shown symbolically below in figure 23b. a represents the quantity in a grid box and b indicates the quantity that was added to a neighboring grid box at the edges of the model cloud. Mass was conserved in these diffusion processes.

unsmoothed trials:	rear edge		forward edge	
location	-1	0	0	+1
concentration	0	a	a	0
total sum of squares		$2*a^2$		

↓ wake diffusion ↓ non wake diffusion

location	-1	0	0	+1
concentration	-b	a+b	a-b	b
sum of squares	$b^2 + a^2 + 2*a*b + b^2$		$a^2 - 2*a*b + b^2 + b^2$	
total sum of squares		$2*a^2 + 4*b^2$		

Figure 23a: Cause of squared mass variation: unsmoothed advection

smoothed trials:	rear edge		forward edge	
location	-1	0	0	+1
concentration	0	a	a	0

total sum of squares $2*a^2$

↓ wake diffusion ↓ non wake diffusion

location	-1	0	0	+1
concentration	0	a	a-b	b

sum of squares a^2 $a^2 - 2*a*b + b^2 + b^2$

total sum of squares $2*a^2 - 2*a*b + 2*b^2$

Figure 23b: Cause of squared mass variation: smoothed advection

In the example above, the unsmoothed advection caused two types of diffusion. The wake diffusion caused the concentration, a, to be spread between two grid boxes. Since one of the grid boxes was negative, this action increased the value of the sum of the squares of the masses. The second type of diffusion was entirely positive and resulted in a

decrease in the sum of the squares of the masses. The two processes almost canceled and the resulting increase in the sum of the squares of the masses was of order b squared. b was the value that was diffused each timestep due to errors introduced by the finite difference approximations and was much smaller than a. Thus, the sum of the squared masses grew slowly. In the unsmoothed advection the wakes grew to be of the same magnitude as the main cloud, but only after there were several alternating wakes of alternating sign which probably aided in canceling the growth of this quantity.

When the smoothing scheme was introduced, the wake diffusion was eliminated and thus the unbalanced non-wake diffusion acted alone and reduced the sum of the squares of the masses. This decrease was of order a*b and was, thus, more rapid than the growth in the unsmoothed case. As the smoothed cloud grew in size, the number of grid boxes that were not adjacent to the wake region grew relatively and absolutely. Thus the rate of decrease in the sum of the squares of the masses was smaller in the later timesteps. This reduction in the decay rate of the sum of the squares is shown in the later timesteps of figure 22. The decay rate was very high in the first 100 timesteps but dropped rapidly thereafter. The quantity was virtually constant after timestep 1000.

viii. Discussion

The smoothed version of the advection scheme gave improved results over the unsmoothed scheme. The cloud that was produced conserved mass and moved at an acceptable speed. The main flaw in the smoothed scheme was that the positive numerical diffusion was not balanced by the wake particles and thus the area weighted sum of the squares of the concentrations decreased significantly during the advection. This decrease was an indicator of the scale of the numerical diffusion introduced by finite differencing errors.

c. Nine point initialization

i. Description of initialization

In an attempt to simulate more realistic clouds, the multi-point initializations used in the unsmoothed trials were repeated. The nine point initialization was centered on gridpoint (10,26).

ii. Diagrams of advection

The results of the advection are shown below in figures

24a through 24h.

```
                10
                 1
          0     0     0     0
          0     0     3     3
       1061  1108  1126    15
       1079  1111  1128    17
25 -   1093  1108  1126    15
          0     0     3     3
          0     0     0     0
```

24a. Nine point initialization smoothed:

advection pattern at t=0001

```
                10
                 1
          0     0     0     0
          0     0     6     6
       1029  1104  1140    30
       1045  1110  1145    35
25 -   1061  1105  1140    30
          0     0     6     6
```

24b. Nine point initialization smoothed:

advection pattern at t=0002

```
                10
                 1
          0     0     0     0     0
          0     0     9     9     0
       1012  1100  1154    45     0
       1014  1108  1162    53     1
25 -   1013  1101  1154    45     0
          0     0     9     9     0
```

24c. Nine point initialization smoothed:

advection pattern at t=0003

```
                10
                 1
          0     0     0     0     0
          0     0    25    30     2
        804  1053  1239   155    10
        799  1077  1271   184    12
25 -    819  1055  1239   155    10
          0     0    26    30     3
          0     0     0     0     0
```

24d. Nine point initialization smoothed:

advection pattern at t=0010

```
                                  15
                                   |
                0     0     0     0     0     0     0
                0   125   203   155    68    18     0
              374   879   795   413   155    43     4
              380  1236  1033   530   195    54     8
25 -          380   880   798   414   156    43     4
                0   122   210   158    69    19     0
                0     0     0     0     0     0     0
```

24e. Nine point initialization smoothed:

advection pattern at t=0100

```
                                  20
                                   |
                0     0     0     0     0     0     0     0
                0   121   228   253   173    87    33     1
              188   523   613   490   321   168    70    18
              218   747   791   613   384   199    83    23
25 -          185   518   614   493   322   169    70    18
                0   117   226   254   177    88    34     2
                0     0     0     0     0     0     0     0
```

24f. Nine point initialization smoothed:

advection pattern at t=0300

```
                                        30
                                         |
                0     0     0     0     0     0     0     0     0
                9   106   201   248   221   153    85    39     6
              110   345   473   474   392   266   157    72    22
              122   461   573   547   453   317   184    87    26
25 -          107   343   474   477   397   279   159    73    22
                4    98   193   249   225   157    90    40     7
                0     0     0     0     0     0     0     0     0
```

24g. Nine point initialization smoothed:

advection pattern at t=0600

```
                        50
                         |
          0     0     0     0     0     0     0     0     0     0
         59   145   207   235   231   198   146    79    41     7
         60   225   338   388   383   334   251   151    75    23
         60   240   369   429   426   374   281   181    87    26
25 -     60   225   341   391   387   339   255   155    75    23
         62   146   210   241   238   204   153    85    42     8
          0     0     0     0     0     0     0     0     0     0
```

24h. Nine point initialization smoothed:

advection pattern at t=1440

iii. Description of advection

The concentrations in this trial formed a pattern that was very similar to the one formed in the previous trial. The major difference was during the early timesteps. The pattern immediately expanded to cover five latitudinal grid boxes in the frontal portion of the cloud, but this expansion did not occur in the rear. The expansion in the rear would have been negative and was eliminated by the smoothing algorithm. The cloud also expanded to the front and formed an arrow shaped distribution, pointing into the wind. The arrow became more and more indistinct and, by timestep 0100, the pattern had become elliptical. The latitudinal extent of the cloud remained, as before, at a constant five grid boxes. The longitudinal extent also expanded at very nearly the same rate as in the previous trial. The cloud was ten grid boxes long in this direction by the end of one day of advection. The most noticeable improvement over the one point initialization was the absence of the trailing particles at the edge of the cloud.

iv. Cross sections

Cross sections through the cloud at selected timesteps are shown below in figures 25a through 25d.

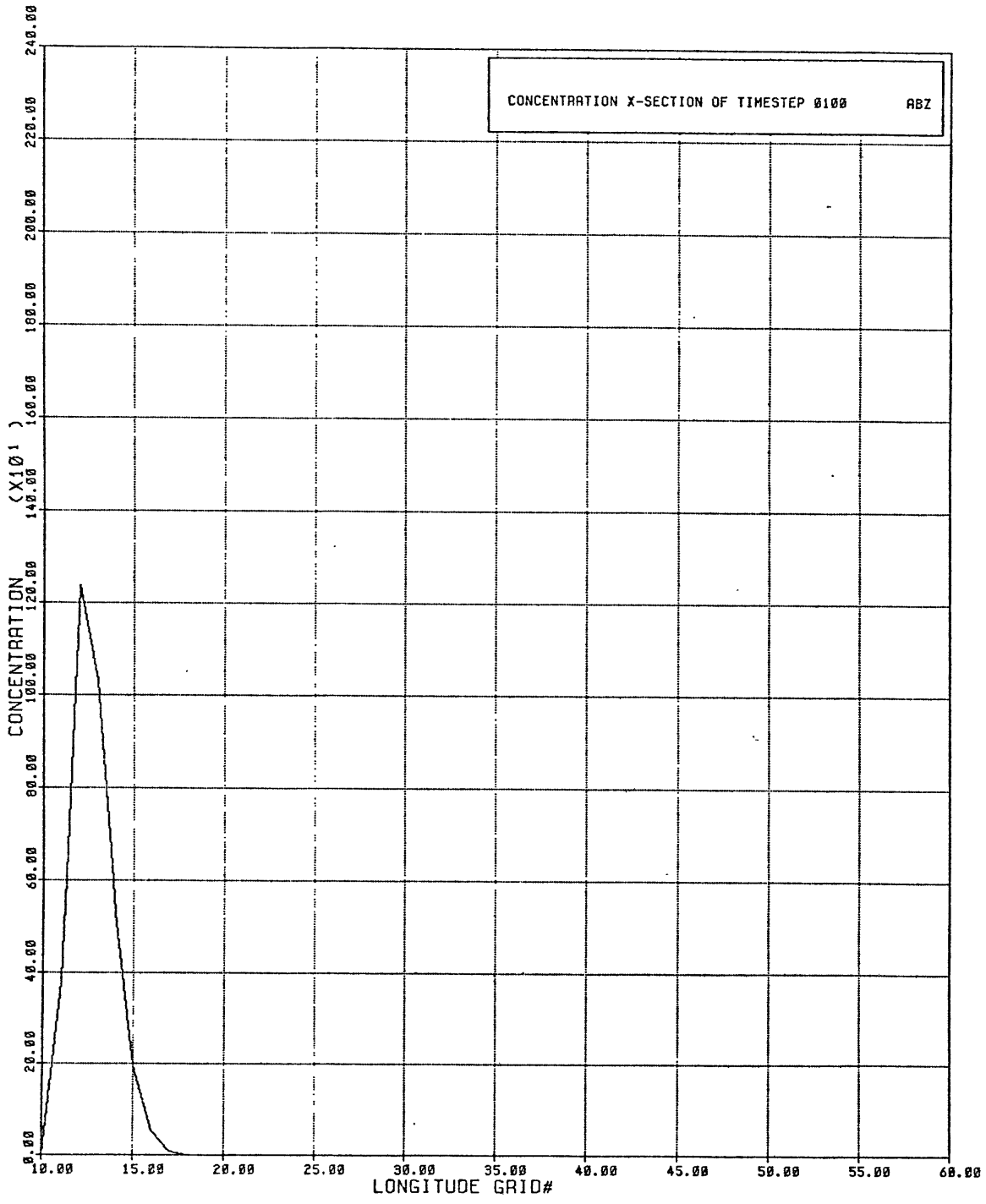

25a. Nine point initialization smoothed:

cross-section at t=0100

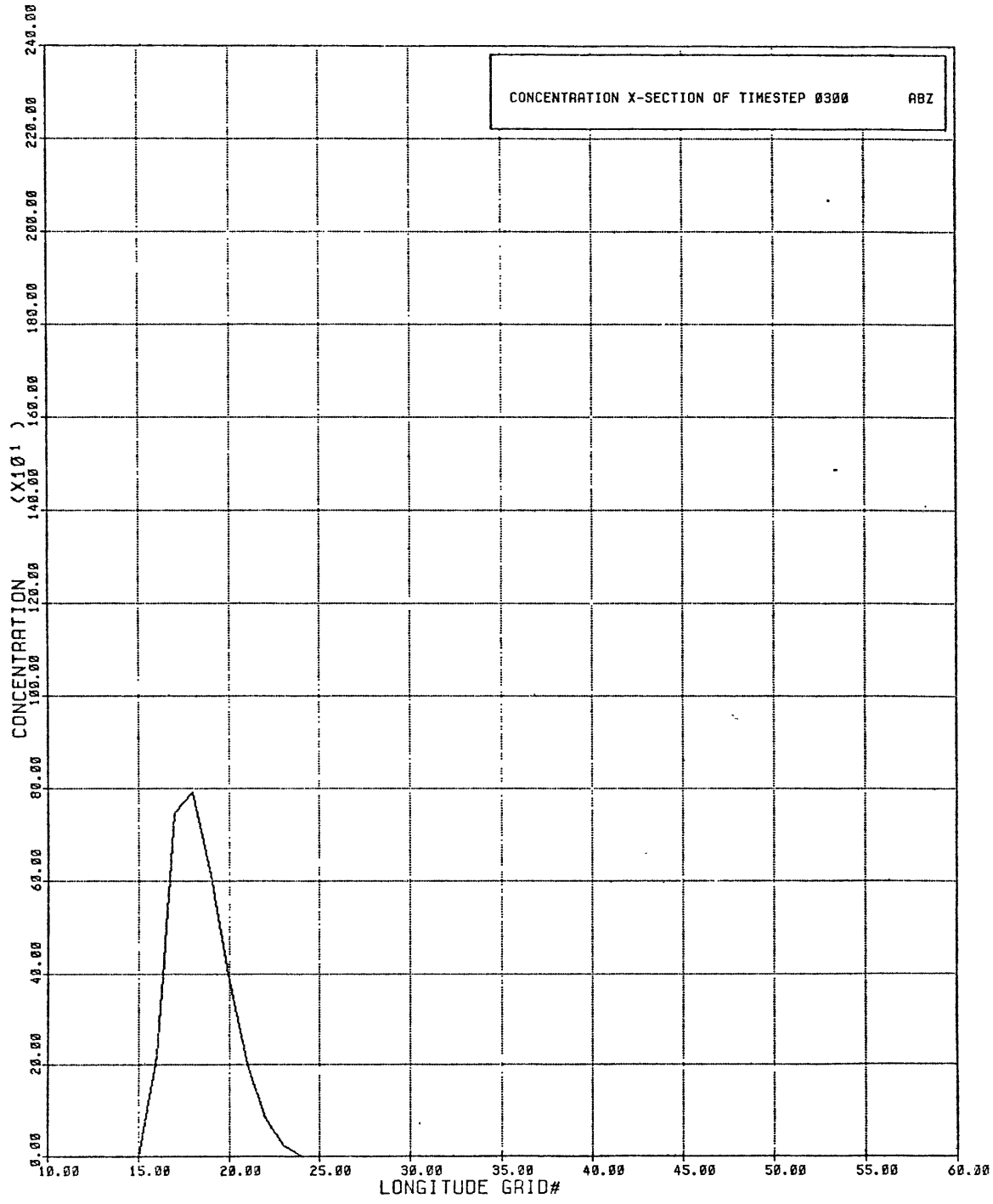

25b. Nine point initialization smoothed:

cross-section at t=0300

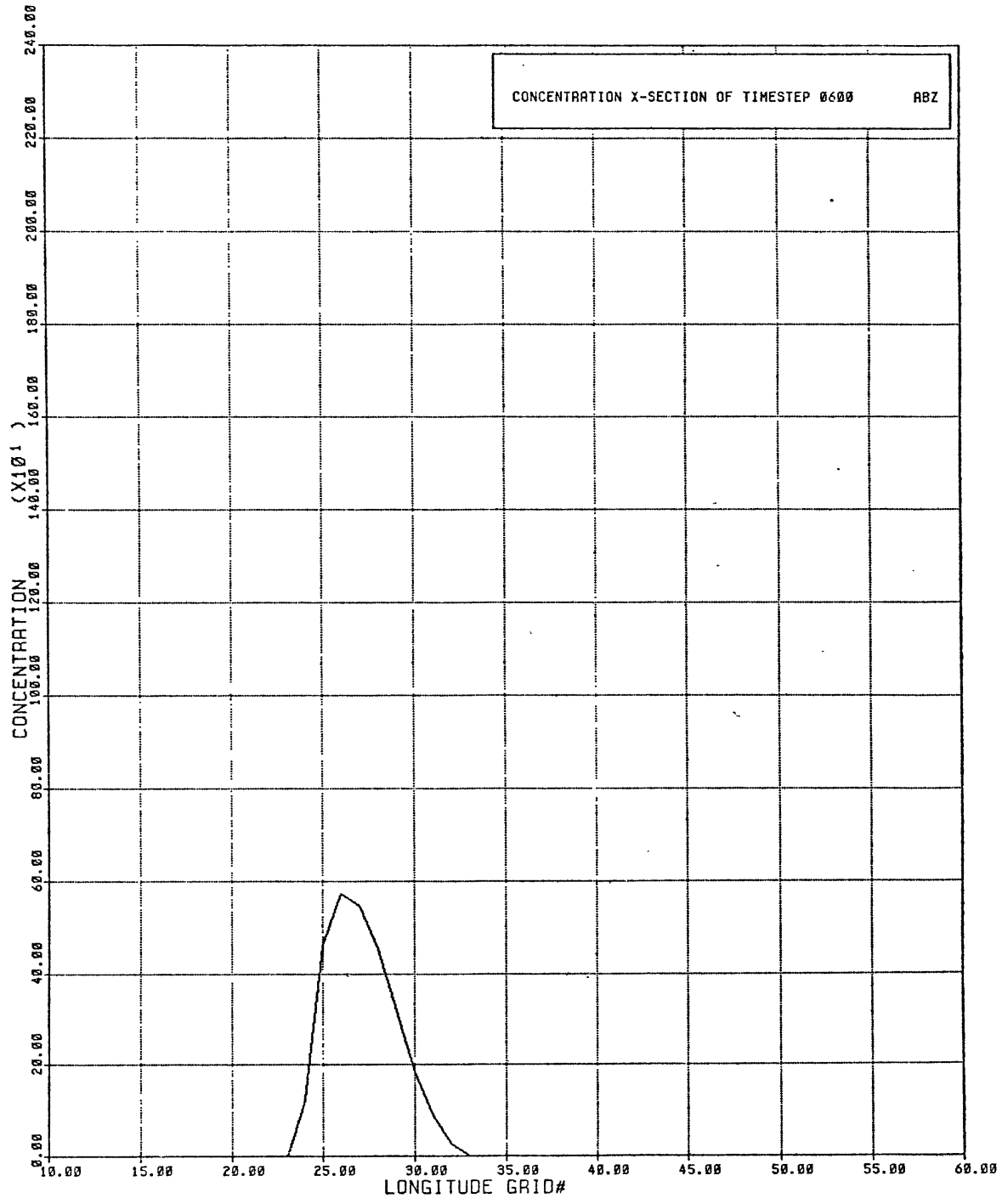

25c. Nine point initialization smoothed:

cross-section at t=0600

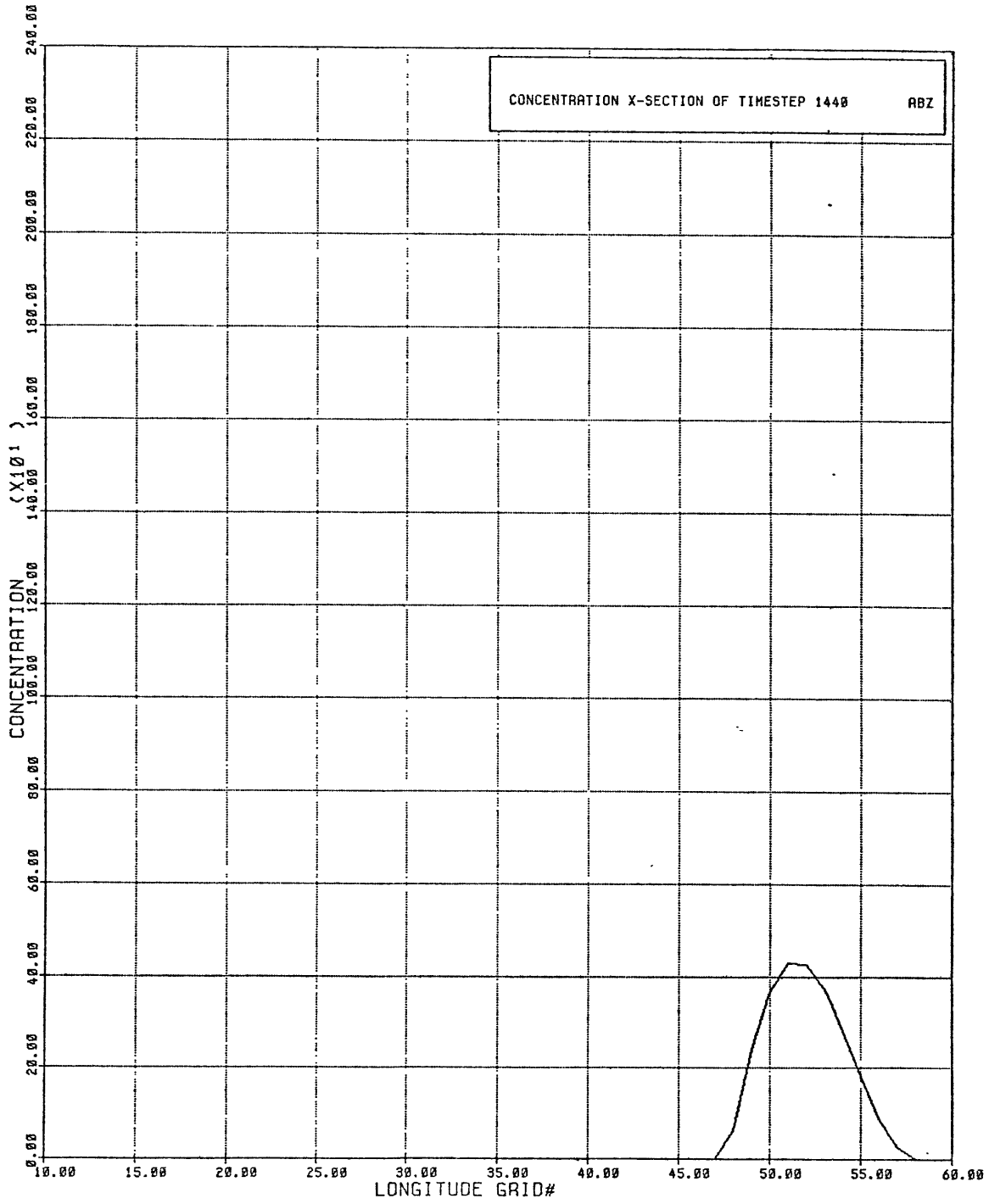

25d. Nine point initialization smoothed:

cross-section at t=1440

After the early timesteps, the cloud appeared to be very similar to the cloud produced in the previous initialization. The peak values and shape were both almost exactly the same. The peak value was slightly smaller than in the forward positive area of the nine point unsmoothed trial. This was not unexpected since the peak value at initialization was considerably smaller than in the previous trial.

v. Velocity of the cloud

The location of the centroid of the model cloud still lagged the location that would have been predicted if it had moved with the local wind velocity. The of the longitudinal location of the centroid, is shown in figure table 8, for selected timesteps.

timestep	predicted location of centroid	actual location of centroid	percentage lag
0001	10.03147	10.0206	35
0010	10.3147	10.259	18
0100	13.147	12.80	11
1000	41.47	39.0	8

Table 8: Nine point initialization smoothed: lag in the centroid

The lag was smaller than in the one point initialization, especially during the early timesteps. This was because a relatively smaller portion of the cloud was bordering the wake formation region. As with the previous trial, the percentage lag decreased to a small value after 1000 timesteps.

vi. Conservation of mass

A graph of the area weighted sum of the concentrations is shown below in figure 26.

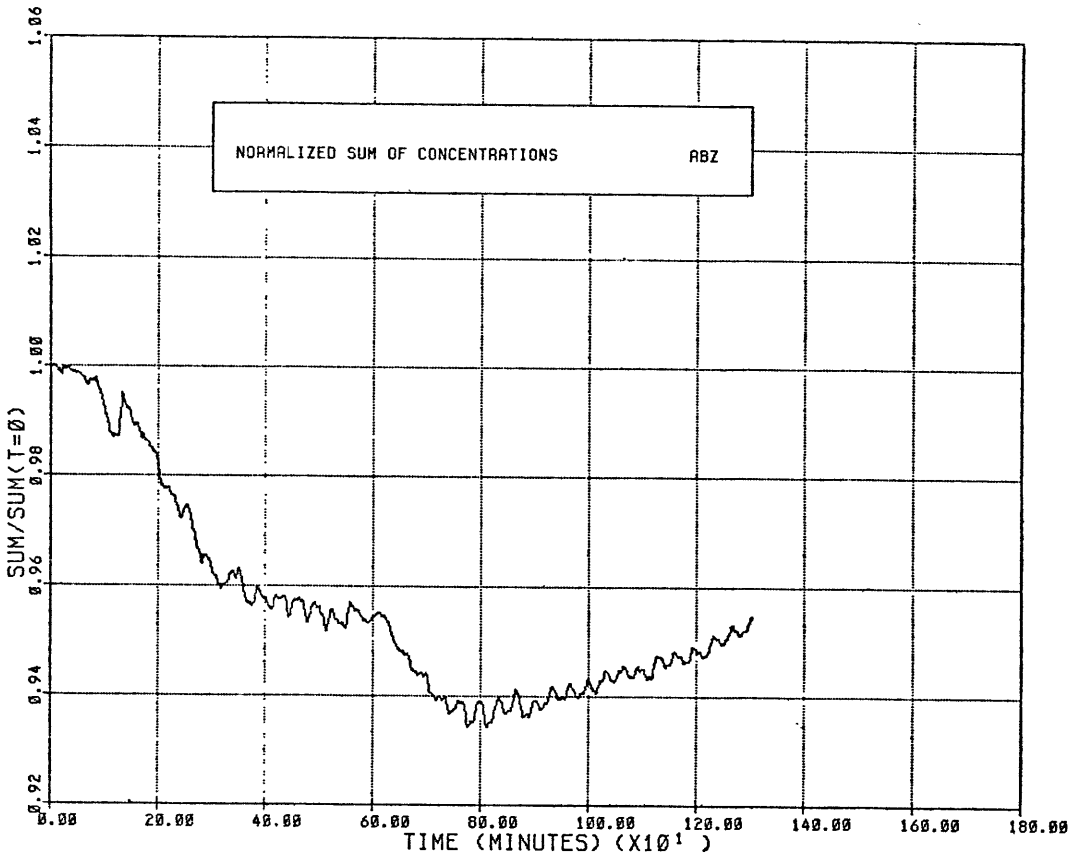

Figure 26: Nine point initialization smoothed: normalized mass

The mass of the cloud was again well preserved. Nearest integer rounding was used in this trial. The short period artifact of the smoothing was also present.

vii. Conservation of squared mass

A graph of the area weighted sum of the squares of the concentrations is shown below in figure 27.

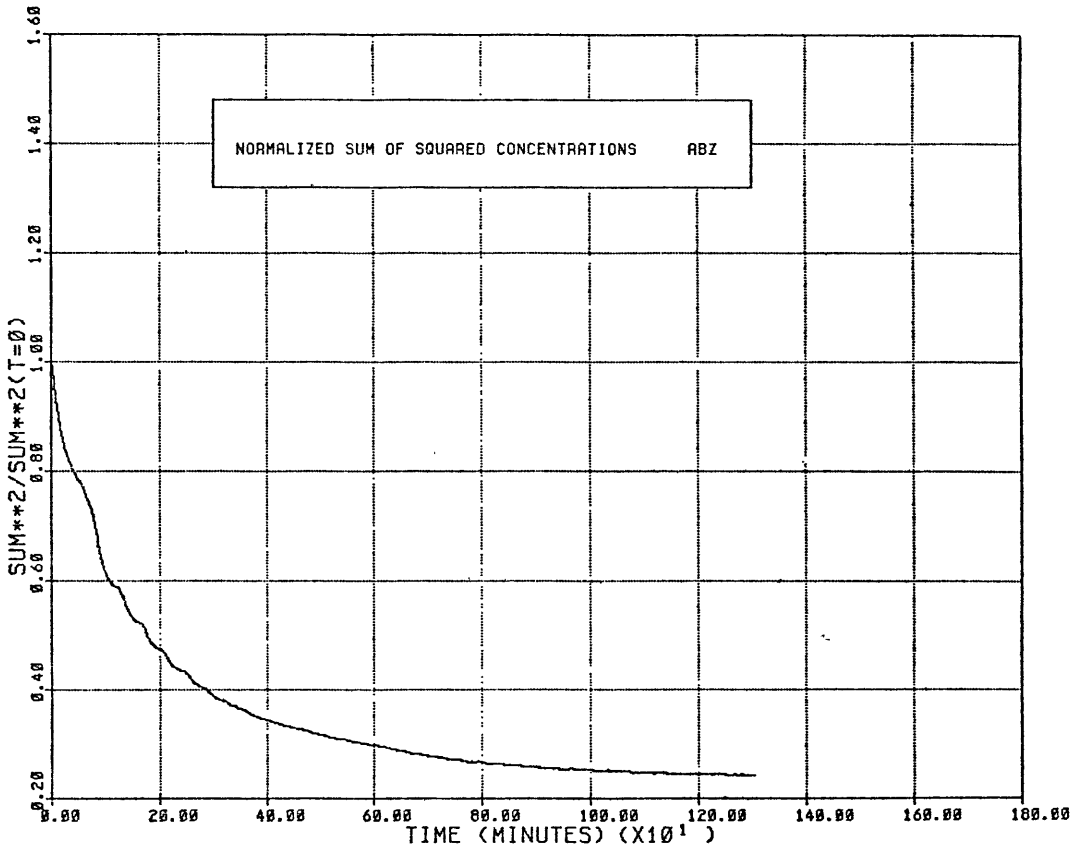

Figure 27: Nine point initialization smoothed: normalized squared mass

The squared mass dropped more slowly in this trial than in the one gridpoint initialization. This was because some of the gridpoints were removed from the high gradient regions at the lee side of the cloud where the action of the smoothing scheme was evident. The squared mass dropped sharply until about timestep 0400 and then began to level off to an, apparently, steady state value. The oscillation caused by the smoothing scheme had become a noticeable factor in the drop rate of this quantity. This oscillation was small, however, compared to the systematic drop in the squared mass.

d. Sixty-nine point initialization

i. Description of initialization

The 69 point initialization was also attempted with the smoothed scheme. The center of the initial concentration distribution was at gridpoint (11,26). The one gridpoint shift from the central location of the other smoothed initializations was for the purpose of avoiding the region near the edge of the grid. The height field produced by the interpolation scheme described in Appendix A dropped rapidly to zero in this region. The winds implied by this high gradient of height values were unrealistic and were to be

avoided.

ii. Diagrams of advection

The results of the advection are shown below in figures 28a through 28h.

				15					
	0	0	0	0	0	0	0	0	0
	0	0	1	2	4	2	1	0	0
	0	0	15	76	133	86	21	2	0
	1	13	197	951	1620	1013	241	23	1
	1	66	916	4307	7259	4499	1048	96	3
	2	111	1523	7118	11969	7400	1717	155	6
25-	1	66	915	4306	7259	4500	1049	96	3
	1	13	197	950	1620	1014	241	23	1
	0	0	15	76	133	86	21	2	0
	0	0	1	2	4	2	1	0	0
	0	0	0	0	0	0	0	0	0

28a. Sixty-nine point initialization smoothed:

advection pattern at t=0001

					79				
	0	0	1	2	4	2	1	0	0
	0	0	12	71	133	91	24	3	0
	1	9	175	919	1619	1044	263	28	1
	0	52	851	4209	7256	4594	1116	112	4
	0	90	1427	6975	11964	7540	1816	178	8
25-	0	52	850	4208	7256	4596	1117	112	4
	1	8	175	918	1619	1045	263	28	1
	0	0	12	71	133	91	25	3	0
	0	0	1	2	4	2	1	0	0

28b. Sixty-nine point initialization smoothed:

advection pattern at t=0002

					79				
	0	0	1	2	4	2	1	0	0
	0	0	9	66	132	96	28	4	0
	1	5	153	887	1617	1075	286	34	2
	0	39	787	4111	7250	4688	1185	129	6
	0	68	1333	6831	11956	7679	1917	203	10
25-	0	39	786	4109	7250	4691	1186	129	6
	1	4	153	886	1617	1076	286	34	2
	0	0	9	66	132	96	29	4	0
	0	0	1	2	4	2	1	0	0

28c. Sixty-nine point initialization smoothed:

advection pattern at t=0003

0	0	1	2	4	2	1	0	0
0	0	0	31	121	125	56	13	0
1	0	25	644	1567	1274	457	86	9
0	0	363	3400	7128	5314	1696	276	26
0	0	642	5793	11788	8601	2664	416	38
0	0	360	3396	7126	5318	1702	277	27
1	0	25	642	1566	1276	458	86	10
0	0	0	31	121	125	57	13	0
0	0	1	2	4	2	1	0	0

28d. Sixty-nine point initialization smoothed:

advection pattern at t=0010

0	0	1	2	4	0	0	0	0	13	2	0	0
0	0	0	0	0	0	7	214	279	180	75	20	0
1	0	0	0	0	0	1136	1782	1281	621	228	64	12
0	0	0	0	0	2408	5805	5388	3094	1305	436	118	23
0	0	0	0	0	2466	9269	7736	4159	1675	540	142	29
0	0	0	0	0	2388	5791	5405	3111	1317	439	118	23
1	0	0	0	0	0	1120	1789	1297	632	232	65	12
0	0	0	0	0	0	2	213	281	182	76	21	0
0	0	1	2	4	0	0	0	0	14	3	0	0

28e. Sixty-nine point initialization smoothed:

advection pattern at t=0100

0	0	0	51	103	88	61	33	4	0
0	0	179	461	507	362	201	93	28	0
0	715	1641	1826	1374	830	425	187	66	16
1012	3344	4318	3630	2404	1342	650	279	103	26
1005	5021	5679	4513	2891	1578	755	320	117	33
1011	3324	4329	3649	2428	1360	660	282	104	27
0	689	1626	1842	1392	850	436	192	69	17
0	0	166	463	523	377	210	96	30	0
0	0	0	48	103	89	62	34	6	0

28f. Sixty-nine point initialization smoothed:

advection pattern at t=0300

0	0	0	65	173	231	195	135	74	36	5	0
0	0	126	508	728	674	505	321	180	83	27	0
0	334	1163	1740	1687	1338	914	555	305	146	57	12
206	1655	2925	3146	2699	1985	1296	765	412	200	81	22
189	2520	3732	3789	3147	2272	1461	854	456	219	90	24
214	1621	2920	3157	2723	2007	1317	780	420	205	84	23
0	308	1122	1739	1714	1366	940	576	318	154	61	14
0	0	101	490	732	691	523	335	190	90	30	0
0	0	0	57	167	235	203	143	82	39	9	0

28g. Sixty-nine point initialization smoothed:

advection pattern at t=0600

0	0	23	147	267	335	302	237	173	108	57	25	0	0
0	102	415	733	834	794	673	511	347	219	120	54	15	0
105	616	1189	1437	1430	1267	1024	761	523	334	190	90	29	0
366	1279	1843	2030	1928	1654	1304	955	654	416	240	123	46	6
374	1513	2093	2275	2127	1808	1419	1036	710	452	265	135	53	9
379	1248	1826	2036	1953	1684	1335	982	674	431	252	129	50	8
69	539	1135	1447	1463	1305	1065	803	560	359	210	102	34	1
0	57	353	696	842	821	707	546	385	249	141	66	21	0
0	0	0	112	244	328	318	254	190	126	64	32	0	0

28h. Sixty-nine point initialization smoothed:

advection pattern at t=1440

iii. Description of advection

The advection pattern, in this trial, initialized as a cloud of considerable extent, was qualitatively quite similar to the other initializations. The pattern did not exhibit any of the immediate spreading that was evident in the previous trials. The latitudinal extent of the cloud remained constant at the nine gridpoints of the initialization. The longitudinal extent grew slowly from nine to fourteen gridpoints by the end of one day. The trailers were again present. They arose at the lee edge and at the north and south edges of the cloud. They formed because there were regions of very low gradients of concentration in the initialization. The concentrations in these regions were not advected and were left behind as trailers. Any advection in this region was lost to the truncation error introduced by the integer arithmetic. This trial was calculated with a more primitive version of the smoothing algorithm which could not eliminate all of the trailers. In order to conserve space, they have been left off of the above diagrams when the cloud has left them far behind.

iv. Cross-sections

Cross sections through the cloud at selected timesteps

are shown below in figures 29a through 29d.

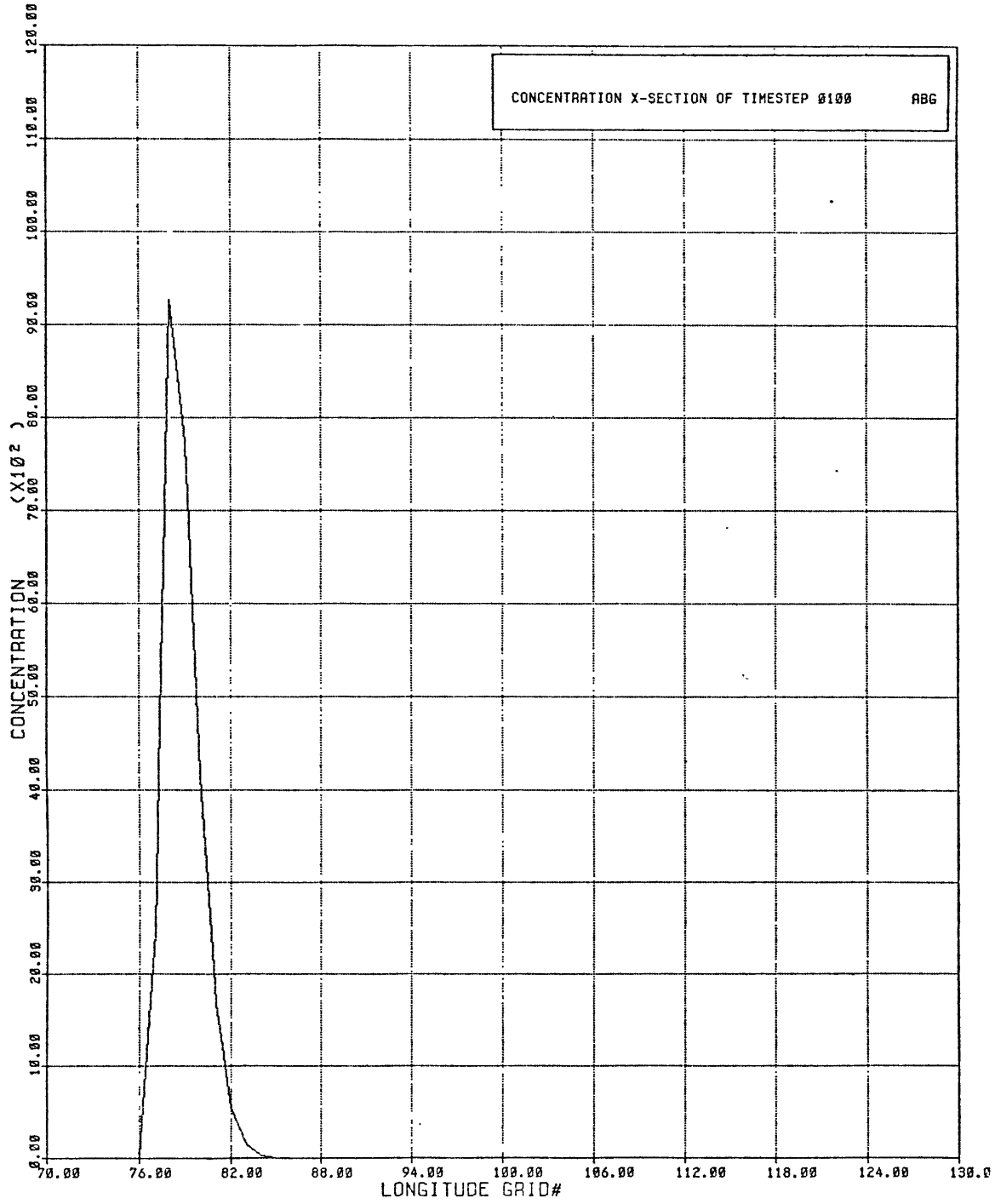

29a. Sixty-nine point initialization smoothed: cross-section at t=0100

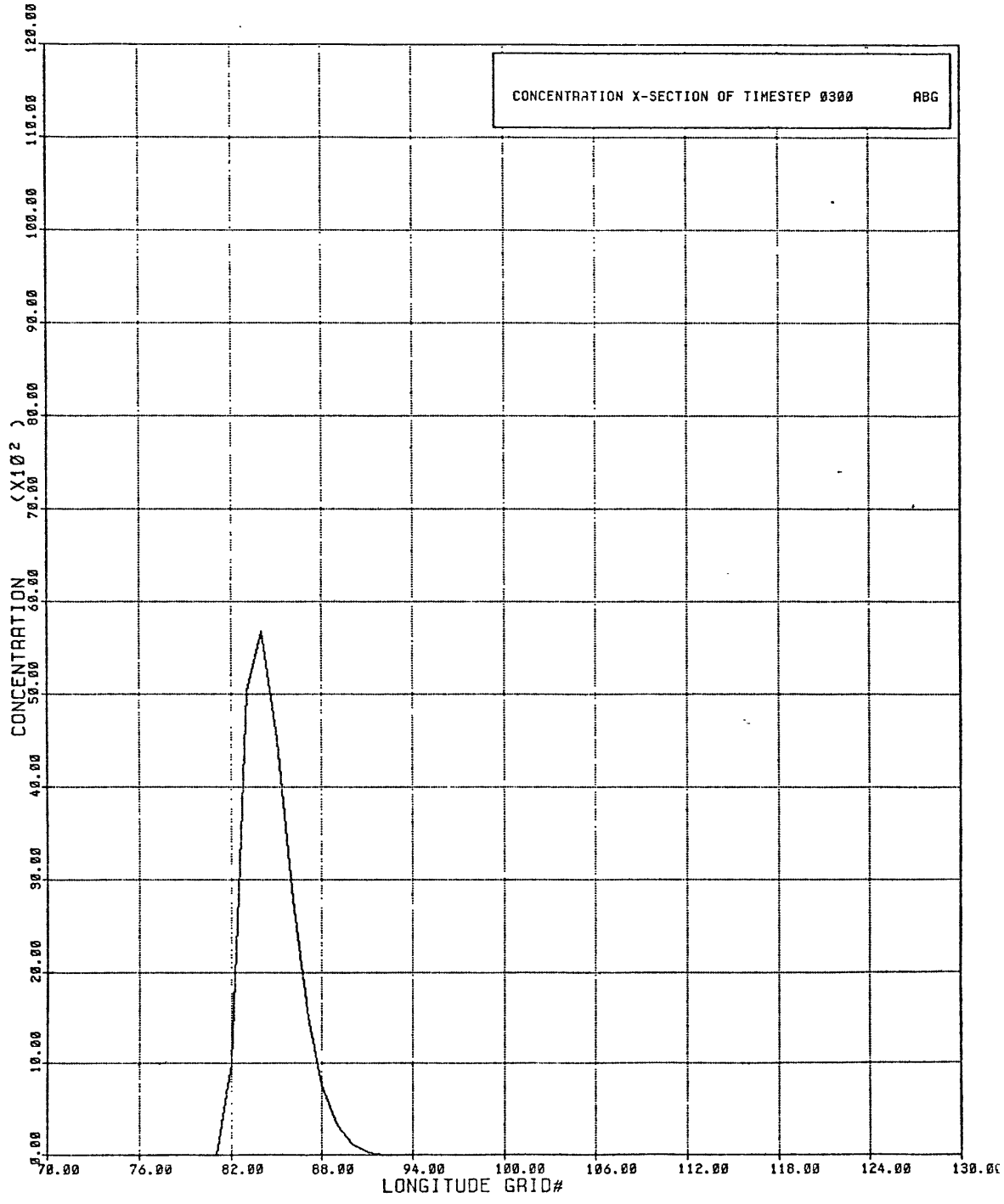

29b. Sixty-nine point initialization smoothed:

cross-section at t=0300

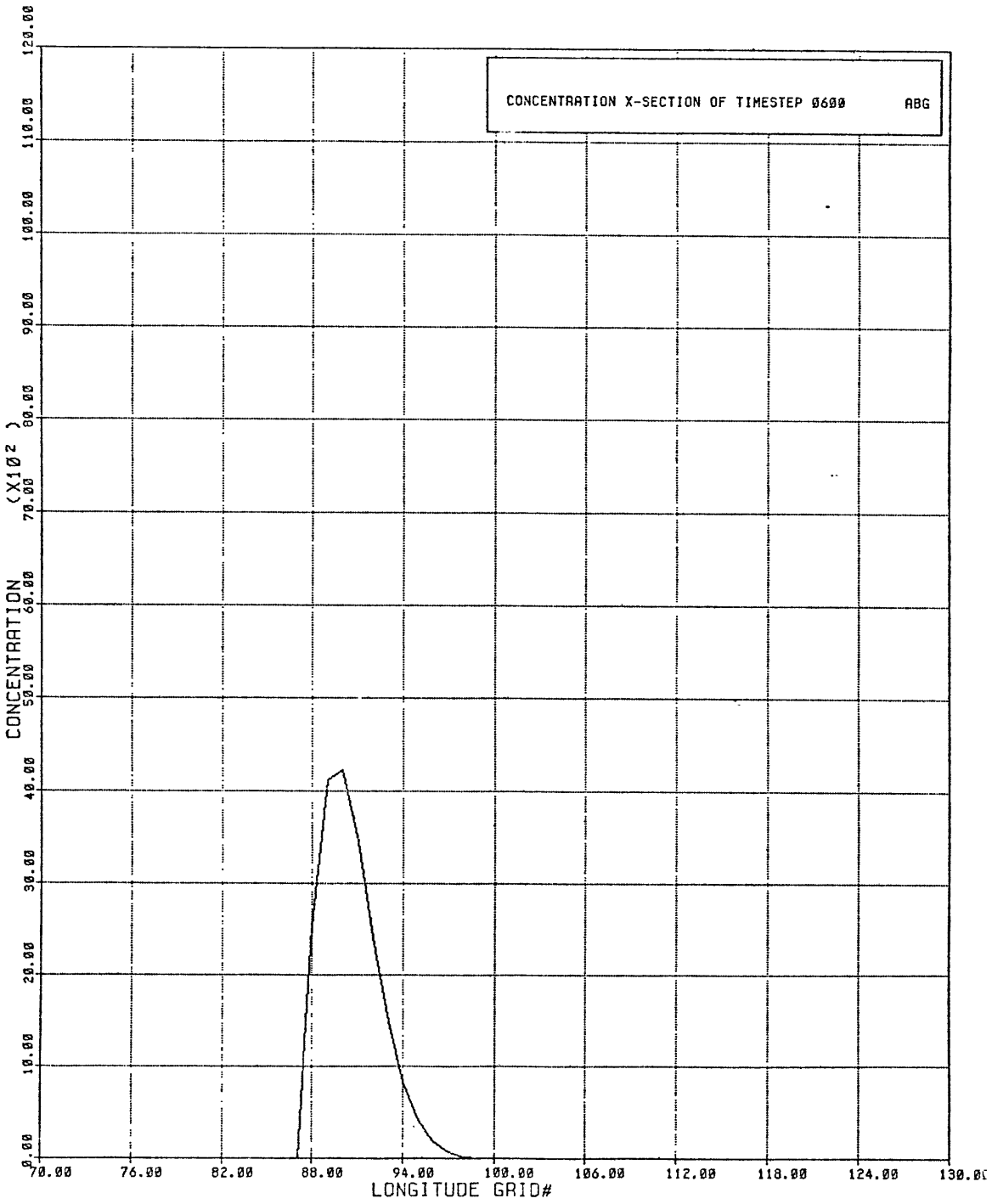

29c. Sixty-nine point initialization smoothed:

cross-section at t=0600

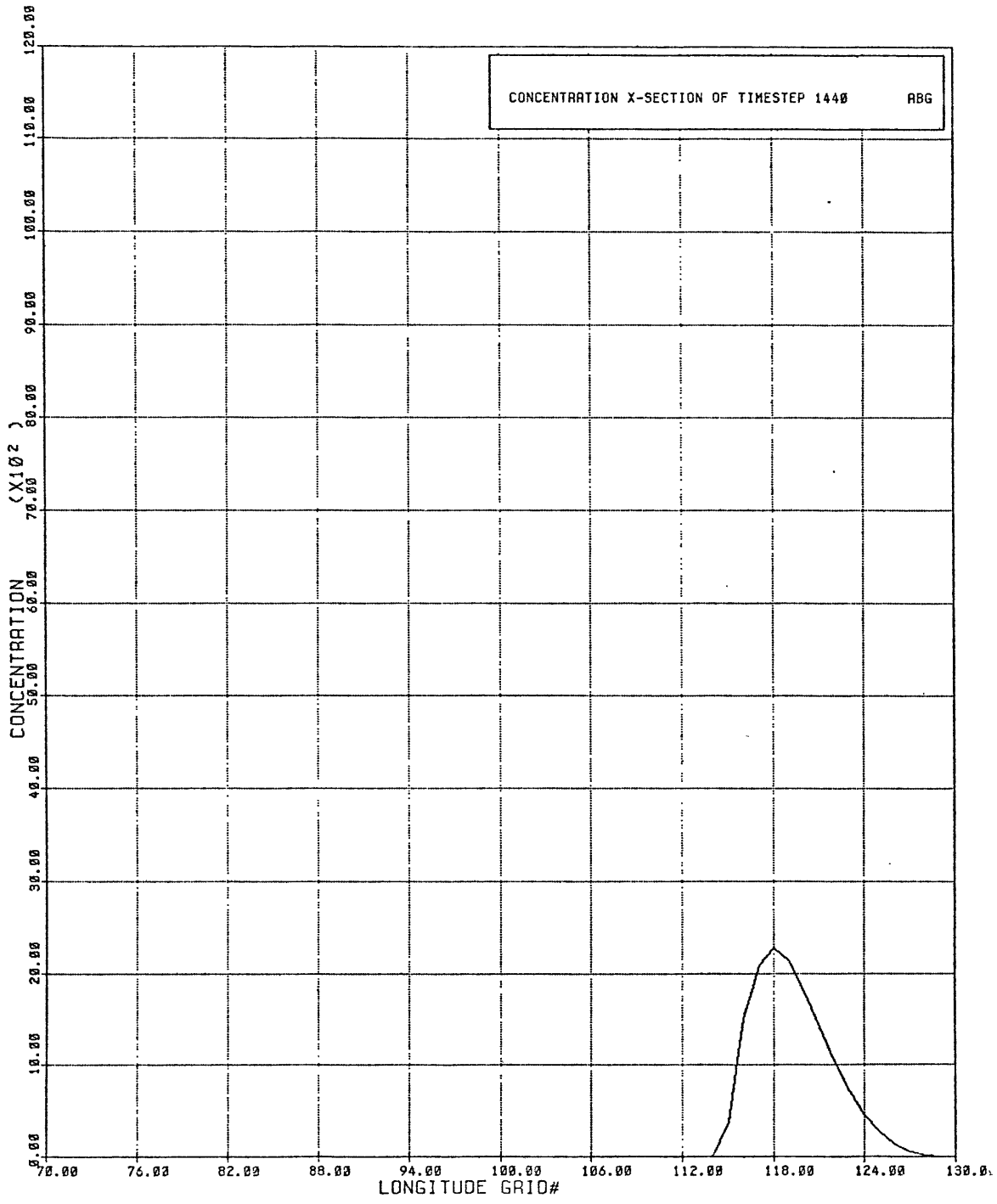

29d. Sixty-nine point initialization smoothed:

cross-section at t=1440

v. Velocity of the cloud

The lag in the location of the cloud caused by the elimination of the negative wake was sharply reduced. With the 69 point initialization, the values in the negative wake that were eliminated were very small when compared to the main cloud values. A table showing the lag at selected timesteps is shown below in table 9.

timestep	predicted location of centroid	actual location of centroid	percentage lag
0001	76.03147	76.03125	0.7
0010	76.3147	76.311	1
0100	79.147	78.953	6
1000	107.47	106.14	4

Table 9: Sixty-nine point initialization smoothed: lag in the centroid

The lag in the early timesteps grew from a negligible value to a few percent. The reason for this growth was the elimination of the buffer of small concentrations at the lee end of the cloud that suppressed wake formation and thus the lags that were due to wake elimination. By timestep 0100, the lee end of the cloud contained large concentrations and wake elimination had noticeable effects on the speed of the cloud.

As before, as the cloud spread in the longitudinal direction, the fraction of grid boxes exposed to the wake elimination shrank and the cloud began to attain the predicted velocity and close the percentage gap between its actual and predicted locations.

vi. Conservation of mass

A graph of the area weighted sum of the concentrations is shown below in figure 30.

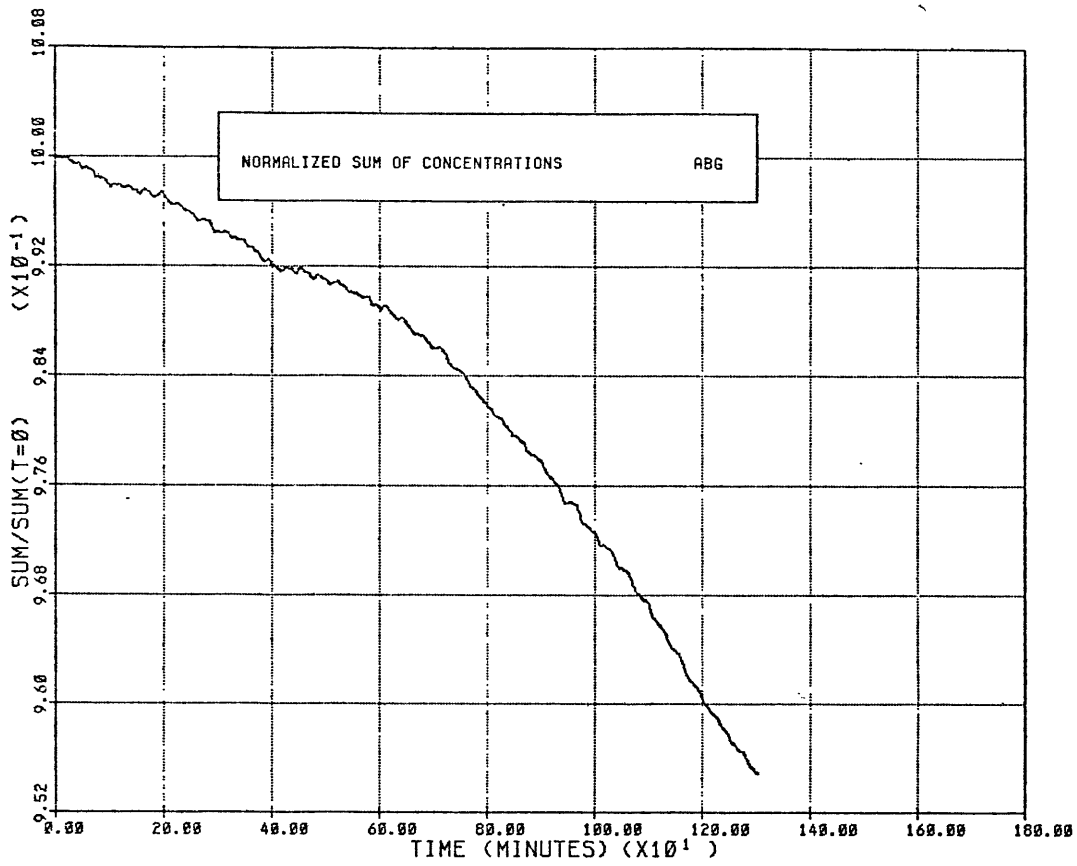

Figure 30: Sixty-nine point initialization smoothed: normalized mass

The mass in this trial was lost slowly through truncation error. The model in this trial used truncation rounding in some of its integer arithmetic. However, the mass is still fairly well conserved.

vii. Conservation of squared mass

A graph detailing the time history of the area weighted sum of the squares of the concentrations is shown below in figure 31.

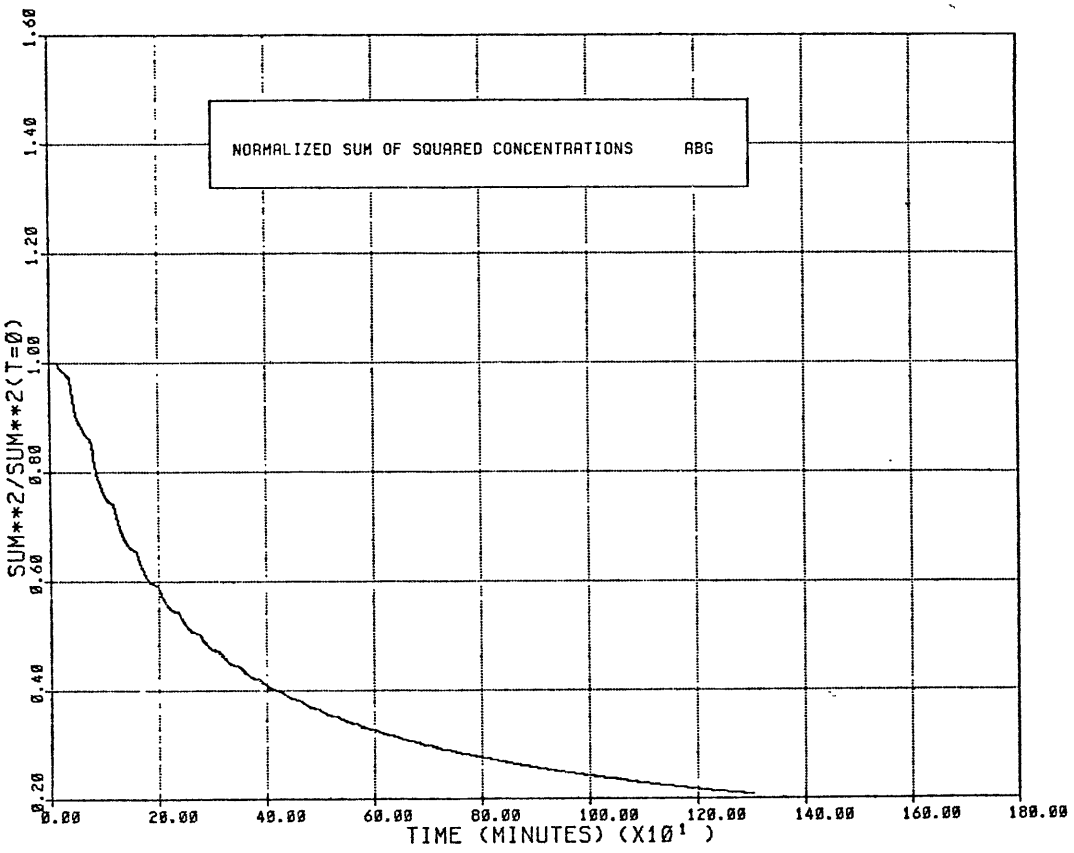

Figure 31: Sixty-nine point initialization smoothed: normalized squared mass

The squared mass decreased, as in the other smoothed trials, rapidly at first. The rate of decrease became smaller in later timesteps and the value approached an, apparently, steady state of about one fifth of the value at initialization. The oscillations caused by the elimination of trailers by the smoothing scheme were very evident in this trial. They were still small compared to the general downward trend in the squared mass.

3. Trial with deposition

a. Discussion

The eventual goal of this advection model is to predict the amount of fallout that would reach the ground after a nuclear explosion. In order to test the model's predictions for such deposition, a trial that incorporated a scheme for this deposition was attempted.

b. Description of deposition scheme

The deposition scheme that was used in this diagnostic trial was very crude. The scheme assumed that the particles in a grid box were uniformly distributed with respect to height up to the level at which the advection was calculated. In this particular case, the concentration of particles was assumed to have been constant from the ground up to the 30000 Pa level. The scheme then assumed that the particles were all falling at a single mean terminal velocity, v_f. In a certain amount of time, all particles in the lowest $v_f * \Delta t$ meters of the cloud fell and were deposited on the ground. The scheme then assumed that the concentration field instantly readjusted so that the concentration was again independent of height. This assumption essentially defined an infinite vertical

diffusion constant. The process just described is detailed in the diagram below in figure 32.

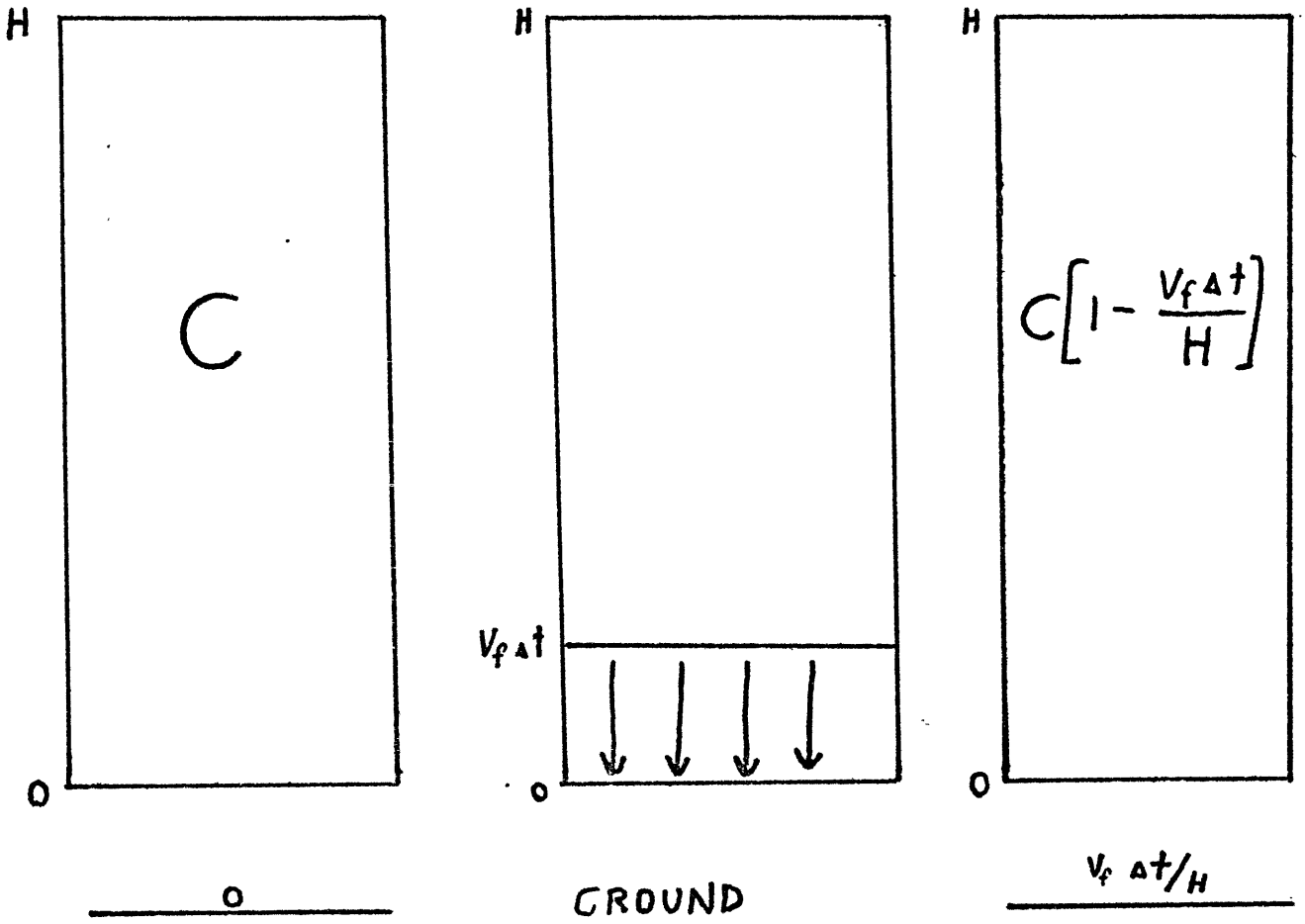

Figure 32: Process of deposition

While this deposition scheme made some rather unrealistic assumptions, it lead immediately to a simple modification of the advection equations that permitted direct computation of the deposition on the ground. If (16) is modified to account for the drop in concentration after the readustment of the

concentration field, the result is:

$$\frac{DC}{Dt} = \frac{dC}{dt} - \frac{g\,P}{2\,om\,\sin(th)\,R_e\,p\,\cos(th)\,r\,T} J(C,z) = \frac{v_f\,C}{H} \qquad (36)$$

where H is the vertical depth of the cloud. Computationally, this modification just indicates that a certain fixed fraction of the concentration in a grid box is deposited on the ground each timestep. Thus the concentrations in the model cloud should tend to decay in an exponential manner.

c. Description of initialization

The cloud was initialized using the 69 point pattern of concentrations. The center of the cloud was at gridpoint (11,26)

d. Deposition parameters

The model removed a fraction of the concentration in each grid box each timestep and placed it in a corresponding grid box representing the ground. The fraction was determined by the last term in the equation above. The values of the constants were set at H=9300 meters which was a typical height

value in the height field, and v_f =.48 m s-1. The value for the velocity was taken from Glasstone (1977). It is the approximate value for the particles that carry the bulk of the radioactivity from an explosion. Thus, in every timestep, (C)*(.48m s-1)*(60s timestep-1)/(9300 m) = .003*C was placed on the ground and .997*C remained in the atmosphere to be advected. The model used integer arithmetic to calculate the remaining concentration in the cloud and used floating point arithmetic to calculate deposition. The floating point arithmetic was used for the deposition because many of the deposited amounts were small and the computational cost in time caused by the use of the floating point arithmetic was small compared to the time required for the advectional calculations.

e. Diagrams of advection

The results of the advection are shown below in figures 33a through 33h.

10

	0	0	1	2	4	2	1	0	0
	0	0	15	76	133	86	21	2	0
	1	13	196	948	1615	1010	240	23	1
	1	66	913	4294	7237	4486	1045	96	3
	2	111	1518	7097	11932	7378	1712	155	6
25 -	1	66	912	4293	7237	4487	1046	96	3
	1	13	196	947	1615	1011	240	23	1
	0	0	15	76	133	86	21	2	0
	0	0	1	2	4	2	1	0	0

33a. Trial with deposition:

advection pattern at t=0001

```
                                10
                                 |
      0     0     1     2     4     2     1     0     0
      0     0    12    71   133    91    24     3     0
      1     9   173   913  1609  1038   261    28     1
      0    52   845  4184  7212  4567  1109   112     4
      0    90  1419  6934 11892  7495  1806   177     8
25 -  0    52   844  4182  7212  4568  1111   112     4
      1     9   173   912  1609  1039   261    28     1
      0     0    12    71   133    91    24     3     0
      0     0     1     2     4     2     1     0     0
```

33b. Trial with deposition:

advection pattern at t=0002

```
                                10
                                 |
      0     0     1     2     4     2     1     0     0
      0     0     9    66   132    96    28     4     0
      1     5   152   878  1602  1065   282    34     2
      0    39   779  4074  7184  4647  1173   129     6
      0    68  1322  6771 11848  7610  1900   201    10
25 -  0    39   778  4072  7184  4648  1176   129     6
      1     5   151   877  1602  1067   283    34     2
      0     0     9    66   132    96    28     4     0
      0     0     1     2     4     2     1     0     0
```

33c. Trial with deposition:

advection pattern at t=0003

```
                                10
                                 |
      0     0     1     2     4     2     1     0     0
      0     0     0    31   121   125    56    13     0
      1     0    26   625  1518  1236   443    85     9
      0     0   352  3299  6916  5157  1645   271    26
      0     0   625  5623 11439  8347  2586   404    38
25 -  0     0   351  3294  6915  5161  1651   271    26
      1     0    25   623  1517  1238   444    86     9
      0     0     0    31   121   125    56    13     0
      0     0     1     2     4     2     1     0     0
```

33d. Trial with deposition:

advection pattern at t=0010

```
                                      15
                                       |
      1     2     4     2     0
      0     0     0     0    20   169   216   145    61    17     0
      0     0     0     0   854  1319   950   464   179    53     9
      0     0     0  1781  4294  3992  2291   967   327    95    18
      0     0     0  1831  6866  5733  3087  1244   406   116    23
25 -  0     0     0  1769  4278  4005  2306   974   328    97    18
      0     0     0     0   844  1332   960   472   182    54     9
      0     0     0     0    18   166   218   150    62    17     0
      1     2     4     2     0
```

33e. Trial with deposition:

advection pattern at t=0100

```
                                  20
                                  |
          0     0   103   195   195   161    95    42    11     0
          0   293   724   749   555   339   192    93    31     0
        402  1369  1774  1479   973   542   271   138    55    11
        402  2044  2308  1838  1173   636   311   155    62    14
25-     408  1363  1780  1496   981   548   274   139    56    11
          0   279   715   755   560   343   195    95    32     0
          0     0    98   191   195   164    98    44    13     0
```

33f. Trial with deposition:

advection pattern at t=0300

```
                                  30
                                  |
          0    32   114   165   166   150   117    84    51    18     0
          0    83   264   300   261   192   166   141    96    38     5
         35   269   488   538   440   288   180   166   126    60    15
         32   421   629   646   530   334   196   166   135    69    18
25-      36   261   489   540   446   293   181   166   127    61    15
          0    71   258   302   265   197   166   145   100    39     6
          0    27   109   163   166   152   119    86    53    20     0
```

33g. Trial with deposition:

advection pattern at t=0600

```
                          50                                        60
                          |                                         |
   31    22    17    43   77    87    84    82    80    79    77   76   45   12    0
    0     0     6    40   82   115   122   121   120   119   118  105   72   38    5
    0     0     0    18   82   139   166   166   166   166   165  157  123   64   19
    0     0     0    10   67   134   166   166   166   166   166  166  144   79   24
25- 0     0     0    18   81   139   166   166   166   166   166  161  127   67   20
    0     0     6    42   83   116   124   122   122   121   120  108   75   41    8
   29    21    16    46   80    91    89    88    86    85    83   82   50   17    0
```

33h. Trial with deposition:

advection pattern at t=1440

f. Description of advection.

The advection pattern was very similar to the smoothed advection of the 69 point initialization. The major difference was due to the loss of particles to the ground. The concentrations decreased significantly, and by the later timesteps, the cloud had lost most of its mass (see section h). The latitudinal extent of the cloud decreased to seven gridpoints. This was due to the failure of the cloud to refill the northern and southern layers that were left empty when trailers were left behind. The smaller total concentration in this cloud was the reason why this trial did not fill these layers where the nondepositing trial did. During later timesteps, the cloud began to develop a line of trailers that were left behind. The smoothing scheme was not aggressive enough to eliminate these lines and, thus, they persisted and formed a long trail behind the main cloud.

The most notable problem in the advection pattern was the end of particle loss due to deposition in the later timesteps. The concentrations in the center of the cloud did not fall below 166 units and eventually a large number of grid boxes attained this same minimum value. This problem can be attributed directly to the integer arithmetic that was used to calculate the concentrations that remained in the cloud after

the deposition. When a grid box contained 166 units of concentration, the resulting deposition was .498 units. The remaining cloud concentration was corrected to 166 - .498 = 165.502 units, which was rounded up to 166 units. Thus, the concentration never could never drop below 166 units except through numerical diffusion in the advection scheme. This diffusion was a very slow process in the later timesteps.

g. Cross-sections

Cross sections through the cloud are shown for selected timesteps in figures 34a through 34d.

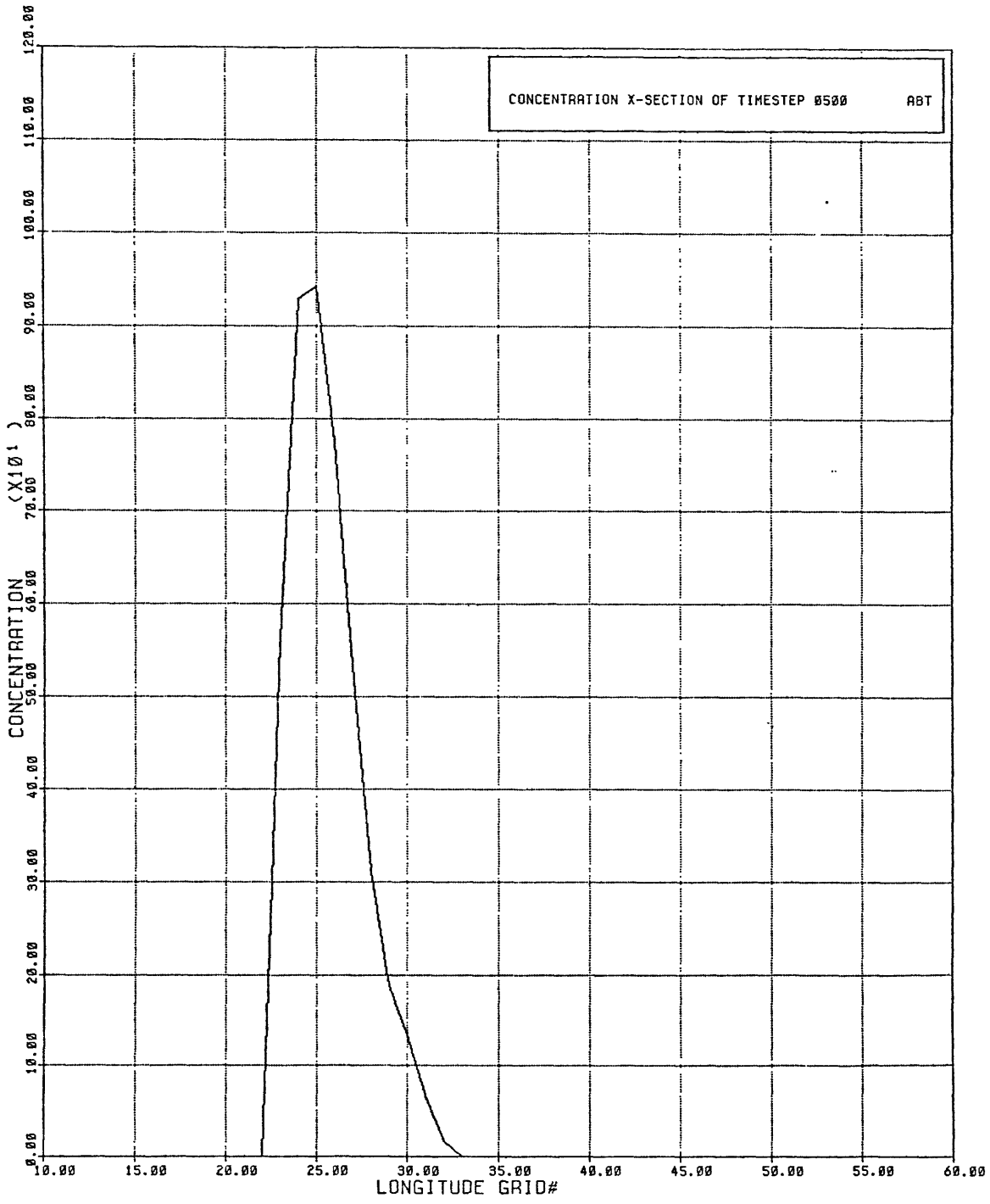

34a. Trial with deposition:

cross-section at t=0500

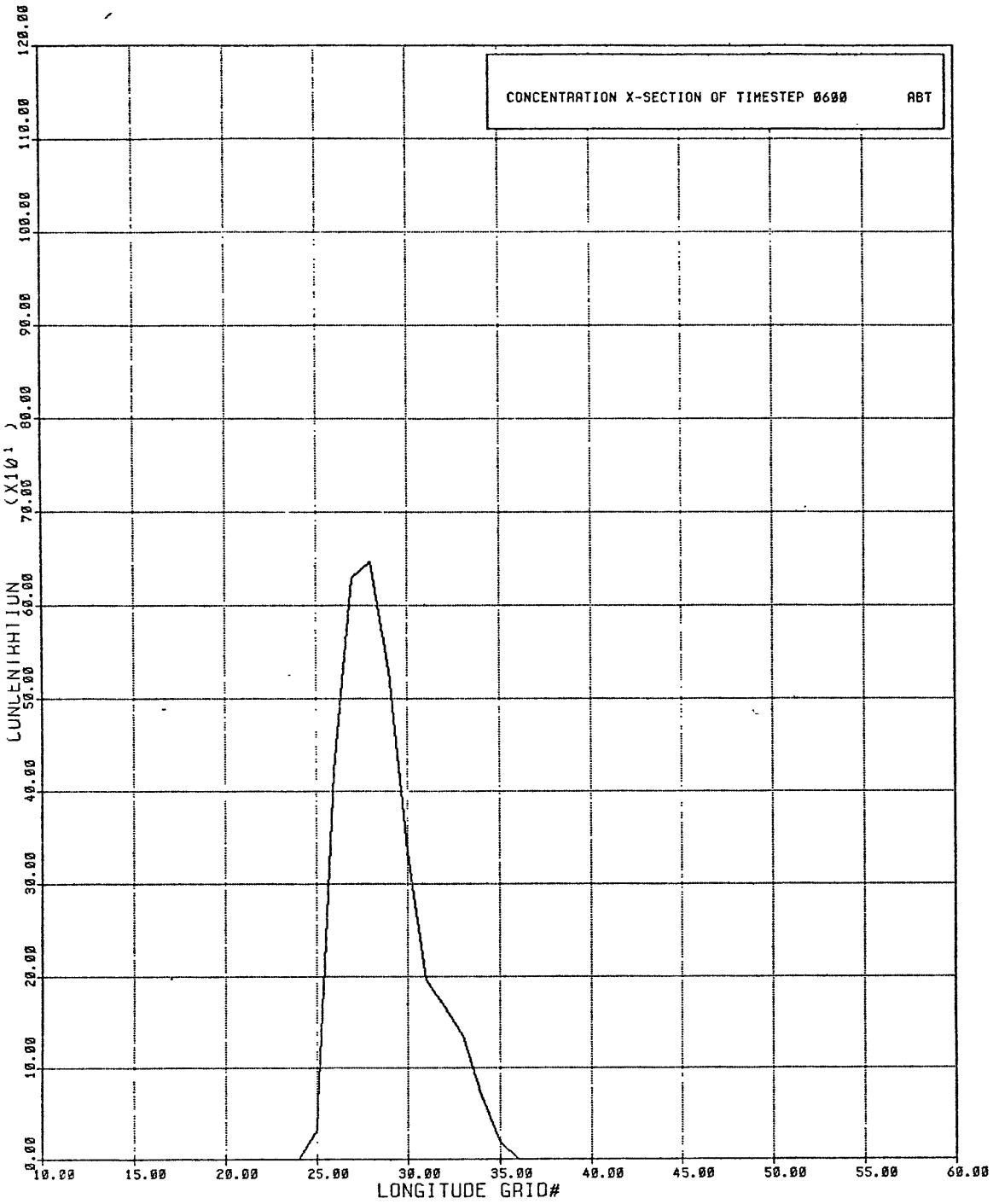

34b. Trial with deposition:

cross-section at t=0600

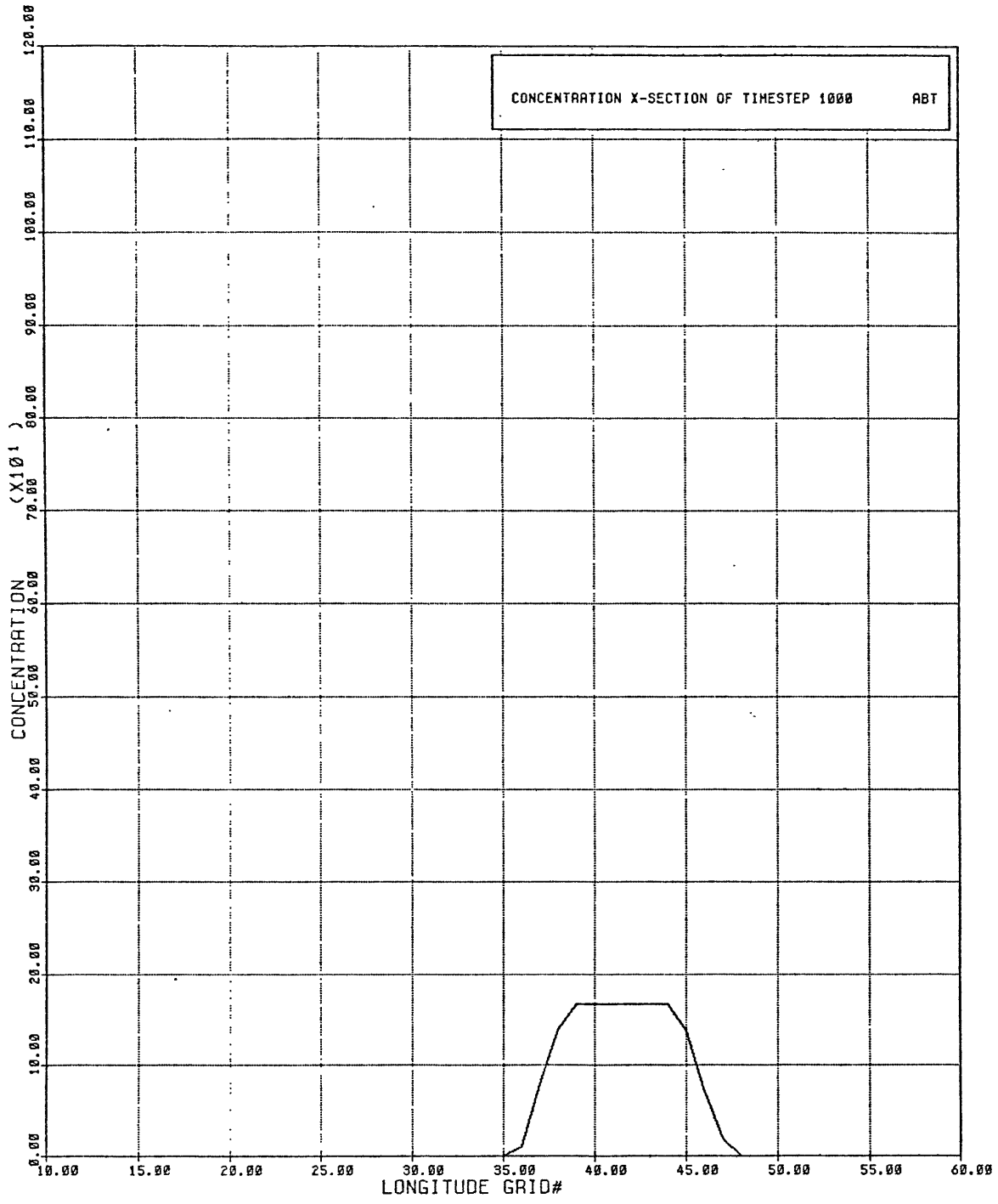

34c. Trial with deposition:

cross-section at t=1000

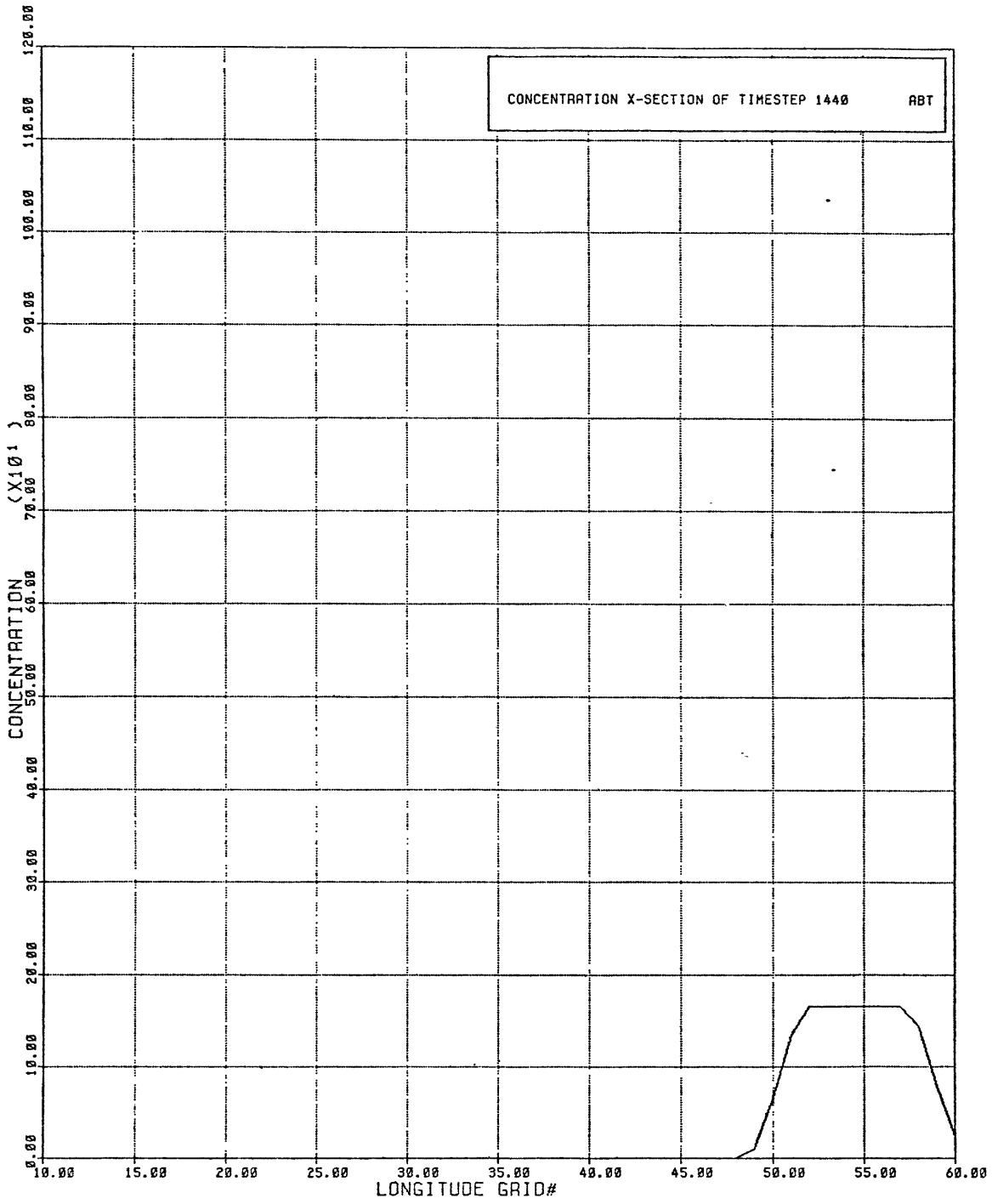

34d. Trial with deposition:

cross-section at t=1440

These cross sections show a cloud that was very similar in shape to the case with no deposition. The exception was the development of the cutoff that was at 166 concentration units. This flat region was kept high by the rounding errors just described in section f.

h. Conservation of mass

The deposition scheme removed a fixed fraction of the concentration from each grid box during each timestep. As was expected, this caused the sum of the area weighted concentrations to drop exponentially until the integer truncation error halted the loss of particles from the cloud. From that point on, mass was almost perfectly conserved. This pattern is shown in figure 35.

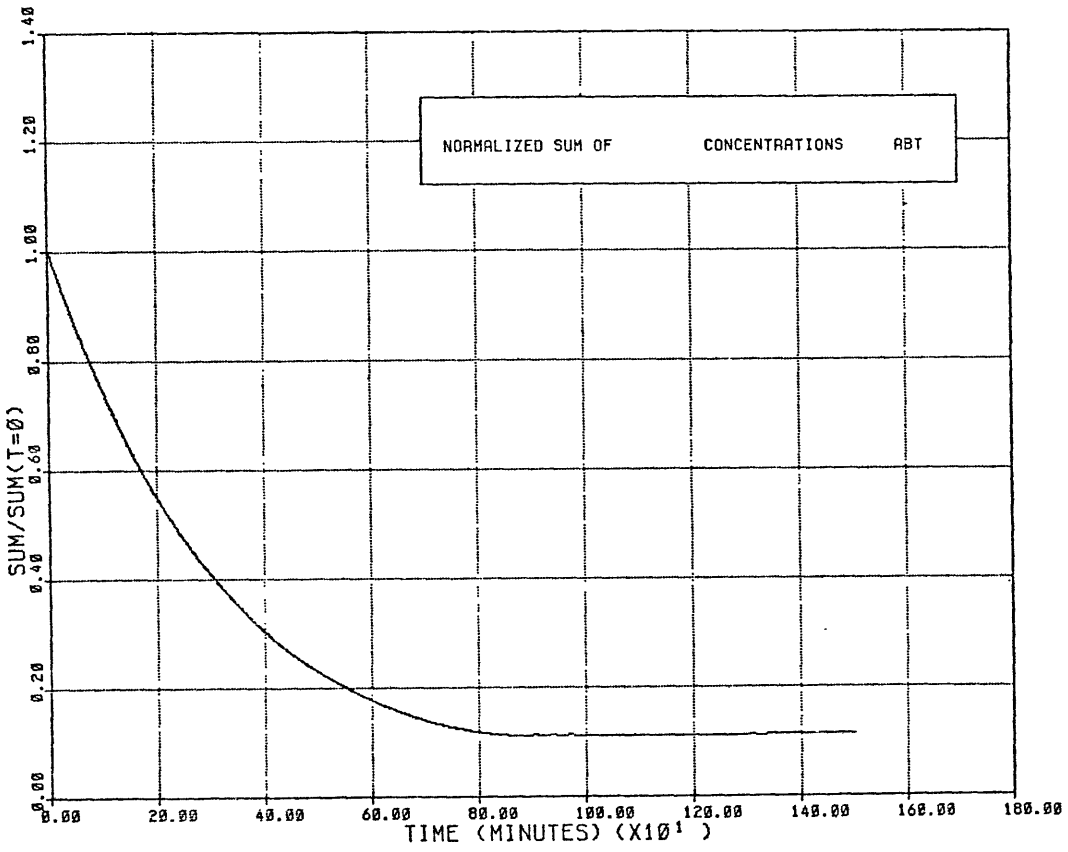

Figure 35: Trial with deposition: normalized mass

i. Conservation of squared mass.

The area weighted sum of the squared concentrations decreased rapidly. This was a result of diffusion and the loss due to deposition. The almost steady state value that was approached in the later timesteps was about three orders of magnitude lower than the value at initialization. The steady state was reached as diffusion and deposition stopped in the later timesteps. This pattern is shown in figure 36.

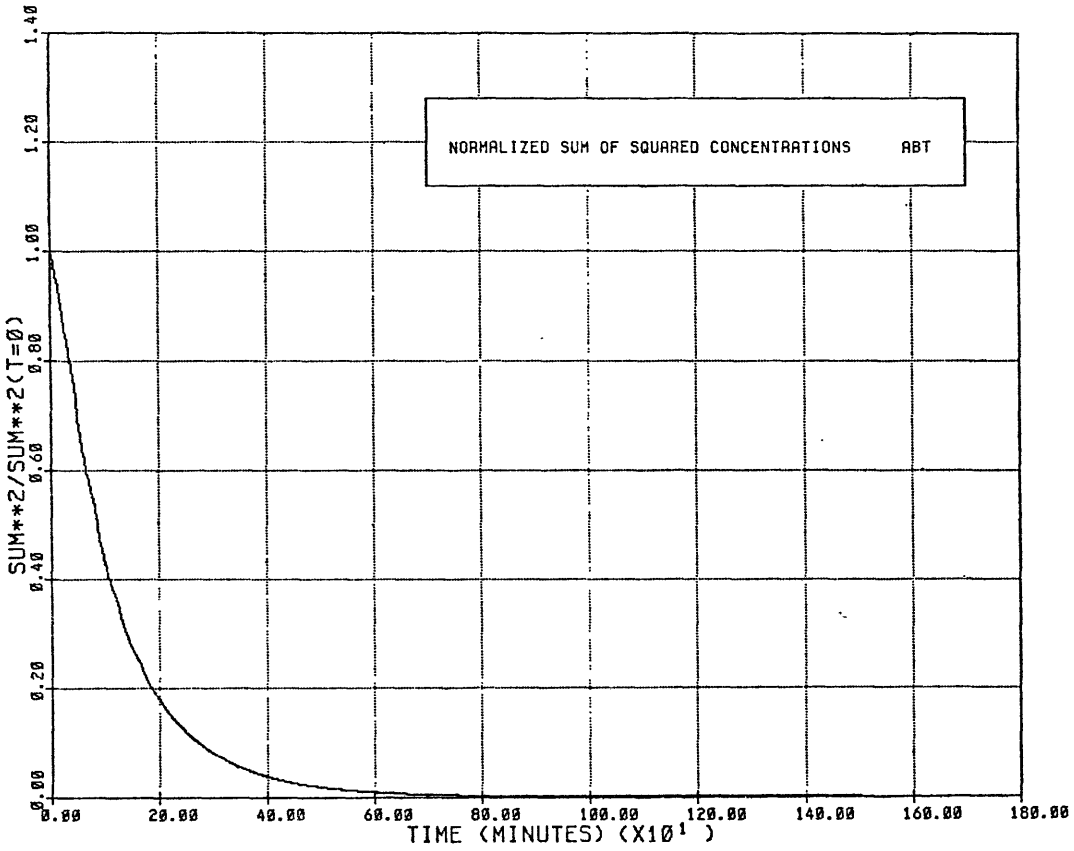

Figure 36: Trial with deposition:
normalized squared mass

j. Diagrams of deposition

The pattern of deposition on the ground at selected timesteps is shown below in figures 37a through 37i.

```
                  10
                  !
0.0   0.0   0.2   0.4   0.3   0.1   0.0
0.0   0.6   2.9   4.9   3.0   0.7   0.1
0.2   2.7  12.9  21.8  13.5   3.1   0.3
0.3   4.6  21.4  35.9  22.2   5.2   0.5
0.2   2.7  12.9  21.8  13.5   3.1   0.3
0.0   0.6   2.8   4.9   3.0   0.7   0.1
0.0   0.0   0.2   0.4   0.3   0.1   0.0
25
```

37a. Trial with deposition:

deposition pattern at t=0001

```
                  10
                  !
0.0   0.1   0.4   0.8   0.5   0.1   0.0
0.1   1.1   5.6   9.7   6.2   1.5   0.2
0.4   5.3  25.5  43.5  27.2   6.5   0.6
0.6   8.8  42.2  71.7  44.8  10.6   1.0
0.4   5.3  25.5  43.5  27.2   6.5   0.6
0.1   1.1   5.6   9.7   6.2   1.5   0.2
0.0   0.1   0.4   0.8   0.5   0.1   0.0
25
```

37b. Trial with deposition:

deposition pattern at t=0002

```
                  10
                  !
0.0   0.1   0.6   1.2   0.8   0.2   0.0   0.0
0.1   1.6   8.2  14.5   9.4   2.4   0.3   0.0
0.5   7.6  37.8  65.1  41.2  10.0   1.0   0.0
0.8  12.8  62.6 107.3  67.7  16.3   1.6   0.1
0.5   7.6  37.8  65.1  41.2  10.0   1.0   0.0
0.1   1.6   8.2  14.5   9.4   2.4   0.3   0.0
0.0   0.1   0.6   1.2   0.8   0.2   0.0   0.0
25
```

37c. Trial with deposition:

deposition pattern at t=0003

```
                  10
                  !
          0.1   0.1   0.1
    0.1   1.6   3.9   3.2   1.1   0.2
0.1   3.2  23.7  47.3  33.9  10.2   1.5   0.1
0.6  18.8 114.3 213.4 145.4  40.3   5.4   0.4
1.1  32.5 191.4 352.3 237.0  64.5   8.2   0.6
0.6  18.7 114.2 213.4 145.5  40.5   5.4   0.4
0.1   3.2  23.7  47.3  34.0  10.2   1.6   0.1
    0.1   1.6   3.9   3.2   1.1   0.2
          0.1   0.1   0.1
25
```

37d. Trial with deposition:

deposition pattern at t=0010

```
                                                  15
                                                  |
      0.0   0.0   0.3   0.6   1.2   0.6   0.2   0.0   0.0   0.0   0.0   0.0   0.0
      0.0   0.0   0.1   1.8   8.9  22.6  35.3  36.9  24.8  11.0   3.4   0.5   0.0
      0.3   0.1   3.2  40.0 164.1 291.1 309.3 208.1  99.8  36.9  11.0   2.3   0.1
      0.0   0.6  22.1 259.6 975.41448.61125.4 587.3 234.2  76.3  20.8   4.6   0.5
      0.0   1.1  38.4 422.51576.92359.51722.2 833.0 314.6  97.9  26.0   5.8   0.7
25 -  0.0   0.6  22.0 259.1 974.61447.61128.2 589.6 235.8  76.6  20.9   4.7   0.5
      0.3   0.1   3.2  39.9 163.4 289.2 309.9 210.4 100.8  37.5  11.1   2.3   0.1
      0.0   0.0   0.1   1.8   8.9  22.7  35.1  36.9  25.3  11.5   3.4   0.5   0.0
      0.0   0.0   0.3   0.6   1.2   0.6   0.2   0.0   0.0   0.0   0.0   0.0   0.0
```

37e. Trial with deposition:

deposition pattern at t=0100

```
                                                  15
                                                  |
      0.0   0.0   0.9   1.8   3.6   1.8   0.2   0.0   0.0   0.0   0.0   0.0   0.0   0.0   0.0   0.0   0.0   0.0   0.0   0.0   0.0
      0.0   0.0   0.1   1.8   8.9  22.6  35.4  48.2  57.5  65.7  70.6  76.6  75.0  61.8  38.5  21.2   8.9   2.7   0.2   0.0
      0.3   0.1   3.2  40.0 164.1 291.1 352.8 371.7 378.0 373.4 360.7 329.5 261.3 169.0  95.2  47.4  21.2   7.3   1.5   0.0
      0.0   0.6  22.1 259.6 975.41501.41501.11356.71206.31073.3 948.4 756.5 513.5 299.7 155.4  72.7  31.6  12.0   3.0   0.2
      0.0   1.1  38.4 422.51576.92407.82320.81996.91715.21482.81278.9 982.8 638.5 363.5 183.9  84.2  36.0  13.5   3.6   0.3
25-   0.0   0.6  22.0 259.1 974.61501.31502.41357.51210.51077.5 950.1 762.0 517.6 303.7 156.8  73.5  31.8  12.1   3.1   0.2
      0.3   0.1   3.2  39.9 163.4 289.2 352.2 374.1 377.7 372.9 361.9 330.5 264.0 171.2  96.2  48.0  21.8   7.6   1.6   0.0
      0.0   0.0   0.1   1.8   8.9  22.7  35.2  47.6  57.7  66.6  70.5  76.3  75.3  62.5  39.3  21.9   9.2   3.0   0.3   0.0
      0.0   0.0   0.9   1.8   3.6   1.8   0.2   0.0   0.0   0.0   0.0   0.0   0.0   0.0   0.0   0.0   0.0   0.0   0.0   0.0
```

37f. Trial with deposition:

deposition pattern at t=0300

```
                                  10                                                                  30
                                  |                                                                   |
      0.0   0.0   1.8   3.6   7.2   3.6   0.2   0.0   0.0   0.0   0.0   0.0   0.0   0.0   0.0
      0.0   0.0   0.1   1.8   8.9  22.6  35.4  48.2  57.5  65.7  70.6  76.6  80.2  85.2  82.4
      0.3   0.1   3.2  40.0 164.1 291.1 352.8 371.7 378.0 373.4 360.7 340.2 327.3 308.3 287.9
      0.0   0.6  22.1 259.6 975.41501.41501.11356.71206.31073.3 957.7 854.4 763.6 680.0 607.7
      0.0   1.1  38.4 422.51576.92407.82320.81996.91715.21482.81287.31127.5 986.7 869.2 765.3
25-   0.0   0.6  22.0 259.1 974.61501.31502.41357.51210.51077.5 959.6 859.8 766.6 685.5 610.9
      0.3   0.1   3.2  39.9 163.4 289.2 352.2 374.1 377.7 372.9 361.9 340.1 327.9 308.7 288.6
      0.0   0.0   0.1   1.8   8.9  22.7  35.2  47.6  57.7  66.6  70.5  76.3  80.0  84.8  82.1
      0.0   0.0   1.8   3.6   7.2   3.6   0.2   0.0   0.0   0.0   0.0   0.0   0.0   0.0   0.0

                                        25                                  30
                                        |                                   |
            0.0   0.0   0.0   0.0   0.0   0.0   0.0   0.0   0.0   0.0   0.0   0.0   0.0   0.0
           83.2  84.8  85.4  87.4  89.7  79.9  66.5  50.1  34.0  20.7  10.7   4.0   0.5   0.0
          266.5 242.5 231.9 216.9 202.3 164.1 118.9  85.3  55.8  37.1  20.8   8.6   2.2   0.0
          547.7 489.2 434.3 393.7 335.5 263.2 186.0 115.5  72.9  45.5  27.9  13.1   3.8   0.4
          682.0 601.4 537.5 472.3 405.2 309.9 214.8 133.7  78.6  48.7  30.1  14.7   4.5   0.5
25 -      550.4 492.0 436.3 394.8 337.8 265.6 187.5 117.0  73.6  45.7  28.1  13.2   3.8   0.4
          266.7 242.7 231.7 216.2 202.4 165.4 120.5  87.0  57.0  38.1  21.7   9.1   2.3   0.1
           83.4  85.0  86.1  87.4  90.2  80.5  67.5  51.1  34.9  21.4  11.2   4.3   0.6   0.0
            0.0   0.0   0.0   0.0   0.0   0.0   0.0   0.0   0.0   0.0   0.0   0.0   0.0   0.0
```

37g. Trial with deposition:

deposition pattern at t=0600

				10										20						
	0.0	0.0	3.0	6.0	12.0	6.0	0.2	0.0	0.0	0.0	0.0	0.0	0.0	0.0	0.0	0.0	0.0	0.0	0.0	0.0
	0.0	0.0	0.1	1.8	8.9	22.6	35.4	48.2	57.5	65.7	70.6	76.6	80.2	85.2	82.4	83.2	84.8	85.4	87.4	
	0.3	0.1	3.2	40.0	164.1	291.1	352.8	371.7	378.0	373.4	360.7	340.2	327.3	308.3	287.9	266.5	242.5	231.9	216.9	
	0.0	0.6	22.1	259.6	975.4	1501.4	1501.1	1356.7	1206.3	1073.3	957.7	854.4	763.6	680.0	607.7	547.7	489.2	434.3	394.2	
	0.0	1.1	38.4	422.5	1576.9	2407.8	2320.8	1996.9	1715.2	1482.8	1287.3	1127.5	986.7	869.2	765.3	692.0	601.4	537.5	472.5	
25 -	0.0	0.6	22.0	259.1	974.6	1501.3	1502.4	1357.5	1210.5	1077.5	959.6	859.8	766.6	685.5	610.9	550.4	492.0	436.3	395.2	
	0.3	0.1	3.2	39.9	163.4	289.2	352.2	374.1	377.7	372.9	361.9	340.1	327.9	308.7	288.6	266.7	242.7	231.7	216.2	
	0.0	0.0	0.1	1.8	8.9	22.7	35.2	47.6	57.7	66.6	70.5	76.3	80.0	84.8	82.1	83.4	85.0	86.1	87.4	
	0.0	0.0	3.0	6.0	12.0	6.0	0.2	0.0	0.0	0.0	0.0	0.0	0.0	0.0	0.0	0.0	0.0	0.0	0.0	

	26													39
	0.0	0.0	0.0	0.0	0.0	0.0	0.0	0.0	0.0	0.0	0.0	0.0	0.0	0.0
	90.5	89.7	93.6	96.3	99.8	105.5	103.1	102.7	104.9	106.7	104.5	96.1	83.1	68.6
	204.7	186.0	166.5	154.0	141.4	120.9	123.0	126.6	120.7	120.7	119.8	114.7	101.4	86.1
	349.3	314.0	283.5	255.7	235.8	212.6	184.2	159.1	141.4	140.9	140.3	136.2	125.3	109.3
	425.9	379.5	336.4	294.8	263.9	249.9	222.9	199.5	167.8	146.1	144.7	140.2	129.0	113.8
25 -	351.3	315.7	283.9	257.0	236.5	213.2	185.6	158.4	141.2	141.6	141.8	137.2	126.1	110.5
	204.3	185.8	166.4	154.5	140.8	123.8	122.0	126.9	129.2	130.3	121.4	116.6	104.1	87.4
	90.7	89.4	93.6	96.2	98.8	103.4	104.8	102.8	102.3	102.9	104.0	96.7	85.0	70.9
	0.0	0.0	0.0	0.0	0.0	0.0	0.0	0.0	0.0	0.0	0.0	0.0	0.0	0.0

	40							47
	0.0	0.0	0.0	0.0	0.0	0.0	0.0	0.0
	55.0	42.1	30.0	18.6	9.0	2.8	0.1	0.0
	70.5	56.1	41.6	27.5	15.8	7.0	1.9	0.0
	92.9	75.9	59.1	42.7	26.1	12.7	3.6	0.4
	97.1	80.7	63.9	47.5	30.5	15.2	4.6	0.6
25 -	93.6	76.7	60.3	43.3	27.0	12.8	3.8	0.4
	72.4	57.3	42:5	28.8	16.4	7.7	2.1	0.0
	57.0	44.1	31.7	20.0	10.0	3.4	0.3	0.0
	0.0	0.0	0.0	0.0	0.0	0.0	0.0	0.0

37h. Trial with deposition:

deposition pattern at t=1000

15

	0.0	0.0	3.0	6.0	12.0	6.0	0.2	0.0	0.0	0.0	0.0	0.0	0.0	0.0	0.0	0.0	0.0	0.0
	0.0	0.0	0.1	1.8	8.9	22.6	35.4	48.2	57.5	65.7	70.6	76.6	80.2	85.2	82.4	83.2	84.8	85.4
	0.3	0.1	3.2	40.0	164.1	291.1	352.8	371.7	378.0	373.4	360.7	340.2	327.3	308.3	287.9	266.5	242.5	231.9
	0.0	0.6	22.1	259.6	975.4	1501.4	1501.1	1356.7	1206.3	1073.3	957.7	854.4	763.6	680.0	607.7	547.7	489.2	434.3
	0.0	1.1	38.4	422.5	1576.9	2407.8	2320.8	1996.9	1715.2	1482.8	1287.3	1127.5	986.7	869.2	765.3	682.0	601.4	537.5
25	0.0	0.6	22.0	259.1	974.6	1501.3	1502.4	1357.5	1210.5	1077.5	959.6	859.8	766.6	685.5	610.9	550.4	492.0	436.3
	0.3	0.1	3.2	39.9	163.4	289.2	352.2	374.1	377.7	372.9	361.9	340.1	327.9	308.7	288.6	266.7	242.7	231.7
	0.0	0.0	0.1	1.8	8.9	22.7	35.2	47.6	57.7	66.6	70.5	76.3	80.0	84.8	82.1	83.4	85.0	86.1
	0.0	0.0	3.0	6.0	12.0	6.0	0.2	0.0	0.0	0.0	0.0	0.0	0.0	0.0	0.0	0.0	0.0	0.0

30

	0.0	0.0	0.0	0.0	0.0	0.0	0.0	0.0	0.0	0.0	0.0	0.0	0.0	0.0	0.0	0.0	0.0	0.0
	87.4	90.5	89.7	93.6	96.3	99.8	105.5	103.1	102.7	104.9	108.1	119.4	122.8	128.6	129.0	127.6	122.6	117.3
	216.9	204.7	186.0	166.5	154.0	141.4	120.9	123.0	126.6	120.7	120.7	119.9	119.1	116.9	116.2	114.6	114.1	113.0
	394.2	349.3	314.0	283.5	255.7	235.8	212.6	184.2	159.1	141.4	140.9	140.5	140.5	141.0	140.7	141.2	141.2	141.3
	472.5	425.9	379.5	336.4	294.8	263.9	249.9	222.9	199.5	167.8	146.1	144.8	144.5	144.2	144.4	144.1	144.1	144.0
25	395.2	351.3	315.7	283.9	257.0	236.5	213.2	185.6	158.4	141.2	141.6	142.0	141.5	141.6	141.8	141.7	141.7	142.1
	216.2	204.3	185.8	166.4	154.5	140.8	123.8	122.0	126.9	129.2	130.3	121.6	120.9	119.9	117.3	116.8	115.9	114.3
	87.4	90.7	89.4	93.6	96.2	98.8	103.4	104.8	102.8	102.3	102.9	112.1	117.8	120.2	123.7	124.0	121.1	118.0
	0.0	0.0	0.0	0.0	0.0	0.0	0.0	0.0	0.0	0.0	0.0	0.0	0.0	0.0	0.0	0.0	0.0	0.0

45

	0.0	0.0	0.0	0.0	0.0	0.0	0.0	0.0	0.0	0.0	0.0	0.0	0.0	0.0	0.0	0.0	0.0	0.0
	111.0	105.4	100.3	93.6	86.3	82.9	79.5	71.6	61.9	51.5	42.4	33.5	25.4	17.1	9.5	3.1	0.2	0.0
	111.7	111.0	109.6	109.5	110.7	111.5	107.8	101.4	90.3	77.8	65.0	52.7	40.3	28.5	16.7	7.9	2.2	0.0
	141.7	141.7	142.1	142.0	142.7	142.9	143.1	138.4	127.3	111.5	95.1	78.1	61.7	44.7	28.4	14.1	4.5	0.6
	144.3	143.9	144.4	144.5	144.4	144.9	144.7	141.8	131.5	116.8	99.7	83.4	66.4	50.0	33.0	17.3	5.7	0.9
25	142.1	142.6	142.2	142.6	143.1	143.4	143.8	139.3	128.3	112.5	96.1	79.2	62.7	45.8	29.4	14.7	4.7	0.6
	113.5	112.4	111.9	111.7	111.9	113.7	110.2	103.7	92.5	79.8	66.4	54.4	41.7	29.7	17.7	8.6	2.6	0.1
	113.5	108.2	103.5	97.0	91.2	87.1	83.9	75.6	65.5	55.3	46.1	36.5	27.8	18.9	10.7	3.8	0.5	0.0
	0.0	0.0	0.0	0.0	0.0	0.0	0.0	0.0	0.0	0.0	0.0	0.0	0.0	0.0	0.0	0.0	0.0	0.0

37i. Trial with deposition:

deposition pattern at t=1440

k. Description of deposition

The deposition pattern reproduced fairly realistically the deposition pattern that would be likely to result from a nuclear explosion (see figure 9.105 in Glasstone, (1977)). The amount deposited grew very rapidly near the explosion and quickly became a large, narrowly distributed peak. As the cloud drifted downwind, the amount of particulate matter in the cloud decreased and so the deposition rate was lower. The deposition pattern spread downwind across the grid but the maximum amplitude that was attained grew smaller at increasing distance from the explosion.

l. Cross sections through deposition pattern

Cross sections through the deposition pattern are shown below in figures 38a through 38c.

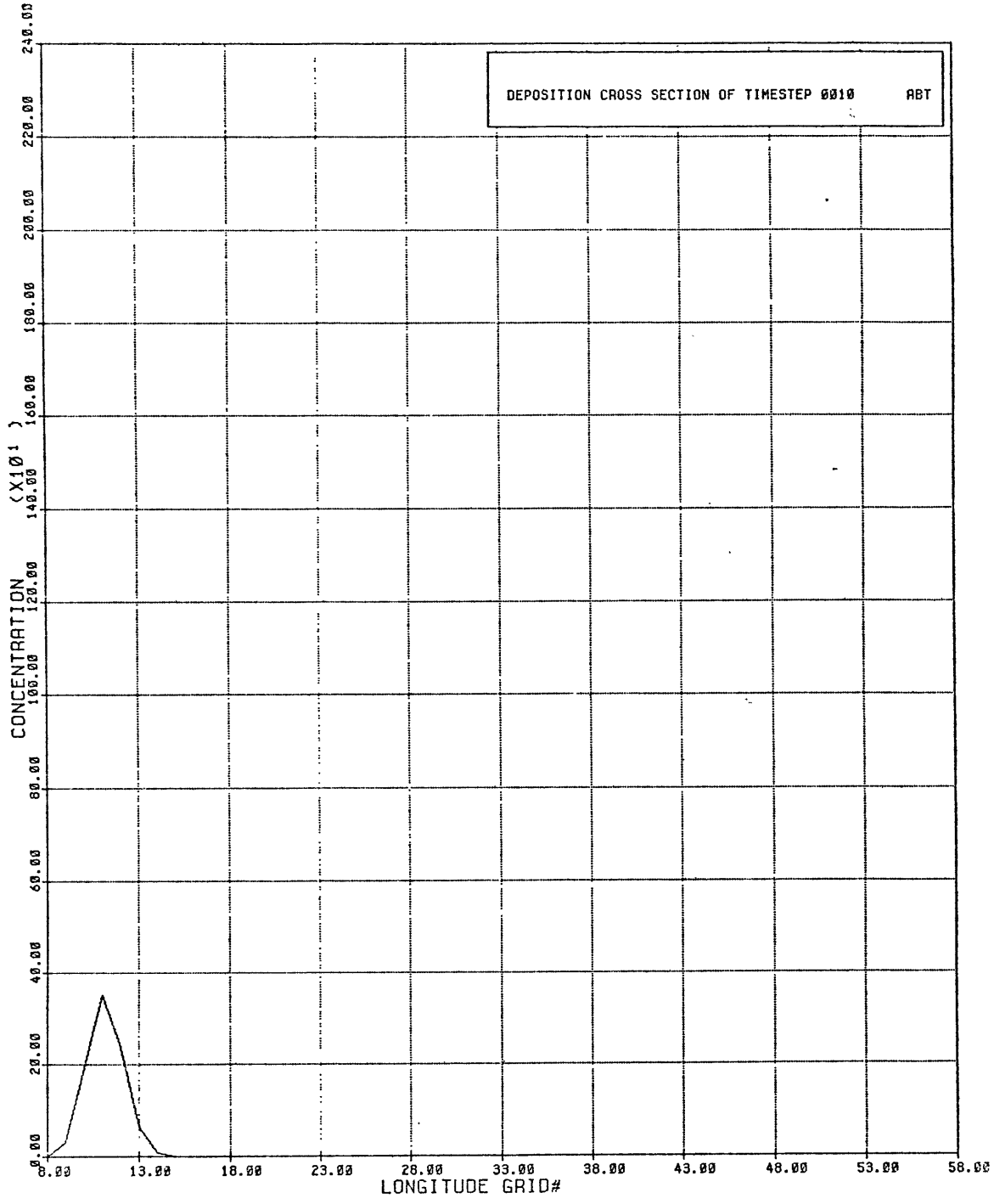

38a. Trial with deposition:

deposition cross-sections at t=0010

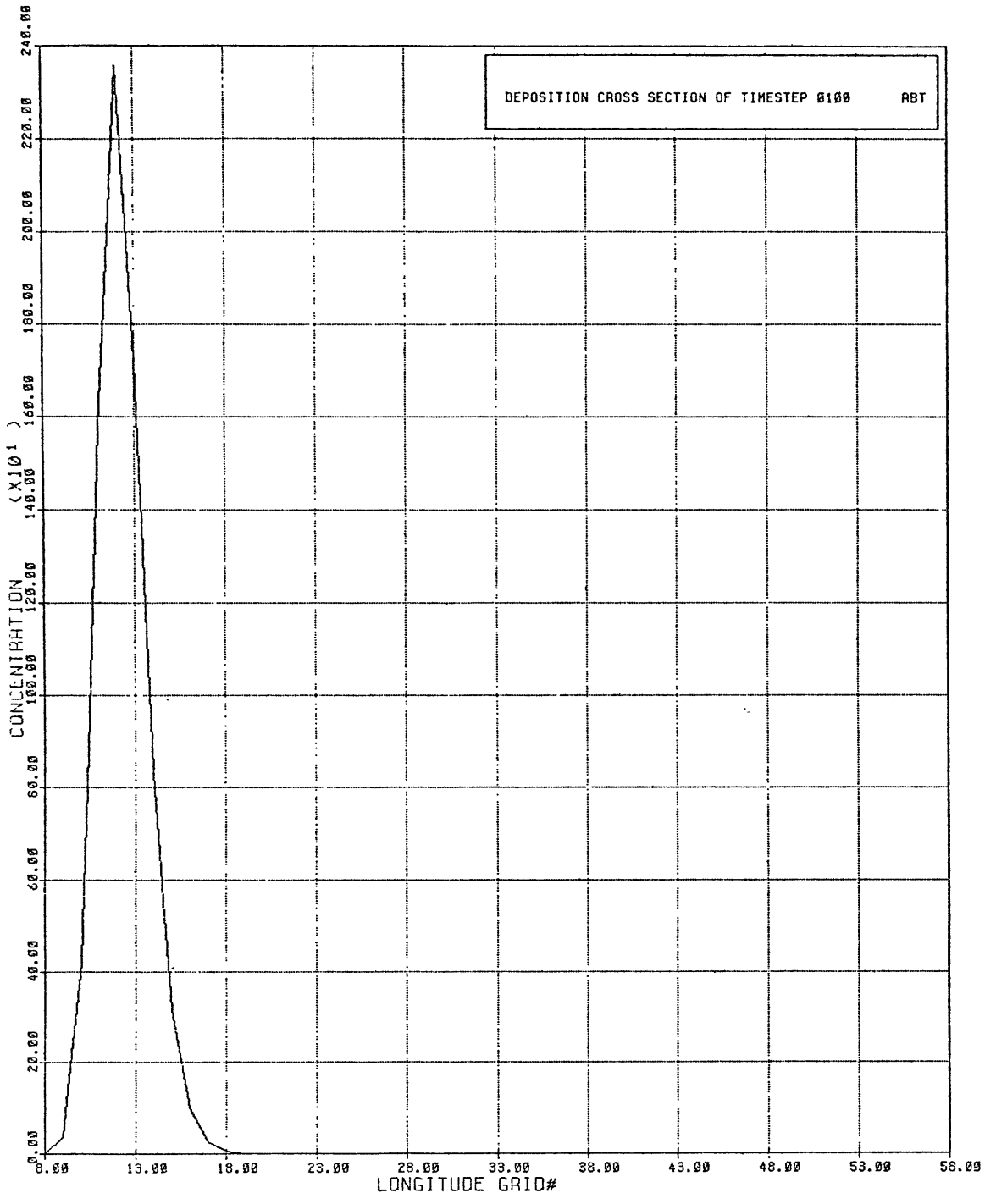

38b. Trial with deposition:

deposition cross-sections at t=0100

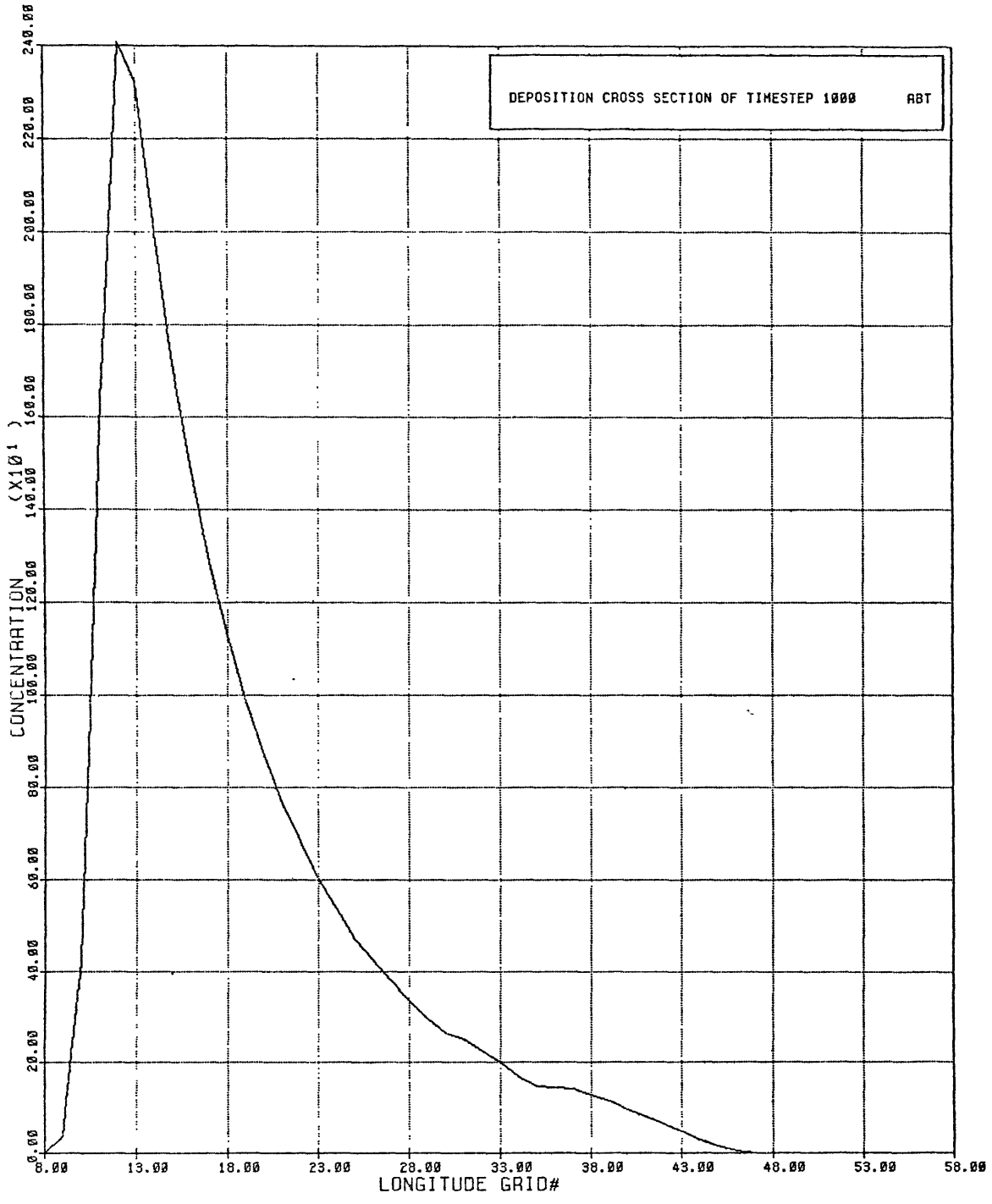

38c. Trial with deposition:

deposition cross-sections at t=1000

The cross-sections illustrate the peak near the explosion and the nearly exponential decay downwind. The drop was not exponential at the eastern portion of the pattern. The values were higher than an exponential decay would have produced because they were produced by a cloud that, because of the truncation error discussed above, was not losing mass as it deposited debris on the ground. The enhancement of the eastern portion was larger than was implied by the cross-section of timestep 1000. At timestep 1000, the particle cloud was over gridpoints (38,26) to (43,26) and was depositing in that region. The deposition pattern eventually became flat at the level that had already been reached at gridpoints (35,26) through (37,26), where the cloud had just passed.

V. Conclusions

A. Unsmoothed model

The Arakawa scheme in its pure form is not suitable for the long term advection of particulate clouds. The scheme was developed with the goal of conserving certain quantities during long term numerical integration. These quantities, mass and squared mass, were conserved fairly well in the trials that were tested here. The total mass was always conserved to within a few percent with the error easily attributed to the truncation errors that were inherent to the integer arithmetic that was used. The squared mass was not conserved quite as well. The quantity always grew monotonically to 1.7 to two times its original value. The origin of this growth has been discussed and the magnitude of the growth was not very large considering that the factor of two growth occurred over 1400 iterations. With more accurate time differencing schemes, this quantity can be conserved more closely, (Arakawa (1970)).

Unfortunately, these quantities were conserved at the expense of producing unrealistic results. The wakes produced by the scheme tended to almost totally obscure the actual cloud. Indeed, it was difficult to even define the actual

cloud in these trials. It certainly was not the entire distribution; the negative concentrations are not realistic. The positive area to the front of the distribution was also not, by itself the actual cloud. The mass and velocity of this positive area did not agree with what should be present in such a cloud. As pointed out in Orzag (1971), the wakes contained information about the distribution that lagged the proper location of the cloud.

The entire distribution, including the wakes, produced by the pure scheme had a centroid that was in the location predicted for particles moving at the local wind velocity. It seems likely that this agreement is only preserved for clouds embedded in very idealized wind fields. In the trials presented here, the wakes spread into regions of the grid where an actual cloud should not have been present. The concentrations were thus advected by winds that a real cloud should never have experienced. In the simplified cases studied here, the wakes always felt a pure zonal wind that varied only very little through the grid, thus the location of the centroid was not affected by the different winds that the wake was experiencing. This would not, generally, be the case in the real atmosphere.

The pure scheme results in the extreme expansion of the cloud. This poses problems for the advection as described above, but also is unrealistic in itself. One of the ultimate

goals of this model is to predict the deposition rate of radioactive particles falling to the ground after being carried by the wind from an unwind nuclear detonation. The spurious growth of the cloud implies that exposures to radioactive debris would occur over a much larger region than is realistic. In particular, the model would predict that exposures (possibly negative, the meaning of which is an enigma) even far upwind of the explosion. This does not occur in nature and is a major shortcoming of this model.

B. Smoothed model

In order to eliminate the difficulties associated with the wakes, a smoothing scheme was introduced which modified the pure Arakawa scheme. This scheme was very successful at controlling the wakes and restoring realistic results to the advection scheme. The wakes were totally eliminated by the method described in Appendix B, and the upwind growth of the cloud was halted.

The clouds that were produced did exhibit some numerical diffusion, but it was greatly reduced and exclusively positive. The spatial extent of the clouds was significantly reduced. The clouds were smaller than even just the forward positive areas in the unsmoothed trials. The most rapid

diffusion occurred during the early timesteps of the advection that were initialized with clouds covering only one or nine grid boxes. This was not an unexpected result because finite differencing schemes generally have difficulty with objects that vary over a small scale. The minimum stable size in the latitudinal direction appears to be five grid boxes. When the one and nine point initializations grow to this width, the growth ceased for the remainder of the trial. It is likely that slow growth would have continued if floating point arithmetic had been used. With integer arithmetic, very small expansions were systematically rounded to zero. The growth in the direction of motion was more pronounced, but still not very rapid after the initial timesteps. The clouds, in all of the trials, only expanded to between ten and thirteen gridpoints after over 1000 iterations.

Since this small rate of numerical diffusion was entirely positive and was not counterbalanced by negative wake diffusion, the sum of the squared mass necessarily decreased in these trials. This is the major flaw of the smoothed scheme. The amount of the decrease of this quantity is a measure of the amount of numerical diffusion that has affected the cloud. This problem should not preclude useful predictions from being made. In nature, clouds experience physical diffusion due to turbulent motions in the atmosphere. In an actual cloud, therefore, the sum of the squared masses would drop. In the simplified trials presented here the

natural rate of diffusion was set at zero. If natural diffusion is to be incorporated into this model, the value of the diffusion constant in (17) should be reduced to account for the numerical diffusion already present in the model. Thus a modified equation (17) would be:

$$\frac{DC}{Dt} = \left[D_{E(natural)} - D_{E(numeric)} \right] \nabla^2 (C) \qquad (37)$$

This smoothed model predicts very well the location of a particle cloud embedded in a height field of constant pressure. In order to make predictions about the actual deposition of radioactive debris, some additions must be made to the scheme.

1. An appropriate diffusion constant must be chosen This constant may be negative if the numerical diffusion rate is determined to be larger than the natural diffusion rate.
2. Depending on the type of debris that is under study, a rate of decay should be incorporated into the model. For many long lived isotopes, such as Strontium-90, this decay rate can be safely ignored.

3. A modification should be made to the smoothing scheme, if possible, to prevent the spurious lag in the velocity

of the centroid of the distribution.

C. Deposition case

The deposition trial worked very well, especially considering the crude deposition scheme that was used. The pattern that was produced closely approximated the typical "teardrop" patterns that actually occur in the aftermath of nuclear explosions. The spurious enhancement of the eastern portions of the pattern could be easily eliminated with the use of floating point, rather than integer, arithmetic in the calculation of the concentrations remaining in the cloud after deposition. If only long range deposition is to be considered, then a more sophisticated scheme must be used. The simplest scheme that eliminates the deposition near the explosion assumes a vertical diffusion constant of zero. In this scheme the cloud, with finite vertical extent, falls at the terminal velocity of the particles contained in it. As the cloud falls it is advected by the wind at the level to which it has fallen. (The height fields at several standard pressure levels are easily obtainable and can be used to calculate these winds.) When the bottom of the cloud hits the ground, then deposition begins to occur. Deposition continues to occur until the top of the cloud reaches the ground. This

scheme should produce a region of deposition that is offset from the explosion and represents solely long range deposition.

D. Summary

The model described here was tested on very idealized and simplified fields of wind and concentration. The physical diffusion in the atmosphere was ignored and the decay rate of radioactive particles was similarly neglected. The deposition scheme was of the crudest nature. A major simplification was made when the model incorporated only one layer. This ignored all vertical variation in the wind and concentration fields.

The purpose of this study was not to make meaningful predictions of actual fallout dispersion patterns. Rather, it was to develop and study the properties of a scheme which can be used to make such predictions. This paper discussed the numeric instabilities of the advection scheme and the rates of spurious numerical diffusion that are to be expected in a simulation of fallout dispersion. The instabilities were serious but a smoothing scheme was presented which eliminated the instabilities while still producing realistic results. This paper should provide the groundwork for more detailed studies of the long range dispersion of particles produced by

nuclear detonations.

REFERENCES

Arakawa, A., (1966), "Computational Design for Long-Term Numerical Integration of Fluid Motions: Two Dimensional Incompressible Flow. Part 1.", Journal of Computational Physics, 1, 119-143.

Arakawa, A., (1970), "Numerical Simulation of Large-Scale Atmospheric Motions", Numerical Solution of Field Problems in Continuum Physics, (American Mathematical Society, Providence, RI), 24-40

Arakawa A., and Lamb. V., (1977), "Computational Design of the Basic Dynamical Processes of the UCLA General Circulation Model", Methods in Computational Physics, Volume 17: General Circulation Models of the Atmosphere, (Academic Press, New York, NY), 173-265

Bretherton, F., and Karweit, M., (1975), "Mid-Ocean Mesoscale Modeling", Numerical Models of Ocean Circulations, (National Academy of Sciences, Washington, DC), 237-249

Davidson, B., Friend, J., and Seitz, H., (1966), "Numerical models of diffusion and rainout of stratospheric radioactive materials", Tellus, 18, 301-315

Dyer, A., (1966), "Artificial radio-activity, ozone and volcanic dust as atmospheric tracers in the Southern Hemisphere", Tellus, 18, 416-419

Fjortoft, R., (1953), "On the Changes in the Spectral Distribution of Kinetic Energy for Twodimensional, Nondivergent Flow", Tellus, 5, 225-

Glasstone, S., and Dolan, P., (1977), The Effects of Nuclear Weapons, (United States Department of Defense and United States Department of Energy, Washington, DC)

Holton, J., (1979), An Introduction to Dynamic Meteorology, Second Edition, (Academic Press, New York, NY)

Houghton, J., (1979), The Physics of Atmospheres, (Cambridge University Press, Cambridge, United Kingdom)

Kao, S.-K., and Henderson, D., (1970), "Large-Scale Dispersion of Clusters of Particles in Various Flow Patterns", Journal of Geophysical Research, 75, 3104-3113

Lilly, D., (1965), "On the Computational Stability of Numerical Solutions of Time-Dependent Non-Linear Geophysical Fluid Dynamics Problems", Monthly Weather Review, 93, 11-26

Lilly, D., (1969), "Numerical Simulation of Two-Dimensional Turbulence", The Physics of Fluids Supplement, 2, 240-249

Molenkamp, C., (1967), "Accuracy of Finite-Difference Methods Applied to the Advection Equation", Journal of Applied Meteorology, 7, 160-167

Orzag, S., (1971). "Numerical simulation of incompressible flows within simple boundaries: accuracy", Journal of Fluid Mechanics, 49, 75-112

Pedlosky, (1979), Geophysical Fluid Dynamics, (Springer-Verlag, New York, NY)

Roache, (1976), Computational Fluid Dynamics, (Hermosa Publishers, Albuquerque, NM)

Tanaevsky, O., and Blanchet, J., "Meteorological study of the course of radioactive debris", Tellus, 18, 434-439

Wit J., and Zagurek, M., (1981), "Fallout and the Land-Based MX", Arms Control Today, 11, 4-5

Appendix A: Height field generation scheme

The data used to construct the height field used in the advection calculation is transmitted from several hundred observing locations across the North American continent. The observing stations are scattered in a non-systematic manner across the continent. It is necessary to construct a height field from these observations so that there is a height value defined for each gridpoint in the model.

The scheme presented here to construct a height field is not the only one which would produce acceptable height fields. It is just one method of interpolating between the scattered observations. The results of this interpolation are acceptable and agree well with other human and computerized analysis of the same data. Where discrepancies arise between the results produced by this method and the results produced by other methods, the differences can be explained in the ambiguity of the field defined by the scattered observations. The mechanism of the interpolation is described below.

The scheme places all the scattered observations in the grid. It then finds a nearest neighboring observation for each of the observations. Lines are drawn between all of these pairs of observations. The values of the heights on these lines are linear interpolations between the endpoints.

The grid then contains a network of lines that connect many of the observations together. Two interpolating passes are then conducted. In the first, the scheme searches for filled grid boxes with the same longitudinal gridpoint values and draws linearly interpolated lines between them. This usually fills most of a grid with height values. The second pass repeats this process, but between values with the same latitudinal gridpoint value. This forms another grid that is mostly filled. The two grids are then averaged to form the final interpolated height field. The result, at this stage, contains frequent discontinuities in the first derivative of the field in the region of the lines that were drawn between the observations. In order to eliminate these discontinuities, the averaged interpolation was smoothed. The smoothing scheme was chosen so as to eliminate short period variations in the field. Each gridpoint value was modified to be the weighted average of itself and the neighboring gridpoint values. For a central height value located at gridpoint (ln,lt), the following quantities were defined:

```
cc =   height(ln,lt)

dd = ( height(ln+1,lt) + height(ln-1,lt)
     + height(ln,lt+1) + height(ln,lt-1))/4

ee = ( height(ln+1,lt+1) + height(ln+1,lt-1)
     + height(ln-1,lt+1) + height(ln-1,lt-1))/4
```

```
ff = ( height(ln+2,lt) + height(ln-2,lt)
     + height(ln,lt+2) + height(ln,lt-2))/4

gg = ( height(ln+2,lt+1) + height(ln+1,lt+2)
     + height(ln+2,lt-1) + height(ln+1,lt-2)
     + height(ln-2,lt+1) + height(ln-1,lt+2)
     + height(ln-2,lt-1) + height(ln-1,lt-2))/8

hh = ( height(ln+2,lt+2) + height(ln+2,lt-2)
     + height(ln-2,lt+2) + height(ln-2,lt-2))/4
```

The smoothed value at the gridpoint was the weighted average of all these quantities. The weighting function was the value of a Gaussian normal curve with a standard deviation equal to the distance between two adjacent gridpoints. Thus, for example, cc was weighted by normal(0)=.3989, and gg was weighted by normal($\sqrt{1^2+2^2}$)=.2136. Using this weighting function, the average was:

$$\text{height}(ln,lt) = \frac{.3989*cc+.3521*dd+.3108*ee+.2420*ff+.2136*gg+.1468*hh)}{(.3989+.3521+.3108+.2420+.2136+.1468)}$$

This produced fields that were very smooth and represented the large scale, synoptic, variations in the actual height field.

Appendix B: Concentration field smoothing scheme

The problems presented by the wakes are discussed in detail in the main body of this paper. A simple scheme for eliminating these wakes is presented here. This is by no means the only possible, or even the best, method of eliminating these wakes. It is, however, a simple, straightforward method.

The effects of the Arakawa advection scheme only extend to the eight nearest neighbors of a grid box with a non-zero concentration. Thus, in the initial wake forming phase, the wake can only be one layer thick. The following diagram shows, schematically, the region of possible wake formation around each grid box with a positive concentration. The wind is blowing from the left to the right. Wakes do not form around all grid boxes with concentrations. The negative wakes will not form if the concentrations in the wake region are sufficiently positive so as to remain positive even after the advection scheme subtracts concentration. In the trials tested in this paper, wakes will also not form if the magnitude of the wake is truncated or rounded to zero by the integer arithmetic used in the advection.

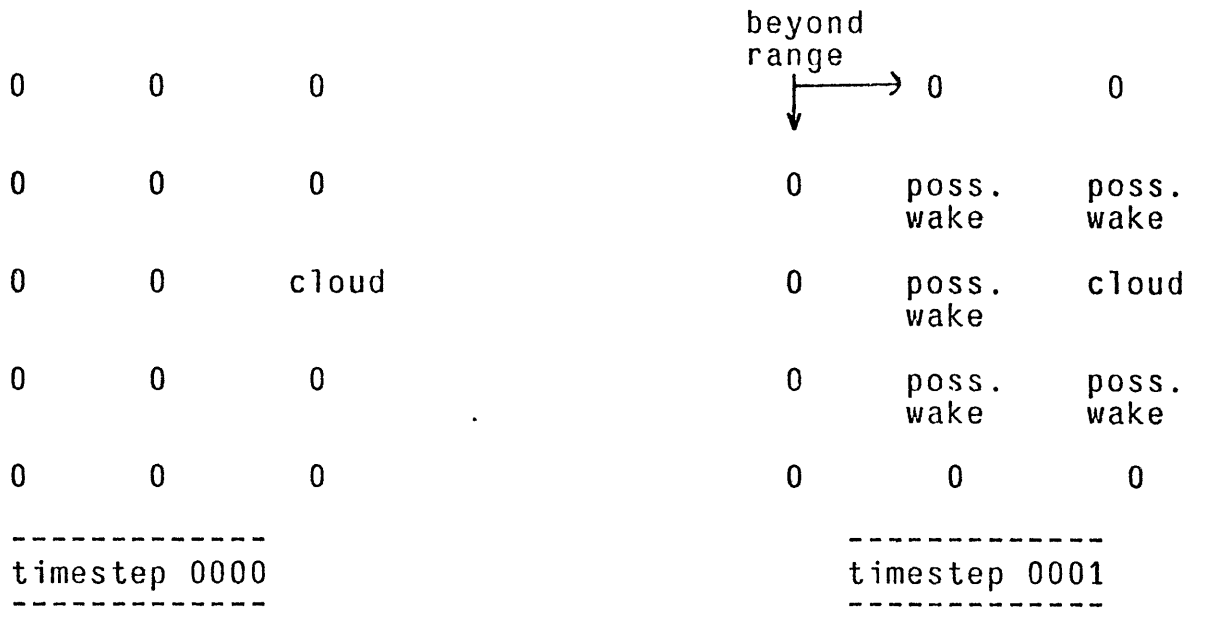

Figure 39: Wake formation regions

As the diagram shows, when a wake forms, all the grid boxes containing wake particles are, in the first timestep of wake formation, adjacent or diagonally adjacent to a grid box occupied by cloud particles.

The wake elimination scheme eliminates the negative wake every timestep and, thus, a wake never grows beyond the one layer dimension. A secondary positive wake is never formed.

The method of elimination is very straightforward. The scheme searches for a negative concentration produced by the advection scheme. When a negative value is found, the scheme searches for the largest positive value that is adjacent or

diagonally adjacent to the negative grid box. The concentration in the negative grid box is then added to the largest neighboring positive value and the value in the negative grid box is set to zero. The negative value is added to the largest nearby value instead of the absolute nearest neighbor because it is possible that the absolute nearest neighbor will be smaller in magnitude than the wake value. An addition would then result in just another negative value. As long as the CFL criteria is honored, there will always be a adjacent or diagonally adjacent cloud concentration that is larger than the wake concentration.

The elimination sometimes results in trailers being formed. These are described in the particular trials in which they occur. Trailers result when the elimination of negative wakes isolates particles, which were in regions of low concentration gradients, that were being left behind by the advection scheme. In addition to eliminating the wake, the smoothing scheme made an attempt to eliminate these trailers. In the trials studied here, several different versions of the smoothing scheme were used. They differed in their aggressiveness in eliminating the trailers. The earliest version of the smoother only eliminated single isolated particles. Other versions eliminated pairs, triplets and quadruplets of isolated particles. The most aggressive version eliminated long lines of trailers were only attached to the bulk of the cloud by a one gridpoint thick string of

concentrations. When found, a trailer was eliminated without regard for conservation of mass. The concentrations in the trailers were small and this did not introduce any significant errors.

The search for, and elimination of trailers was a time consuming process and was conducted only infrequently during the advection. The short period oscillations in the sum of the squares of the area weighted concentration and squares of concentrations are a result of trailers being eliminated by the smoothing scheme.